

**Charge transfer pumping for XUV lasers using femtosecond laser
induced plasmas interacting with neutrals from a pulsed gas jet**

Vom Fachbereich Physik
der Universität Hannover
zur Erlangung des Grades

Doktor der Naturwissenschaften

Dr. rer. nat.

genehmigte Dissertation

von

Dipl.-Phys. Valeriy Vorontsov

geboren am 08.11.1975 in Omsk, Rußland

2005

Referent : Prof. Dr. B. Wellegehausen

Korreferent: Prof. Dr. B. Chichkov

Tag der Promotion: 4. Februar 2005

Abstract

Valeriy Vorontsov

Charge transfer pumping for XUV lasers using femtosecond laser induced plasmas interacting with neutrals from a pulsed gas jet

This dissertation introduces a novel setup for investigations of charge transfer pumping at high densities and desirable geometries, which makes this approach very promising for the realization of lasers in the extreme ultraviolet (XUV) spectral range. The new approach consists of a femtosecond laser produced plasma colliding with a pulsed gas jet. For this scheme, the widths of the plasma and gas fronts are correspondingly steep, allowing effective ion-neutral charge exchange interactions at densities of reagents in excess of 10^{16} cm^{-3} , necessary to achieve inversion densities required for high gain and lasing at XUV transitions.

For basic studies and the optimization of the setup, the well-known charge transfer reaction $\text{C}^{4+} + \text{H}_2 \rightarrow \text{C}^{3+} (n=3) + \text{H}_2^+$ was investigated in detail, and clear selective pumping of levels with $n=3$ of C^{3+} ions was observed. A strong increase in intensities was also obtained for the $3d-2p$ ($\lambda=23.8 \text{ nm}$) and $2p3s-2p^2$ ($\lambda=37.4 \text{ nm}$) lines of O^{3+} and O^{2+} ions, as a result of the reactions $\text{O}^{4+} + \text{H} \rightarrow \text{O}^{3+} + \text{H}^+$ and $\text{O}^{3+} + \text{H} \rightarrow \text{O}^{2+} + \text{H}^+$, correspondingly. As a promising scheme for XUV gain experiments, the reaction $\text{C}^{6+} + \text{H} \rightarrow \text{C}^{5+} (n=3,4) + \text{H}^+$ was studied, and selective pumping of the 4-2 transition at 13.5 nm and of the 3-2 transition at 18.2 nm, well known from recombination pumped lasing experiments, was achieved.

A thoroughful analysis based on time resolved measurements allows to perform a quantitative comparison of the obtained results with a kinetic model of charge transfer pumping. These data confirm that highly selective charge exchange pumping has been realized for the first time at densities of both reagents of up to $2.8 \times 10^{16} \text{ cm}^{-3}$, which is sufficient for XUV lasing experiments.

Based on the achieved data and first test experiments with a line focus geometry, it is predicted that for a picosecond pump laser with 2.5 J, a gain-length-product of 10 appears feasible for the C^{5+} transition at 18.2 nm. In addition, advantages of new charge exchange schemes with potential lasing transitions in Na-like ions are presented and discussed.

Keywords: charge transfer pumping, XUV lasers, femtosecond laser produced plasma

Zusammenfassung

Valeriy Vorontsov

Ladungsaustauschpumpen von XUV Lasern durch Wechselwirkung von Femtosekundenlaser-induzierten Plasmen mit einem gepulsten Gasstrahl

Die Dissertation stellt einen neuentwickelten experimentellen Aufbau für die Untersuchungen von Ladungsaustausch-Pumpprozessen bei hohen Teilchendichten und geeigneten Geometrien für die Verwirklichung von Lasern im extremen ultravioletten (XUV) Spektralbereich vor. Durch Einsatz von Femtosekundenlasern für die Plasmaerzeugung und gepulsten Gasstrahlen für Neutralteilchen werden im Wechselwirkungsbereich von Plasma und Gasstrahl steile Dichtegradienten erreicht, die Ladungsaustauschreaktionen bei Teilchendichten von über 10^{16} cm^{-3} ermöglichen, die für eine hohe Verstärkung und einen Laserbetrieb auf XUV-Übergängen erforderlich sind.

Für grundlegende Untersuchungen und die Optimierung des Versuchsaufbaus wurde die bekannte Ladungsaustauschreaktion $\text{C}^{4+} + \text{H}_2 \rightarrow \text{C}^{3+} (n=3) + \text{H}_2^+$ verwendet. Die Experimente zeigen deutlich, dass selektives Pumpen der Niveaus $n=3$ des C^{3+} Ions erreicht wird. Eine starke Erhöhung der Linienintensität wird auch für die Übergänge $3d-2p$ ($\lambda=23,8 \text{ nm}$) und $2p3s-2p^2$ ($\lambda=37,4 \text{ nm}$) der O^{3+} und O^{2+} Ionen als Folge der Ladungsaustauschreaktionen $\text{O}^{4+} + \text{H} \rightarrow \text{O}^{3+} + \text{H}^+$ und $\text{O}^{3+} + \text{H} \rightarrow \text{O}^{2+} + \text{H}^+$ beobachtet. Als besonders geeignetes Schema für einen XUV Laser wurde die Reaktion $\text{C}^{6+} + \text{H} \rightarrow \text{C}^{5+} (n=3,4) + \text{H}^+$ untersucht, und es konnte selektives Pumpen auf dem 4-2 Übergang bei 13,5 nm und auf dem 3-2 Übergang bei 18,2 nm, der als Rekombinations-Laserübergang bekannt ist, demonstriert werden.

Eine ausführliche Analyse von zeitaufgelösten Messungen und ein quantitativer Vergleich mit einem entwickelten kinetischen Modell für den Ladungsaustausch bestätigt, dass erstmals selektives Pumpen bei Teilchendichten beider stoßenden Komponenten von bis zu $2,8 \times 10^{16} \text{ cm}^{-3}$ erzielt wurde.

Erste Testexperimente mit einem Linienfokus ergeben, dass für den 18,2 nm-Übergang von C^{5+} ein Pikosekunden-Pumplaser mit einer Energie von 2,5 J erforderlich sein wird, um ein Verstärkungs-Längen-Produkt von 10 zu erzielen. Zusätzlich werden neue Ladungsaustauschschemata mit Laserübergängen in Na-ähnlichen Ionen vorgestellt und deren Vorteile diskutiert.

Schlagworte: Ladungsaustausch, XUV Laser, Femtosekundenlaserplasma

CONTENTS

Abstract

Zusammenfassung

Contents

| | |
|--|-----------|
| 1. Introduction | 3 |
| 2. Principles of short wavelength lasers | 6 |
| 2.1 Lasing medium and operating modes | 7 |
| 2.2 Gain formulations and methods for gain measurements | 9 |
| 2.3 Main mechanisms of pumping | 12 |
| 2.3.1 electron collisional pumping | 12 |
| 2.3.2 recombination pumping | 15 |
| 2.3.3 alternative pumping mechanisms | 18 |
| 2.4 Conclusion | 20 |
| 3. Population inversion by charge transfer pumping | 21 |
| 3.1 Basics of charge exchange mechanism | 21 |
| 3.2 Cross section data | 24 |
| 3.3 Rate equations | 27 |
| 3.4 Charge transfer pumping rate | 29 |
| 3.5 Estimations of gain with charge transfer excitation | 31 |
| 4. Status of experimental investigations on charge transfer pumping | 33 |
| 4.1 Typical scenarios of charge exchange interaction | 33 |
| 4.2 Interaction of high Z-ions with a solid easily evaporated obstacle | 35 |
| 4.3 Conclusion | 41 |
| 5. Novel experimental setup (<i>charge transfer between fs-laser produced ions and neutrals from a gas jet</i>) | 42 |
| 5.1 Experimental arrangement and diagnostics | 43 |
| 5.2 Ti:Sapphire laser system | 45 |
| 5.2.1 Description of the system | 45 |
| 5.2.2 Intensity in focus | 48 |

| | |
|---|-----------|
| 6. Experimental results | 50 |
| 6.1 Charge exchange between C^{4+} ions and hydrogen as a model system | 51 |
| 6.1.1 observation of selective pumping of $n=3$ level of C^{3+} ions | 52 |
| 6.1.2 comparison of results with different pulse duration lasers | 60 |
| 6.2 Theory versus experiment | 62 |
| 6.3 Observation of charge transfer excitation in oxygen ions | 68 |
| 6.3.1 dramatic increase in intensities of O^{2+} and O^{3+} ions | 69 |
| 6.4 Investigations on possible lasing transition of C^{5+} ions at 18.2 nm | 72 |
| 6.4.1 Selective pumping of $n=3,4$ levels with He and H_2 gases | 72 |
| 6.5 Conclusion | 75 |
| | |
| 7. Perspectives of charge exchange lasers | 76 |
| 7.1 Ideal geometry for lasing experiments – uniform plasma column interacting with a uniform gas stream having a sharp boundary | 77 |
| 7.2 Hydrogen like Beryllium as an ideal candidate for lasing | 81 |
| 7.3 Extensions to non-Hydrogenic ions – lasing in Na-like ions with higher efficiency | 83 |
| 7.4 The idea of quasi-steady state charge transfer pumping | 86 |
| 7.4.1 results on pumping of Ne-like Silicon ions | 86 |
| 7.4.2 $3p-3s$ transition of O^{3+} at 307 nm as an ideal tool for lasing by charge transfer in a normal operating laser mode with cavity | 89 |
| | |
| 8. Summary | 91 |
| | |
| References | 95 |
| | |
| Acknowledgements | |
| Lebenslauf | |
| List of publications | |

1. Introduction

In the past two decades considerable progress in the development of soft-x-ray or XUV lasers (spectral range from 0.2 to 100 nm) with collisional and recombination pumping using laser-produced and capillary discharge plasmas was achieved [Proceedings 2002]. However, the low efficiency of the presently operating XUV lasers, which is typically at the 10^{-7} level [data from “9th X-ray laser conference 2004”] limits the use of these lasers for applications and provides further motivation for investigations of other more efficient pumping schemes. Among the alternative pumping schemes for XUV lasers, charge exchange is one of the most promising candidates because of its quasi-resonant character, which makes it possible to populate the quantum levels selectively. The cross section of the process may be two orders of magnitude higher than that for the electron collisional excitation scheme. This makes the charge transfer scheme very advantageous and could dramatically improve the situation with XUV lasers by providing a better conversion efficiency.

In an ion-neutral charge exchange reaction, collisions of ions with neutrals take place, leading to the transfer of an electron from a neutral atom to an excited state of an ion. Straightforward estimates by [Vinogradov and Sobel'man 1972] predicted that a population inversion and lasing effect could be achieved in the short wavelength range at densities of ions and neutrals in the range of 10^{16} - 10^{17} cm⁻³. First attempts for creating population inversion by charge exchange were done already in the 70`s [Dixon and Elton 1977], in experiments with laser-produced plasmas expanding into a uniform background gas. However, the charge-transfer pumping efficiency was very low. The main problem with these experiments was the formation of shock waves, which further ionized gas particles and prevented a direct plasma-gas interaction, and finally the realization of charge-transfer pumping was achieved only at very low ion densities of the order of 10^{14} cm⁻³, which made this approach useless for the realization of XUV lasers. To reach an intermixing of different ion species which are initially separated, several other schemes were investigated. An ion-ion charge exchange process was suggested in [Ruhl et. al. 1997]. In experiments with hot and cold colliding plasmas an increase in intensity of the C⁵⁺ (3d-2p) line at 18.2 nm was reported and explained as an effect of the reaction C⁶⁺ + C²⁺ → C⁵⁺ (n=3) + C³⁺. However, due to a smeared interaction region and difficulties to control parameters of the plasmas during the collision, no

improvement has been reached in further experiments with colliding plasmas. In a work of [Ponomarenko et. al. 1998], a compact gas cloud created by laser ablation was used as a source of neutrals flowing towards the laser produced ions. A sharp density gradient of the gas cloud and a controllable gap between the plasma target and the gas front allowed the realization of efficient and direct charge-exchange interaction at ion densities of 10^{15} cm^{-3} . However, in this approach a further increase of the ion density in the interaction region is found to be problematic, since it is difficult to position the ablation gas cloud close enough to the plasma target.

According to an analytical model of charge-exchange interaction of dense interpenetrating flows developed by [Shaikhislamov 2000], for an efficient charge-transfer pumping at relatively high densities of reagents it is crucial to have both a compact gas stream and a well-localized plasma jet with a steep ion density gradient. At desired particle densities of 10^{16} cm^{-3} the characteristic length of charge exchange which determines the interpenetration of ions into a gas medium is less than 1 mm. Thus, an effective pumping can only be realized on a spatial scale of the order of 1 mm or less, and therefore, the plasma and gas fronts should be correspondingly steep.

The aim of this work is to perform a systematic analysis of charge transfer excitation mechanism, and find and explore suitable experimental scenarios for the realization of charge exchange pumping at densities of ions and neutrals in access of 10^{16} cm^{-3} , which is necessary to achieve gain in the Amplified Spontaneous Emission (ASE) mode. In addition, appropriate candidates for lasing experiments have to be found, and corresponding experimental tests have to be performed.

Furthermore, it is very desirable that the theoretical model developed for this purpose be subject to comparison with the experimental data in order to better understand the processes of charge transfer interaction and its conditions in more detail, and to work out the optimum conditions for the potential laser.

Because of the difficulty to control the front of the ablation plasma, the only way to ensure the front sharpness is to use ultrashort laser pulses for the generation of the plasma and to realize a gas-plasma interaction as close to the plasma target as possible. Therefore, a novel experimental scenario for charge exchange pumping, consisting of a pulsed gas jet interacting with plasmas produced by ultrashort laser pulses will be introduced and tested. With this technique selective charge exchange pumping at the required densities will be demonstrated for a number of reactions.

In connection with the main purpose, studies on charge exchange reactions are also of great interest from a fundamental point of view for laboratory and astrophysical plasmas [Rigazio et. al. 2002].

The work presented here is organized as follows:

In chapter 2, some definitions important for short wavelength lasers as well as basic principles, operating modes, and main mechanisms for creating a population inversion in the XUV spectral range are described.

The basics of charge exchange pumping, different theoretical models for the estimation of the cross section, rate equations, and an estimation of the gain for this excitation mechanism are described and discussed in Section 3.

Chapter 4 emphasizes previous experimental investigations on charge transfer pumping and summarizes the main difficulties and disadvantages of performed experiments.

The novel experimental scenario, allowing the realization of charge exchange interaction at desired densities and geometries, is introduced in Chapter 5. The setup consists of a femtosecond laser for the production of plasmas with steep ion density gradients and a gas jet for the production of neutrals.

In Section 6 the experimental results obtained with the novel setup are presented for a number of different reactions. The optimization of the setup was made by investigations on the well know $C^{4+} + H_2 \rightarrow C^{3+} (n=3) + H_2^+$ charge transfer reaction. Further investigations concern reactions of Oxygen ions with neutrals such as $O^{4+} + H \rightarrow O^{3+} + H^+$ and $O^{3+} + H \rightarrow O^{2+} + H^+$, and the reaction $C^{6+} + H \rightarrow C^{5+} (n=3,4) + H^+$ with possible lasing on the 3-2 transition at 18.2 nm, at which the lasing was already demonstrated with recombination pumping.

Chapter 7 gives a summary on perspectives for charge exchange lasers, discusses an ideal geometry of interaction, and introduces a novel scenario on charge transfer pumping in Na-like ions, which promises even more efficient pumping as compared with the here analyzed Hydrogen like ions.

Finally, in Section 8 the obtained results and future directions are summarized.

2. Principles of short wavelength lasers

Nowadays, x-ray lasers based on laser-produced plasmas have been developed worldwide. Shortly after the first demonstration of a ruby laser at 694.3 nm [Maiman 1960], laser scientists have pursued to make lasers with shorter and shorter wavelength. In the branch of X-ray lasers, plasma sources, and astrophysical fields, the spectral range shorter than 100 nm and down to 0.01 nm can be named as X-ray spectral range with sub-divisions as extreme ultraviolet (XUV) from 100 to 30 nm, soft x-ray for 30- 0.2 nm, and for wavelengths shorter than 0.2 nm hard x-ray or kilovolt x-ray when the photon energy is beyond 1 keV. The relationship between the wavelength λ and the photon energy $h\nu$ is as follows: $h\nu$ (eV) = 1240/ λ (nm), where h and ν are the Planck constant and frequency, respectively.

There are different methods developed to generate coherent photons in the XUV spectral range such as nonlinear optical processes (mostly due to generation of high order harmonics), free electron laser and basic laser principle. Harmonic generation can presently provide coherent XUV radiation down to about the water window (2-4 nm) with ultrashort pulses and efficiencies of about 10^{-7} - 10^{-8} , and are already used for some applications [Brabec and Krausz 2000]. Free electron lasers, based on electrons periodically accelerated in synchrotrons, are presently developed for the generation of radiation down to about 1 nm. They will provide tuneable powerful radiation, but will be extremely costly laser facilities [Neil and Merminga 2002], [Emma et. al. 2004]. X-ray lasers can presently be operated at a variety of wavelengths in the XUV and soft x-ray spectral range and are mostly based on laser produced plasmas. Although considerable progress has been achieved, the efficiency of present x-ray lasers is still small, about 10^{-6} or less, so that an output energy in the mJ-range still requires kJ of pump laser energy. Consequently, there is need for more efficient laser schemes, and the intention of this work is to investigate pumping mechanisms, which promise higher efficiencies. The results achieved with x-ray lasers nowadays can be found in [Proceedings 2002].

In the following chapter, the principles of x-ray lasers, operating modes as well as the main pumping mechanisms are described in detail.

2.1 Lasing medium and operating modes

The main differences of short wavelength lasers with respect to normal visible lasers result from two facts, namely, that they work without cavity and that the transitions involved correspond to transitions of high Z-ions and not to transitions of neutral species, which is typical for visible lasers, or transitions of low Z-ions for the ultraviolet regions. It means that the lasing medium must consist of high Z-ions, which are typically produced either by laser irradiation of solid or gaseous targets, or by a pulsed discharge in a dense gas. Such a medium is called plasma, consisting of ions and free electrons. The main characteristics of a plasma is the temperature of electrons and ions and their densities. It is often assumed that $T_e=T_i$ (equilibrium plasma), and the density of electrons has the following relationship with the density of ions $N_e=(Z-1)N_i$. Due to strong collisional and radiative depopulation of the levels, the population inversion is typically short lived (ns or less depending on the pump processes and involved transitions) and therefore a resonator is difficult to apply. Moreover, the active medium is a plasma which has high a temperature, and mirrors would have to be placed very near to the plasma and therefore would be quickly damaged. This explains why almost all of the present X-ray lasers operate without a resonator, or use in some specific cases a half-cavity (one mirror). Consequently, in such a system high gain must occur only for one pass through the medium, the laser is operated in the Amplified Spontaneous Emission regime (ASE).

A typical experimental realization of an x-ray laser consists of producing the amplifying medium, which is normally created by a line-focused laser beam on a target. The population inversion is produced in an elongated plasma column, where spontaneous emission from a group of inverted atoms is amplified by the same atoms through the plasma column. This results in a narrow divergence monochromatic x-ray beam, which propagates from both ends of the target to the other ends. The x-ray laser emission is normally measured using on-axis grazing incidence spectrometers placed on either side of the plasma column.

There are two main operating modes of X-ray-lasers: transient/self-terminated and quasi-continuous. In the former, the pumping takes place for a short period of time, typically from sub-picoseconds to tens of picoseconds, by heating the plasma at a rate faster than the relaxation rate of the excited state. This became very practical

2. Principles of short wavelength lasers

with the travelling wave pumping performed along the length of the active medium in coincidence with the amplified wave. In case of quasi-continuous pumping, population inversion exists for the duration of the pumping conditions. Then, if the upper levels are metastable with respect to radiative decay to the ground state, and the laser lower levels are depopulated by strong dipole-allowed transitions, the population inversion is created.

A first stage in the development of an x-ray laser is the spectroscopic regime where the possible lasing line gets strong in comparison with other non-lasing lines. The second stage is when the lasing line dominates in the spectrum. The third includes the saturated amplification regime where a significant part of the population inversion is converted into the lasing signals. The gain-length-product gL for these stages corresponds to less than 5, less than 15 and about 15, respectively. For applications of x-ray lasers, the saturated amplification regime is extremely important, because the effective intensity of the laser beam in this regime, for instance at 8 nm, is 10^4 times higher than that from a Planck thermal x-ray source having a radiation temperature of 150 eV [Key et. al. 1995] .

2.2 Gain formulations and methods for gain measurements

It is firstly necessary to relate the increase in intensity passing through the active medium and resulting as amplification of spontaneous emission, to a gain coefficient, and then relate this coefficient to the atomic processes in the plasma.

The macroscopic gain of the active material of the length L can be described by

$$G = e^{gL} \quad (2.1)$$

where g is the small signal gain coefficient, which is determined as the product of the stimulated emission cross section σ_{st} and the population inversion density and given by

$$g = N_u \sigma_{st} - N_l \sigma_{abs} = N_u \sigma_{st} F \quad (2.2)$$

$$\text{where } \sigma_{abs} = \frac{g_u}{g_l} \sigma_{st} \quad \text{and } F = 1 - \frac{N_l g_u}{N_u g_l} \quad (2.3)$$

F is the population inversion factor (assumed 1 for efficient pumping $N_u \gg N_l$).

N_u, N_l are the densities of the upper and lower levels correspondingly, and g_u, g_l are the upper and lower laser state statistical weights.

For the general line broadening mechanism, the stimulated emission cross-section is determined by

$$\sigma_{st} = \frac{\lambda^4 A_{ul}}{8\pi c \Delta\lambda} \quad (2.4)$$

where A_{ul} is the spontaneous transition probability, and $\Delta\lambda$ is the line width. Then the main equation for the gain coefficient will be obtained by combining this equation with Eq.(2.2)

$$g = \frac{\lambda^4 A_{ul}}{8\pi c \Delta\lambda} N_u F \quad (2.5)$$

The cross section for the Doppler broadened lines, which is the typical broadening mechanism in laser produced plasmas for the XUV wavelengths, can be estimated as

$$\sigma_{st} = \frac{\lambda^3}{8\pi} A_{ul} \left(\frac{M}{2\pi k T_i} \right)^{1/2} \quad (2.6)$$

where M is the atomic mass of the lasing ions, and T_i is the ion temperature

2. Principles of short wavelength lasers

We can show that for the 3-2 transition of C^{5+} ions at 18.2 nm, which will be considered later, $A_{32} = 5.7 \times 10^{10} \text{ s}^{-1}$ and for the typical value of $kT_e/M \approx 13$ in a high temperature plasma, $\sigma_{st} \approx 1.5 \times 10^{-15} \text{ cm}^2$. For this value of cross section the required ion density in the upper laser level should be about 10^{16} cm^{-3} for a 1 cm medium length to achieve the value of $gL \approx 15$ (see Eq. 2.1 and 2.2), and one order of magnitude more is necessary for the upper density for a length of 1 mm.

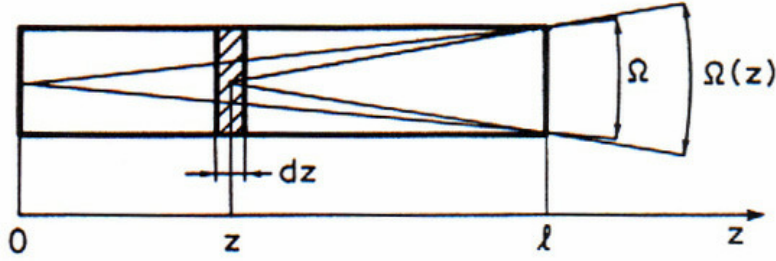


Figure 2.1 Schematic of an amplified-spontaneous emission, amplification along the z -direction.

Since in experiments only a line intensity is detected, one needs to relate this value to the gain in the medium. This can be done by analyzing the situation depicted in Fig. 2.1. The elemental increase of the spectral intensity dI_ν along the z -coordinate is given by the amplification of the incident spectral intensity and the spontaneous emission emitted into the considered solid angle $\Omega(z)$ according to the Eq. 2.7.

$$\frac{dI_\nu}{dz} = gI_\nu + N_u A_\nu h\nu \frac{\Omega(z)}{4\pi} \quad (2.7)$$

where A_ν is the spontaneous emission rate at frequency ν , N_u is the upper state population.

The solution of the eq. (2.7) by integrating over the length z from 0 to L for a Gaussian line (which is more usual due to Doppler main broadening mechanism) is given by [Svelto 1998]:

$$I_\nu = I_s \frac{\Omega}{4\pi} (e^{gL} - 1)^{3/2} (gL e^{gL})^{-1/2} \quad (2.8)$$

where $I_s = \frac{h\nu}{\sigma_{st}\tau}$ is the saturation intensity, τ is the life time of the corresponding transition.

The ASE threshold can be then defined as the situation where the ASE becomes the main mechanism of depopulating. It means, the intensity has to be comparable to the saturation intensity for a given medium. This yields to $gL \approx 10-15$. At this point the population inversion gets modified by the laser beam. A detailed description of the ASE mechanism one can find in [Svelto O. 1998].

The simplest and reliable way to determine the net gain (in the presence of a significant gain coefficient (more than 2 cm^{-1})) is to measure the increase of the output signal as a function of the lasing length. Experimentally it is usually realized by varying the length of the target, and the gain is derived by fitting the data for different lengths of the target to the above-obtained Eq. (2.8).

In case of low gain, population density inversion is often measured. Relative measurements of N_u/N_a are the most straightforward. Such measurement with known statistical weights yield directly a value for the population inversion factor F in equation (2.3). Then, the measured absolute value for the upper state density provides a value for the gain coefficient, while the cross section value is usually known.

In the optically thin plasmas for transitions having levels coupled to the ground state (o) through optical transitions, the ratio of intensities from upper and lower laser states to the ground state I_{uo}/I_{lo} provides direct evidence of population inversion through

$$\frac{N_u}{N_l} = \frac{I_{uo}}{I_{lo}} \frac{A_{lo}}{A_{uo}} \frac{h\nu_{lo}}{h\nu_{uo}} \quad (2.9)$$

where A_{lo} , A_{uo} are corresponding spontaneous emission coefficients, and $h\nu_{lo}$, $h\nu_{uo}$ corresponding energies. For resonance lines, the wavelengths for the transitions $l-o$ and $u-o$ are usually very close and, therefore, the value of measured intensities can be directly employed for the derivation of population inversion (without knowledge of spectral characteristics of the monochromator).

Another way to confirm the lasing action is comparison of the time-dependent spatial divergence of the radiation leaving the medium exit at different wavelengths. In this case, the laser line should show a distinctly smaller divergence with increasing active length and, therefore, this method can be easily checked experimentally.

2.3 Main mechanisms of pumping

2.3.1 electron collisional pumping

The electron collisional excitation scheme was one of the first explored theoretically [Zherikhin *et al* 1976] and realized experimentally [Matthews *et al* 1985]. This scheme is found to be the most robust and simply operated. Several compact, high gain, laser-pumped and discharge pumped soft x-ray amplifiers have been successfully developed based on this scheme [Rocca 1999]. This excitation mechanism resembles that of some of the most widely utilized visible and ultraviolet ion lasers, for instance, the cw-argon ion laser, in which the laser upper levels are predominantly excited by direct electron impact collision from the ground state of the ion stage of interest. Mostly the generation of a population inversion occurs in a quasi-cw regime due to the very favorable radiative lifetime ratio between the laser upper and lower levels. The upper levels are metastable with respect to radiative decay to the ground state, and the laser lower levels are depopulated by strong dipole-allowed transitions.

The first successful demonstration of lasing was done with utilizing the $2p^53p-2p^53s$ transition in Ne-like Selenium [Matthews *et al* 1985]. Ne-like ions have a fully occupied outer shell and are hard to ionize. This is a significant advantage because it allows creating a high relative abundance of the lasing ions over a wide range of plasma parameters. To date, amplification has been demonstrated in the majority of the Ne-like ions having atomic number between 14 and 47. Figure 2.2 demonstrates the principle of this type of pumping with a simplified energy level diagram for the Ne-like Selenium. Firstly, the desirable stage of ions has to be produced in the ground state, and then electron impact excitation takes place. The population inversion is maintained by the very rapid radiative decay of the $3s$ laser lower levels to the ground state through strong dipole-allowed transitions. Therefore, operation of these lasers in a quasi-cw regime requires the plasma to be optically thin for the transitions originating from the laser lower level. This imposes a restriction in the maximum plasma column diameter, which is often significantly relaxed by a Doppler shift in the lines caused by radial velocity gradients in the plasma. The pumping rate and the population inversion increase with the electron density. However, as mentioned

before, the maximum electron density at which an inversion can be maintained is limited by collisional mixing between the upper and lower laser levels. Another disadvantage of Ne-like schemes is the high degree of ionization and consequently the large pump power that is required to obtain lasing at a given wavelength.

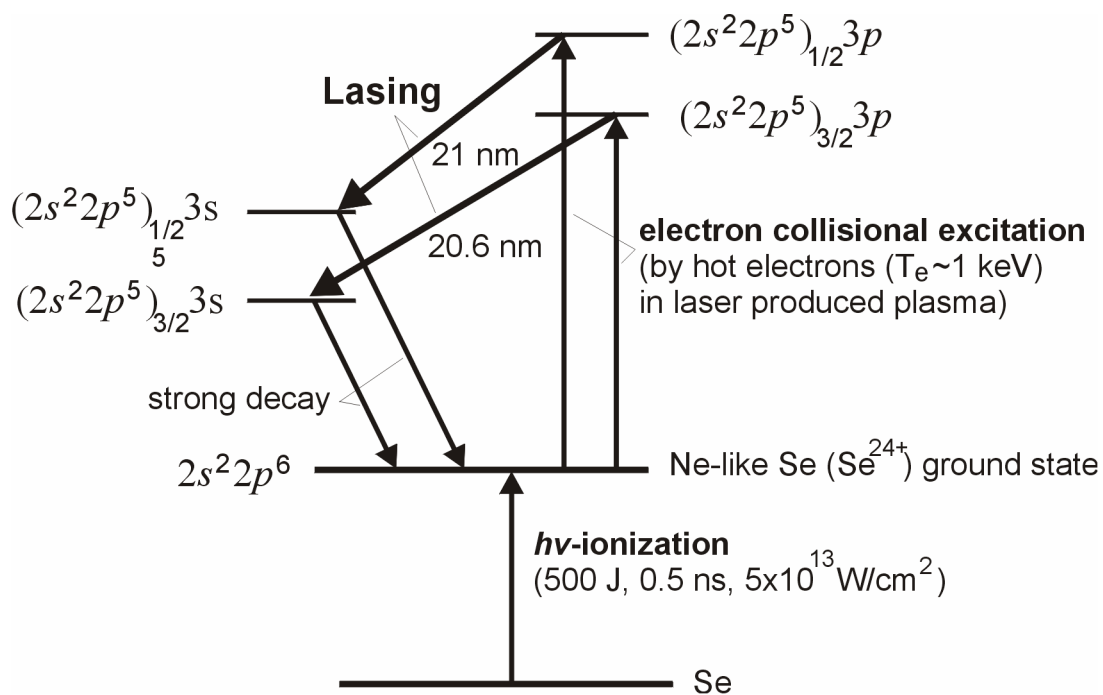


Figure 2.2 The principle of electron collisional pumping with a simplified energy level diagram for the Ne-like Selenium.

Alternatively, the Ni-like sequence has been proposed and successfully utilized to extend collisionally excited lasers to shorter wavelengths. Lasers on the $3d^9 4d-3d^9 4p$ transitions of Ni-like ions are direct analogs to lasers on $2p^5 3p-2p^5 3s$ transitions in closed shell Ne-like ions, but have the advantage of producing amplification at a shorter wavelength for a given state of ionization. This higher quantum efficiency significantly reduces the pumping energy required to achieve lasing by collisional excitation at a selected wavelength. Ni-like soft x-ray lasers were first demonstrated in 1987 in an Eu laser-created plasma [MacGowan et al 1987], producing an amplification of $g/l = 4$ at 7.1 nm. Subsequently, the scheme was isoelectronically extrapolated to a number of ions. Gain has also been observed in Co-like ions, [B. J. MacGowan et al 1990], and also the lasing in the Nd-like

sequence was proposed.[P. L. Hagelstein 1991]. The summarized results on demonstration of lasing in Ne- and Ni- like ions are given in [Daidoo 2002].

Transient electron collisional excitation

The electron impact excitation under rapid transient conditions results to provide much larger population inversions than in quasi-steady state regime. It was first recognized by Afanasiev and Shlyaptsev in 1989, that larger gain coefficients (1–2 orders of magnitude more than in quasi-steady scheme) can be produced by heating the plasma ions into excited states at a rate faster than the ionization rate. This corresponds to time duration of sub-picoseconds to tens of picoseconds.

The larger gain coefficients are a consequence of several phenomena:

- immediately following rapid collisional excitation before collisions have the time to redistribute the populations
- the upper laser level population is larger as a result of its larger rate of excitation. The rate of electron excitation in an overheated plasma is larger, since it depends exponentially on the electron temperature. Due to these differences in the pumping rates of the closely spaced lasing upper and lower levels, this method allows operation at significantly high electron densities, and therefore at increased pumping rates.

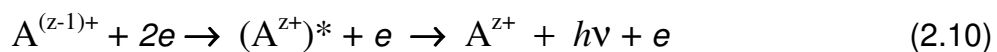
Transient gains in excess of 100 cm^{-1} have been predicted theoretically, and the first experimental demonstration was realized by Nickles P. et. al. in 1997 in the 32.6 nm $3p-3s$ line of Ne-like Ti. The experiment was performed at the Max Born Institute using the hybrid Chirped Pulse Amplification Ti-sapphire/Nd:glass pump lasers. This laser system delivers synchronized long and short laser pulses of 1.2 ns and 0.7 ps duration, respectively. A dual cylindrical lens optics system was used to line focus the two beams onto the target with a width of 30 μm over lengths of 1–5 mm. No laser pulse was detected as long as only one of both laser pulses was used. The first observation of gain was realized with short pulses of more than 2 J and long pulses of more than 3 J. The soft x-ray laser pulse was measured to have a duration of less than 20 ps. A nonlinear increase was clearly observed corresponded to an average gain of 19 cm^{-1} and to a gain-length product of 9.5. This gain coefficient is about seven times larger than that previously reported for the same line in the quasi-steady state regime when pumped by a 0.6 ns duration pulses with an energy of 200–500 J [Boehly I. T. *et al.* 1990].

The short-lived transient population inversions, which are pumped directly from the ground state by electron collisional excitation, last until collisions redistribute the populations among levels. Following this short transient period of high population inversion the gain decreases until the laser level populations finally reach the quasi-steady state value.

It should be emphasized, that in the transient electron collisional excitation scheme a population inversion is created because the transient collisional processes of excitation of the laser upper and lower level occur at different rates, and not because of the faster rate of radiative relaxation of the laser lower level. Therefore, in the transient regime there is no need to limit the transverse dimension of the plasma in order to ensure optical transparency for the lower level radiation. The transient excitation scheme has been also extended to the Ni-like sequence. For example, in [Ozaki et. al. 2002], at a pump energy only of 150 mJ a gain in the $4d-4p$ line of Ni-like Molybdenum at 18.9 nm was demonstrated.

2.3.2 recombination pumping

This pumping mechanism, sometimes referred to collisional recombination or three-body recombination, was first proposed by Gudzenko and Shelepin in 1965. This is the inverse process to electron-collisional ionization. It is assumed that the initial ions, which are one ionization stage higher than the lasing one, capture a free electron into a high bound quantum state followed by cascading downward to the lower states. This combined recombination and cascade processes are illustrated by the equation (2.10) and shown in Fig. 2.3.



The collisional recombination allows the scaling of the wavelength with the principal quantum number n (Fig. 2.3) which provides the lasing at shorter wavelengths in comparison with electron collisional excitation. The collisional recombination rate is proportional to the square of the electron density and extremely sensitive to the electron temperature. Therefore, the generation of a large population inversion by recombination requires a dense and relatively cold plasma. When the

plasma cools, collisional recombination populates highly excited states, and electron collisions rapidly transfer the population to levels of lower energy. Since collisional electron deexcitation is inversely proportional to the square root of the energy difference between the levels, this electronic cascade reaches a level at which electron de-excitation is no longer dominant over radiative decay. At this level, a population inversion is created with respect to a lower level, which is most commonly de-excited by very rapid radiative decay to the ground state of the ion. Hydrogen-like ions have a very favorable energy level structure for the generation of population inversion by collisional recombination. In principle, several transitions can be inverted, but initially much of the attention focused in the very favorable 3–2 transition of these ions. Fig. 2.3 shows, for example, the generation of population inversion in the 3–2 transition of H-like C at 18.2 nm.

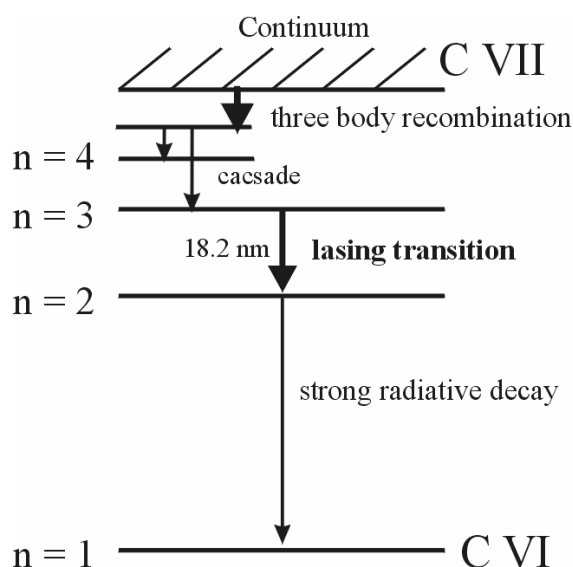


Figure 2.3 Simplified Grotrian diagram of H-like Carbon showing the processes responsible for the generation of population inversion between the $n=3$ and $n=2$ levels in the 18.2 nm C VI recombination laser.

One of the main difficulties with this type of pumping is to satisfy the conflicting plasma conditions: a very highly ionized plasma and a very cold electron temperature. In practice, the problem was traditionally solved utilizing a two-step process. First, a highly ionized and dense plasma is generated by a heating pulse. Second, the plasma is rapidly cooled following the termination of the excitation pulse.

2. Principles of short wavelength lasers

By this method, the plasma is hot during the excitation pulse, allowing for the generation of the required high population density of ions, and cold during the recombination phase. The plasma can be rapidly cooled by an adiabatic expansion, by electron heat conduction to a nearby wall or colder neighboring plasma, or by radiation from high- Z ions introduced as impurities into the plasma. All three cooling mechanisms or combinations of them have been utilized experimentally to generate gain at soft x-ray wavelengths by collisional electron–ion recombination. In particular, important efforts have been devoted to the demonstration and study of amplification in the 18.2 nm $3-2$ line of H-like Carbon [Zhang et. al. 1995]. Initial experiments for creating population inversion by recombination pumping were conducted in plasmas generated by ablating solid carbon targets or carbon fibers with high power laser pulses and cooled by adiabatic expansion. Large amplification was first observed in an experiment in which a 0.3 kJ pulse from a CO₂ laser with about 75 ns pulse width was used to generate a nearly totally ionized carbon plasma column by bombarding a carbon solid target immersed in a strong solenoidal magnetic field [Suckewer et. al. 1985]. The magnetic confinement allowed to maintain a high electron density, while the plasma was cooled by radiation and electron heat conduction to adjacent cooling blades. Laser pulses of about 3 mJ were generated at an efficiency of 10^{-5} . Amplification has also been demonstrated in numerous experiments in which line focus plasmas were cooled by free adiabatic expansion.

Gain also has been reported in the $4f-3d$ and $5f-3d$ lines of Li-like ions [Xu et. al. 1994], [Wagner et. al. 1996], and in Na-like copper ions on $5g-4d$ transition at 11.1 nm [Zhang et. al. 1996].

An important advantage of the recombination scheme with respect to the collisional excitation scheme is its more rapid scaling to shorter wavelengths with nuclear charge Z . However, recombination lasers have suffered the problem of not scaling adequately with plasma column length. This is possibly due to a very high sensitivity of the gain in recombination schemes to the variation of the plasma parameters that can be more pronounced for longer plasma columns, although this problem is not well understood yet.

2.3.3 alternative pumping mechanisms

Among other mechanisms capable of creating a population inversion, more promising are **inner shell excitation**, **resonant photoexcitation**, and **charge exchange pumping**. The latter will be analyzed in detail in the next chapter.

Duguay and Rentzepis originally proposed the generation of large population inversions following the selective x-ray photoionization of inner shell electrons in 1967. The generation of population inversions by this mechanism is possible because at photon energies just above the threshold for inner shell photoionization the cross section is an order of magnitude larger for inner-shell electrons as compared to outer-shell electrons. This process is described by



where [K,L] shows the vacancy of electron in $n=1,2$ or K -, L - shell for the ion, which has more than two shells.

This scheme has the potential advantage of leading to relatively compact lasers with wavelengths shorter than 1.5 nm. The incoherent x-ray photons that pump the laser media would be normally produced by a nearby plasma created by heating a target made of a high- Z material such as gold with an intense ultrashort laser pulse. Experiments have demonstrated total laser energy to incoherent x-ray energy with conversion efficiencies of about 20%. Photons at an energy below the inner-shell binding energy are removed with an appropriate filter to avoid pumping of the laser lower level. The photoionization scheme was demonstrated in the visible region of the spectrum by Silfvast *et. al.* in 1983. The first proposal for inner-shell photoionization lasers at short wavelengths made by [Duguay and Rentzepis 1967] has gained in importance after the development of sufficiently powerful ultrashort pulse laser drivers. However, up to date there is still a lack of lasing with this pumping mechanism in the XUV spectral range.

Resonant photopumping is based on intense line emission to pump the laser upper level. As any resonant process, this mechanism requires a precise wavelength

coincidence between powerful pump lines and lines that can populate a laser upper level by resonant photoabsorption.



The evidence of a population inversion with this type of pumping was obtained in He-like Ne by resonant photoexcitation of the $1s^2-1s4p$ transition in that ion with 1.1 nm radiation from He-like Na plasmas generated by very large pulsed power generators [Porter *et al.* 1992]. Other experiments showed as well the possibility of producing a population inversion [Ilcisin *et. al* 1994], [Qi,*et. al.* 1993], but no convincing gain product was reported.

2.4 Conclusion

Finally, it can be concluded that a demonstration of lasing in the short wavelength range was successfully made with electron collisional and recombination pumping. However, at present, the normal efficiency of the XUV lasers, pumped with short pulse driver lasers, is in the range of 10^{-8} , and with the more effective transient electron collisional excitation an efficiency of 10^{-7} was reported on the 9th X-ray laser conference by J. Dunn (2004). The summarized results on the successful demonstration of lasing for the different types of ions with electron collisional and recombination pumping are given in the table below.

Table 2.1 Summarized results of the main lasing schemes.

| Pumping mechanism | Type of ions | Lasing transition |
|----------------------|------------------|-------------------|
| Electron Collisional | <i>Ne – like</i> | $3p - 3s$ |
| | <i>Ni – like</i> | $4d - 4p$ |
| | <i>Pd-like</i> | $5d - 5p$ |
| Recombination | <i>H – like</i> | $3 - 2$ |
| | <i>Li – like</i> | $4 - 3$ |
| | | $5 - 3$ |
| | <i>Na – like</i> | $5 - 4$ |

It should be noticed, that only the electron collisional excitation mechanism was found to be robust and simply to operate, while the recombination scheme is not easily reproducible and no stable operation with recombination XUV lasers was reported.

Investigations on other promising methods of pumping (inner-shell excitation, photo-excitation, charge exchange), which are capable for producing a more efficient pumping due to a resonant character of the pumping processes and, therefore, higher values of cross-section, so far could only produce a population inversion, but no convincing demonstration of a gain was obtained.

3. Population inversion by charge transfer

A charge exchange reaction in atomic physics is one in which an electron, or several electrons, are transferred from one atomic system to another. Charge exchange was discovered by Henderson in 1923 during the course of the experiments in which α -particles were passed through the absorbing screens of mica. Numbers of singly charged He^+ ions and also neutral He atoms were observed to emerge from the far side of the screens, and these were attributed to the capture of electrons by the α -particles [Bransden and McDowell 1992].

3.1 Basics of charge exchange mechanism

The classical models for the capture of an electron have been developed by [Bohr and Lindhardt 1954], [Grozdanov 1980], Barany et. al.1986]. In the simplest theoretical model of charge exchange, it is assumed that the electrons in the target are at rest and are uniformly distributed over the surface of sphere. Cinematically, reaction requires two collisions to take place. At first the incident ion A of a velocity v_0 strikes an electron in the target B , and since an ion is much heavier than the electron, it is undeflected. On the other hand, it is possible for the electron to acquire the speed v_0 and to make a collision with the target nucleus B in such a way that it is deflected to move in the same direction as the ion A . Those electrons, which are moved with the same velocity as A and in the same direction, are considered to be captured. The detailed analysis of the classical overbarrier model will be given in the next chapter for the derivation of the charge transfer cross section.

In general, the mechanism of charge exchange is very dependant on relative velocities of colliding species v_0 : at high impact velocities $v_0 \gg v_e$ it is quite different from that at low velocities $v_0 \ll v_e$, where v_e is the electronic velocity in the first Bohr orbit of atomic hydrogen. For our experimental conditions the latter situation takes place, as the velocities of ions investigated (about 10^7 cm/s) are smaller than the electronic velocity in the first Bohr orbit of atomic hydrogen $v_e \approx 2 \times 10^8$ cm/s. The interaction time in this case is long compared with the characteristic time required for

3. Population inversion by charge transfer

an electron in the first Bohr orbit to travel the distance a_o , which is 2.4×10^{-17} s, where a_o is the first Bohr radius. At these conditions, a collision complex is formed and the transition probability for the rearrangement is high.

The important feature of this process is its quasi-resonant behavior between the binding energy of the electron in the ground state of the atom and that of the upper laser state of the ion and can be better understood by the diagram shown in Fig. 3.1. The level E_{up} , where the electron is transferred, is determined by the ionization potential of the involved component ($E_{ion}(B)$), and an energy decrement ΔE , which is typically in the range of 10-20 eV.

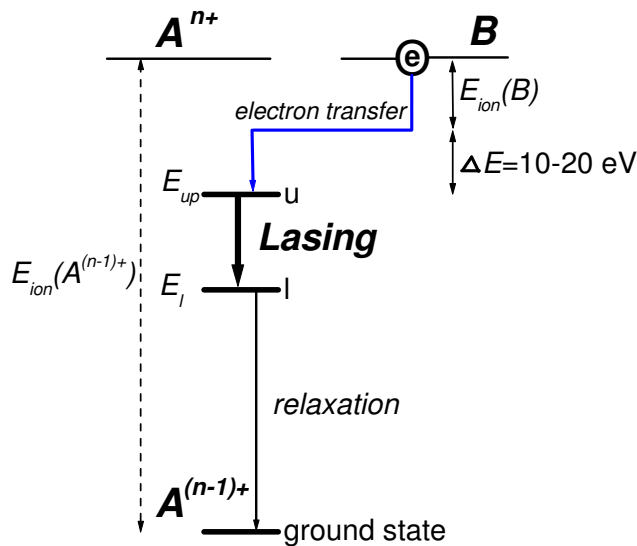


Figure 3.1 Principle of charge transfer pumping mechanism with simplified energy level diagram.

The existence of an energy decrement can be explained from the condition, that the energy ($E_{ion}(A^{(n-1)+}) - E_{up}$) must be definitely higher than ($E_{ion}(B)$) in order to capture the electron, so the reaction must be exothermic. And somewhat more precisely, theoretical calculations show that the energy decrement is usually in the range of 10-20 eV. This is also confirmed by our measurements with investigations on the Silicon ions given in Fig. 7.10 and Fig.7.11 (see chapter 7). As for any collision, one can assume that the probability of interaction is equal zero at the point where ($E_{ion}(A^{(n-1)+}) - E_{up}$) = $E_{ion}(B)$ (i.e. $\Delta E=0$), and then it is getting increased up to a point where the cross section has a maximum ($\Delta E \approx 10-20$ eV). For the larger values

3. Population inversion by charge transfer

of ΔE , the cross section is slightly, but steadily decreasing, as shown for example in Fig. 7.11 for Silicon ions (see chapter 7). In general, the processes of charge exchange interactions are more complicated and the energy decrement for a particular reaction depends not only on relative velocities of the reactants, but also on the symmetry and other properties of the involved reagents. For a detailed description see [Mapleton 1972], and [Bransden and McDowell 1992].

The mechanism of charge exchange can be in general described by the reaction below:



The equation (3.1) represents the capture of an electron by the incident ion (projectile) A with charge $n+$ from atomic target B . The outer electron goes from neutral atom B in an excited level of newly created $A^{(n-1)+}$ ion.

In terms of quantum mechanics, quantal methods must be employed to obtain approximate solutions of the Schrödinger equation for the ion-atom systems. The most attractive is the method of curve-crossing. The concept of pseudo-crossing of potential energy surfaces is utilized to construct an approximation within the framework of the two-state approximation, where the wavefunction is obtained by retaining in the trial function only the initial and final states of interest [Mapleton 1972]. Under these circumstances, the electron to be captured is shared between the two ions during the collision, forming a quasi-molecule. Considering the process of Eq. 3.1, in the absence of interaction the left- and right-hand members of this equation can be imagined to form two quasi-molecules, ΔE is the difference in binding energies of the initial and final states at infinite separation and is in an inverse relationship with a pseudo potential-curve crossing distance. Without interaction the associated potential energy curves have a cross at a critical internuclear distance R_{cr} (R_{cr} is usually about 5-10 *a.u.*). If there is an interaction, these curves usually do not cross, provided that the matrix element of the associated interaction does not vanish. In the region of pseudo-crossing R_c the difference in the two potential energies is the smallest and the capture of electron can occur. This method is adequate only at low velocities of relative motion of colliding systems. By reason of its attractive simplicity the method of curve-crossing has been applied and described extensively [Smirnov 1968].

3.2 Cross section data

Cross section determines the probability of a process involved. In our case it determines the population of the relevant laser levels pumped by charge exchange reaction, and it is therefore very important to estimate this parameter. In regard to charge exchange interaction, the cross section depends primarily on the relative velocity of colliding particles v_o , rather than the incident energy. This is why the cross sections are generally characterized as a function of energy measured in electron-volt divided by the mass of the incident particle in atomic mass units (*a.m.u.*), or as a function of relative velocity. There is the following relationship between these parameters, valid at non-relativistic energies

$$E \approx 20.8v_o^2 \text{ keV/a.m.u.} \quad (3.2)$$

1 *a.m.u.* corresponds to the mass of the proton, and v_o is expressed in atomic units ($v_o = 1 \text{ a.u.}$ corresponds to electronic velocity in the first Bohr orbit of atomic hydrogen $v_e \approx 2.1 \times 10^8 \text{ cm/s}$).

At our experimental conditions, the relative velocity is determined by the laser produced ion velocities, while the gas can be assumed as standing in the way of ions (see chapter 5). The typical velocities of investigated ions are in the range of 10^7 cm/s , which corresponds to the relative velocity of $v_o = 0.05 \text{ a.u.}$ For the Carbon projectile with the mass of 12 the energy is 624 eV. This corresponds to the case of low-energy collisions ($v_o < v_e$).

As discussed before, there are different models developed to make an estimation of charge transfer cross section. We will consider here the Classical Overbarrier Model introduced by [Ryufuku et al. 1980] and elaborated by [Chichkov et.al. 1999], since it allows to make precise calculations at low-energy collisions.

According to the model, the charge transfer corresponds to the transfer of an electron having sufficient energy to overcome the potential barrier between the projected ion and the target nucleus. Electron capture is considered to take place if two conditions are satisfied: - the release of the electron from the orbit about *B* and
- the capture of the released electron by the ion *A*.

The release condition can be derived from the following point. If Z_A and Z_B are the charges of the projectile *A* and the target *B* correspondingly, then the initial

3. Population inversion by charge transfer

energy of the electron, which is bound to B in an orbit with the principal quantum number n is given by

$$E_n = -\frac{1}{2} \frac{Z_B^2}{n^2} \quad (3.3)$$

As the nucleus A approaches the atom ($B^+ + e$), the electron gains an additional electrostatic energy $-Z_A/R$, where R is internuclear distance between A and B . The total energy of the electron before capture is

$$E_n = -\frac{1}{2} \frac{Z_B^2}{n^2} - \frac{Z_A}{R} \quad (3.4)$$

At a point at a distance x , along the internuclear line, the total potential energy acting on the electron become

$$V(x) = -\frac{Z_B}{x} - \frac{Z_A}{R-x} \quad (3.5)$$

The maximum value of this potential and its location are given by the condition

$$\frac{dV(x)}{dx} = 0 \quad (3.6)$$

with the solution $x=x_{max}$, where

$$x_{max} = \frac{R}{1 + \sqrt{Z_B/Z_A}} \quad V(x_{max}) = -\frac{1}{R} (\sqrt{Z_A} + \sqrt{Z_B})^2 \quad (3.7)$$

where $V(x_{max})$ gives the height of the potential wall.

The release condition is taken to be that the diabatic potential of the neutral B perturbed by the Coulomb potential of the projectile should be equal to the initial energy of the electron given by (3.4).

$$E(R) = -\frac{E_{ion}(B)}{2Ry} - \frac{Z_A}{R} = -\frac{1}{2} \frac{Z_B^2}{n^2} - \frac{Z_A}{R} \quad (3.8)$$

where Ry is the Rydberg energy equal to 13.6 eV.

This condition defines the crossing point of two potential curves at the internuclear distance $R=R_n$, where

$$R_n = \frac{2(Z_A - Z_B)}{Z_A^2/n^2 - E_{ion}(B)/Ry} \quad (3.9)$$

Then, the capture condition is that the energy levels $E(R)$ must lie above the potential barrier (Eq. 3.10), and note that the capture can only take place if the kinetic energy $mv_0^2/2$ of the incident ion A is more than the potential energy $(-Z_A/R)$ which binds the electron to A . The condition can be written as

3. Population inversion by charge transfer

$$E(R) > V(x_{\max}) \quad (3.10)$$

This defines the internuclear distance where the overbarrier charge transfer becomes possible

$$R \leq R_{cr} = \frac{2Ry}{E_{ion}(B)} (2\sqrt{Z_A Z_B} + Z_B) \quad (3.11)$$

The cross section strongly depends on the level n_u , in the Eq. 3.12 where the captured electron is transferred



Electron capture into level n_u occurs when $R_n \leq R_{cr}$ or

$$n_u \leq n_{cr} = \left(\frac{Ry}{E_{ion}(B)} \right)^{1/2} Z_A \left(\frac{2\sqrt{Z_A Z_B} + Z_B}{2\sqrt{Z_A Z_B} + Z_A} \right)^{1/2} \quad (3.13)$$

The classical charge transfer cross section σ_{ct} of this process can be written in terms of R_n

$$\sigma_{ct} = \frac{g_i}{g_i + g_B} \pi a_0^2 R_n^2 \approx \frac{1}{2} \pi a_0^2 R_n^2 \quad (3.14)$$

where $g_i = 2n^2$, and $g_B \sim 2n_B^2$ are the statistical weights of the corresponding ion and target states, and $a_0 \approx 0.52 \times 10^{-8}$ cm. The expression for charge transfer cross section in this model is independent on the ion kinetic energy, but this is valid only for $R < R_{cr}$, which corresponds to the low relative velocities range, this is well agreed with the experimental findings [Beijers 1992].

Now we can calculate, for example, that for the charge transfer reaction between C^{4+} ions and hydrogen, in detail investigated later in chapter 6, the capture according to the Eq. 3.13 goes into level $n_u=3$ and the cross section, calculated by the use of Eq. 3.9 and 3.14, is as high as $\sigma_{ct} \approx 2 \times 10^{-15}$ cm² which agrees very well with experimental data [Dijkkamp et. al. 1985].

It must be noticed, that recently other theoretical models for the low impact energies were developed. They are based on quantal molecular close coupling calculations which allow to provide the total and state selective electron capture cross-sections [Harel et. al. 2001]. The detailed description of the method is given in [Errea et. al. 1998]. As a result of the calculations, the authors presented the total and n -partial charge transfer cross-sections for the number of different reactions including the reactions investigated here: between C^{4+} , C^{6+} , Be^{4+} and others. These data will be presented later by considering the particular reaction.

3.3 Rate equations

The rate equation approximations are derived on the basis of a simple notion of considering a balance between the total numbers of ions undergoing the charge transfer reaction and the total numbers of photons being created.

In order to estimate the population inversion with charge transfer pumping, let us consider the lasing on 3-2 transition at 18.2 nm of hydrogen like Carbon ions. The analysis of the lasing on this transition by charge exchange has been done by [Dixon and Elton 1977], [Seely and McKnight 1977], [Elton 1990]. The simplified level diagrams for these ions are shown in Fig. 3.2.

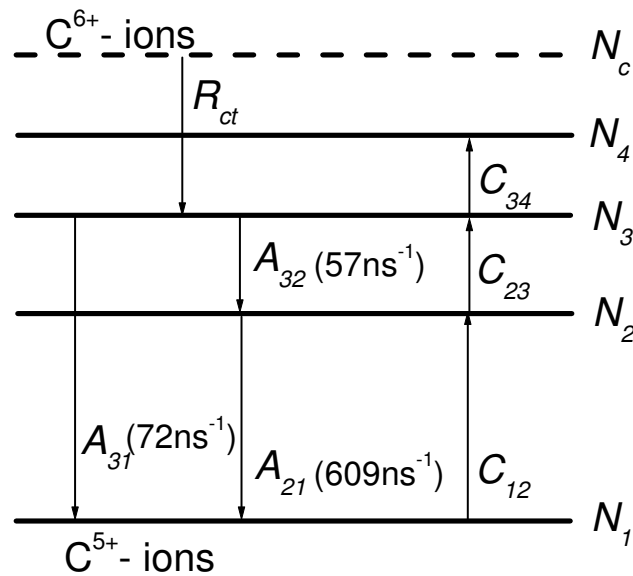


Figure 3.2 Transitions included in the rate equations for the population inversion of the levels of C^{5+} ions. R_{ct} – charge transfer pumping rate, C_{mn} – collisional excitation rates, A_{mn} – spontaneous emission rates, N_n –densities of the levels and N_c – for the density of C^{6+} ions.

Let us assume, that the upper laser state N_3 can be populated only by charge transfer excitation, while the electron-ion recombination rate is of order of 10^7s^{-1} [Irons and Peacock 1974], and is small compared to the charge exchange rate estimated below. The population of the lower excited state N_2 of C^{5+} ions is

3. Population inversion by charge transfer

determined by collisional induced upward transitions and spontaneous downward transitions. In general, the population inversion for the $n=3 \rightarrow 2$ transition is

$$\Delta N = N_3 - N_2 g_3 / g_2 \quad (3.15)$$

In steady state, the rate equations for the upper laser state N_3 and the lower laser state reduce to

$$\begin{aligned} (A_{31} + A_{32} + C_{34})N_3 &= R_{ct} N_c + C_{23}N_2 \\ (A_{21} + C_{23})N_2 &= A_{32} N_3 + C_{12}N_1 \end{aligned} \quad (3.16)$$

where all parameters A_{mn} , R_{ct} , C_{mn} , N_n are described and shown in Fig. 3.2.

With the value of $g_3/g_2 = 3/2$ for the 3-2 transition of C^{5+} ions, the steady state population inversion may be written as

$$\Delta N = \frac{(R_{ct} N_c + C_{23} N_2)(1 - 9A_{32} / 4A_{21})}{A_{31} + A_{32} + C_{34}} - \frac{9C_{12} N_1}{4A_{21}} \quad (3.17)$$

The collisional excitation rates C_{mn} can be found for the corona equilibrium regime [Griem 1964] by the formula:

$$C_{mn} = 4.5 \times 10^{-6} N_e f_{nm} \frac{1}{dE \sqrt{T_e} \exp(dE / T_e)} \quad (3.18)$$

where N_e , T_e are the electron density in cm^{-3} and temperature in eV, dE is the the energy gap in eV, and f_{nm} is the oscillator strength.

Due to the large energy gap between $n=1$ and 2 levels, C_{12} is about seven orders of magnitude smaller than A_{21} , and therefore, the last term in (3.17) can be neglected. The term $C_{23}N_2$ is negligible compared to $R_{ct}N_c$.

Using Eq. (3.17), (3.18) and spontaneous transition probabilities listed in Fig. 3.2, the population inversion is finally given by

$$\Delta N = \frac{6 \times 10^{-12} R_{ct} N_c}{1 + 1.2 \times 10^{-18} N_e T_e^{-1/2} \exp(-23.8 / T_e)} \quad (3.19)$$

where the densities are in units of cm^{-3} and electron temperature is in units of eV.

This expression depends now on the plasma parameters and the rate of charge transfer pumping R_{ct} , which will be derived in the next chapter. The final estimations of population inversion and corresponding gain will be performed in chapter 3.5.

3.4 Charge transfer pumping rate

In a charge exchange pumping process, ions with charge i and density N_i collide with the atoms with density N_a to create the excited in a specific level n ions with charge $(i-1)$ having density $N_{i-1}(n)$.

Considering an elementary collision process, where the ions with N_i and a velocity V_i stream onto the atoms (at rest), the density of ions $N_{i-1}(n)$ formed per time is given by

$$\frac{dN_{i-1}}{dt} = N_i N_a \sigma_{ct} V_i \quad (3.20)$$

where σ_{ct} is the corresponding cross section

Using the notations of the Fig. 3.2, the density of created ions $N_{i-1}(n)$ is N_3 , and $N_i = N_c$. Consequently, the rate R_{ct} in Fig. 3.2 and in Eq. (3.19) can be then given by

$$R_{ct} = N_a V_i \sigma_{ct} \quad (3.21)$$

This holds true, as long as the density of ions and neutrals are not time and space dependent and a unit interaction velocity exists.

At our experimental conditions, the laser produced plasma expands and has therefore the velocity and density distributions of ions changing with time and space. For such a situation, a more detailed analytical model of charge exchange interaction was developed in [Shakhislamov 2000]. In the general case, the equations of charge transfer interaction can be written as:

$$\frac{dn_i}{dt} = -n_i n_a \sigma_i V_i + n_{i+1} n_a \sigma_{i+1} V_{i+1} \quad (3.22)$$

$$\frac{dn_a}{dt} = -n_a \sum_i n_i \sigma_i V_i$$

where n_i and n_a are densities of ions and atoms, V_i - velocity of ions, i - index for ions of charge $Z=i$. They must be completed by the equations of continuity and motion. The time of radiative decay of newly created excited ions is usually much smaller than the inverse rate of charge-transfer $\tau_{ct} = (n_a \sigma_i V_i)^{-1}$ or hydrodynamic time of ions flow. For example, for the charge exchange interaction between C^{4+} ions and hydrogen [Errea et. al. 2000], at usual velocity of ions $V \approx 10^7 \text{ cm/s}$ and required neutral densities in the range of $n_a = 10^{16} \text{ cm}^{-3}$ the ratio of charge exchange and radiative time

3. Population inversion by charge transfer

for C^{3+} ions is $\frac{\tau_{rad}}{\tau_{ct}} \approx 0.01$. Because of this consideration the population of excited

ions in the equations can be neglected. In the most simplified case, only one sort of desirable ions (for example, C^{4+}) can be considered, and all scatterings and decelerations can be neglected, since $V=const$. Then, the equations become:

$$\frac{dn_i}{dt} = \frac{dn_a}{dt} = -n_i n_a \sigma_i V_i \quad (3.23)$$

$$J = n_i n_a \sigma_i V_i$$

where the charge-transfer pumping rate is designated now as J . The equation (3.23) has been analyzed by [Ponomarenko et. al. 1998] and in the case of planar flow of ions, the density distributions are given by

$$n_a = n_a^o \cdot \left(1 + e^{-N_a \sigma_i} \cdot (e^{N_i \sigma_i} - 1)\right)^{-1} \quad (3.24)$$

$$n_i = \frac{dN_i^*}{V_i \cdot dt} = n_i^o \cdot \left(1 + e^{-N_i \sigma_i} \cdot (e^{N_a \sigma_i} - 1)\right)^{-1}$$

where $N_a = \int_0^R n_a^o dR$ is a total number of neutrals along the path of ions up to

the point of observation R , $N_i = \int_0^t n_i^o(R, t) V_i dt$ - a total number of ions flown through

the unit square at the point of observation up to the moment of observation t ; $n_i^o V_i$, n_a^o - ion flow and neutral density taken without interaction.

The exact solution is then given by:

$$J(R, t) = n_i^o(R, t) V_i n_a^o(R) \sigma_i k \quad (3.25)$$

$$\text{where } k = \frac{e^{-N_i \sigma_i + N_a \sigma_i}}{\left[1 + e^{-N_i \sigma_i} (e^{N_a \sigma_i} - 1)\right]^2} \quad (3.26)$$

These final expression for the charge transfer pumping rate $J(R, t)$ will be further applied in chapter 6.2 in order to model the time behaviour of charge transfer induced lines and to compare it with the experimental measurements. These data will allow to obtain the quantitative parameters of charge transfer interaction.

3.5 Estimations of gain with charge transfer excitation

Recall, that the gain coefficient defined in chapter 2 can be stated as

$$g = N_u \sigma_{st} - N_l \sigma_{abs} \quad (3.27)$$

and for the $\sigma_{abs} = \sigma_{st} g_u/g_l$

$$g = \Delta N \sigma_{ct} \quad (3.28)$$

where ΔN can be derived from the Eq. (3.17)

Let us consider again the lasing on the 3-2 transition of hydrogen like Carbon ions at 18.2 nm, for which the population inversion ΔN is determined by the Eq. 3.19.

The charge transfer pumping rate R_{ct} can be estimated with the use of the Eq. 3.21. For the typical velocity of laser produced C^{6+} ions of 3×10^7 cm/s and charge transfer cross section of 0.5×10^{-15} cm², which can be derived from the (3.14) and (3.9) for the hydrogen gas reagent, the pumping rate can be approximated by

$$R_{ct} \approx 1.5 \times 10^{-8} \text{ 1/s} \quad (3.29)$$

Then the final expression for ΔN can be written as

$$\Delta N = \frac{10^{-19} N_c N_a}{1 + 1.2 \times 10^{-18} N_e T_e^{-1/2} \exp(-23.8/T_e)} \quad (3.30)$$

The plasmas, produced by femtosecond laser ablation of solid targets are assumed to be as very dense and cold. The typical density of electrons is in the range of $N_e \sim 10^{22} - 10^{23}$ cm⁻³, and temperature $T_e \sim 150$ eV [Goldstein et. al. 1993], [Theobald et. al. 1999]. Taking into account that for the ideal spherical expansion the plasma density decreases with distance d as $N_e \sim d^{-3}$ and the temperature scales as $T_e \sim d^{-2}$, one can calculate that for the distance $d=1$ mm from the target $N_e \sim 10^{19}$ cm⁻³, and temperature $T_e \sim 1.5$ eV. For these values of the parameters the denominator $[1.2 \times 10^{-18} N_e T_e^{-1/2} \exp(-23.8/T_e)]$ in the Eq. (3.30) is much smaller than 1, and therefore this equation can be further simplified by

$$\Delta N = 10^{-19} N_c N_a \quad (3.31)$$

3. Population inversion by charge transfer

By combining of the Eqs. (3.28) and (3.31), one can obtain the condition for the required ion and neutral densities N_c and N_a . Assuming gain length product $gL \sim 10$ with a 1 cm length, this condition becomes

$$gL = 10 = \Delta N \sigma_{st} L = 10^{-19} N_a N_c \sigma_{st} \approx 10^{-34} N_a N_c \quad (3.32)$$

Here we used the $\sigma_{ct} \sim 10^{15} \text{ cm}^2$ obtained for this transition in the chapter 2 (2.6). Since for the effective charge exchange interaction the densities of the involved components should be equal, we can write $N_a = N_c$ and, then the required ion density for the achievement of $gL \sim 10$ is

$$N_c = \sqrt{10^{35}} \approx 3 \times 10^{17} \text{ cm}^{-3}$$

According to these estimations, one can conclude that a gain-length-product $gL \sim 10$ on the $3d-2p$ transitions at 18.2 nm of C^{5+} ions can be achieved with charge transfer pumping in quasi-steady state if the ion density of C^{6+} ions is $\sim 3 \times 10^{17} \text{ cm}^{-3}$.

However, assuming that charge transfer reaction pumps directly and selectively an upper laser level and a lower laser level is usually unoccupied, we can consider, that all ions, undergoing charge transfer reaction, will be involved in the producing of gain. Based on this, one can apply the formula (2.2) for an estimation of gain by assuming that population inversion factor $F=1$, then the required value of $gL \sim 10$ can be achieved for the density of ions found from the condition

$$gL = N_u \sigma_{st} FL = 10 \quad (3.33)$$

This shows that for the lasing on $3-2$ transition described above, the ion density of C^{6+} ions, which are undergone charge transfer reaction, in the range of 10^{16} cm^{-3} is sufficient.

It should be noticed that the lasing at shorter wavelengths as compared for example with here analyzed lasing at 18.2 nm requires usually higher ion densities, while for the longer wavelengths the lower ion densities are sufficient for achieving gain.

4. Status of experimental investigations on charge transfer pumping

Charge-exchange pumping of highly charged ions in a laser-produced plasma interacting with a neutral gas was proposed as a source of XUV radiation for the first time in 1973 [Vinogradov and Sobelman 1973]. Straightforward estimates predicted that a lasing effect could be achieved in the wavelength range down to ~ 10 nm. Although many investigations have been performed, which showed the selective charge exchange excitation of desired levels, no realization of charge exchange pumping at required densities of 10^{16} - 10^{17} cm^{-3} and appropriate geometries for lasing experiments and with sharp boundaries of involved components has been achieved.

4.1 Typical scenarios of charge exchange interaction

First experimental attempts for the realization of charge-exchange pumping were done by [Dixon and Elton 1977], [Dixon, Seely and Elton 1978] in experiments with laser-produced carbon plasmas expanding into a background gas as depicted in Fig. 4.1a. They observed a population inversion of C^{5+} and C^{4+} , as a result of reactions $\text{C}^0 + \text{C}^{5+,6+} \rightarrow \text{C}^+ + (\text{C}^{4+,5+})^* + \Delta E$, where ΔE is the difference in binding energies of the initial and final states at infinite separation. The levels of preferential population were in agreement with those predicted by charge-transfer mechanisms. Nevertheless, the observed population inversion was independent on the gas type and the gas pressure in the range of most interesting particle densities (10^{16} - 10^{17} cm^{-3}). An explanation provided by the authors was that this population inversion appears due to charge-transfer processes in ion collisions with neutral atoms existing in the same expanding plasma. The role of the background gas was only to stop plasma expansion and to produce a mixing of neutral and ionic plasma components at 10–15 mm distance from the target surface. As a result, the charge exchange pumping was realized only at the ion densities of 10^{13} - 10^{14} cm^{-3} and the efficiency of this process was very low, not more than 10^{-3} of the maximum possible value for the given ion and neutral densities. The reasons of such low efficiency were clarified in further

4. Status of experimental investigations on charge exchange

experiments and numerical simulations discussed in detail in [Ponomarenko A.G et. al. 1998]. When nanosecond laser pulses with energy of a few joules are used to produce a plasma, the plasma radiation and hot electrons can ionize the background gas in a region of up to several millimeters from the target surface. At densities of the surrounding pre-ionized gas larger than $\sim 10^{16} \text{ cm}^{-3}$, plasma expansion generates a shock wave that further ionizes gas particles. As a result, gas is ionized before it comes into contact with highly-charged ions and a mixing between them and neutral gas particles is entirely prevented.

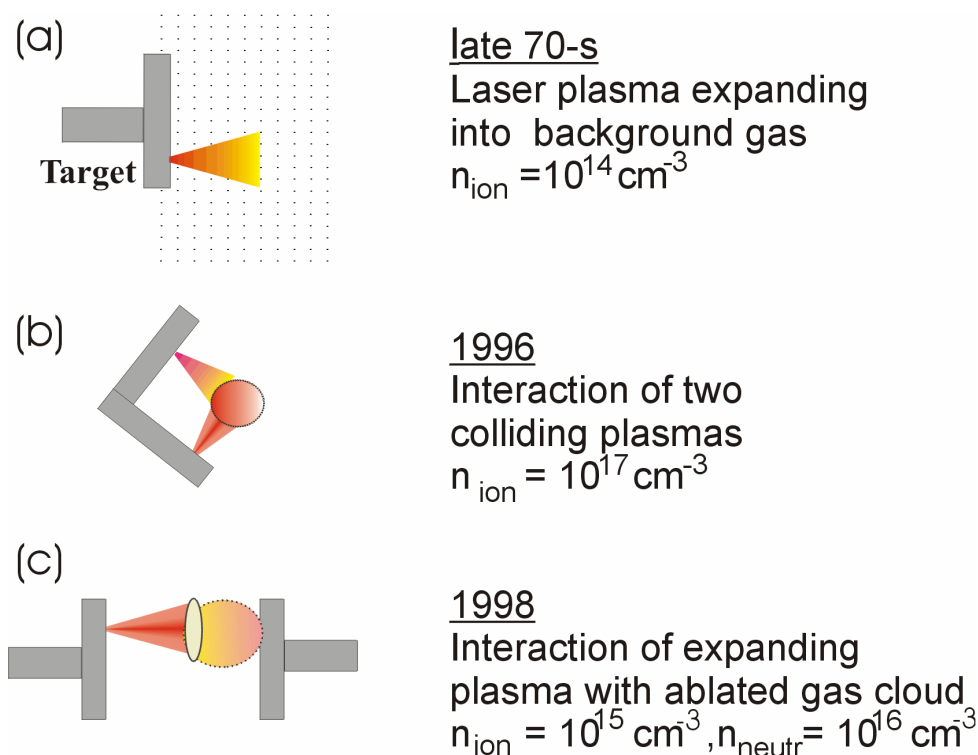


Figure 4.1 Typical experimental scenarios of investigations on charge exchange pumping aimed for realization of XUV lasers.

To achieve sufficient intermixing of different ion species which are initially separated, several other schemes were proposed and investigated. An ion-ion charge-exchange process was also suggested in [Seely and McKnight 1977], since for some reactions the Landau-Zener model predicts relatively large charge-transfer cross-sections of the order of 10^{-15} cm^2 . In experiments with hot and cold colliding plasmas (Fig. 4.1b) [Ruhl et. al. 1997], an increase in intensity of the $\text{C}^{5+} (3d-2p)$ line

4. Status of experimental investigations on charge exchange

at $\lambda=18.2$ nm was reported and explained as an effect of the reaction $C^{6+} + C^{2+} \rightarrow C^{5+} (n=3) + C^{3+}$. The densities of involved particles were in the range of 10^{17} cm^{-3} , but due to difficulties to control parameters in the interaction region, no improvement has been reached in further experiments with colliding plasmas. In [Chichkov et. al. 1999] OFI ionization of gas-cluster mixtures, which should result in two component plasmas with ion-ion charge-exchange, was proposed but not tested so far.

In [Ponomarenko et. al. 1998] a compact gas cloud created by laser ablation was used instead of a uniform gas atmosphere [Fig. 4.1c]. A sharp density gradient of the gas cloud and a controllable gap between the plasma target and the gas front has allowed to realize efficient and direct charge-exchange interaction at densities of neutrals $>10^{16} \text{ cm}^{-3}$ and of ions at about 10^{15} cm^{-3} . However, in this approach a further increase of the ion density in the interaction region, which is required for XUV lasing, seems problematic since it is difficult to position the ablation gas cloud close enough to the plasma target.

4.2 Interaction of high Z-ions with a solid easily evaporated obstacle

Another interesting experimental scenario for the realization of charge exchange excitation could be the setting of easily evaporated material in a way of high Z-ions produced by laser ablation of solid targets. Such a material could be bombarded by fast ions and produce an evaporated gas cloud near the material surface. This would allow to provide localized neutrals, which could further interact with high Z-ions. Successful confirmation of this approach was done by detecting a signal of $4f-3d$ transition at 52.1 nm of O^{5+} ions as a result of reaction $O^{6+} + H \rightarrow O^{5+}(n=4) + H^+$ [Shaikhislamov et. al. 2001], which will be further discussed in some more detail.

This experimental approach is depicted in Fig. 4.2, where the radiation emitted from the region near the obstacle was imaged by a platinum coated concave grating on a set of vacuum photodiodes. The spectral analyses were made in the mode of a spectroheliograph. The experiments were done with aluminum oxide target, in order to investigate the charge transfer interaction between O VII ions and hydrogen atoms. The gain on $4f-3d$ and $4d-3p$ transitions at 52.1 nm of O VI ions has been

4. Status of experimental investigations on charge exchange

already demonstrated by recombination pumping [Wagner et. al. 1996], and therefore the $O^{6+} + H \rightarrow O^{5+}(n=4) + H^+$ reaction, which allows to populate the level $n=4$ selectively (Fig. 4.3), is of special interest for the realization XUV-lasers by pumping with another excitation mechanism.

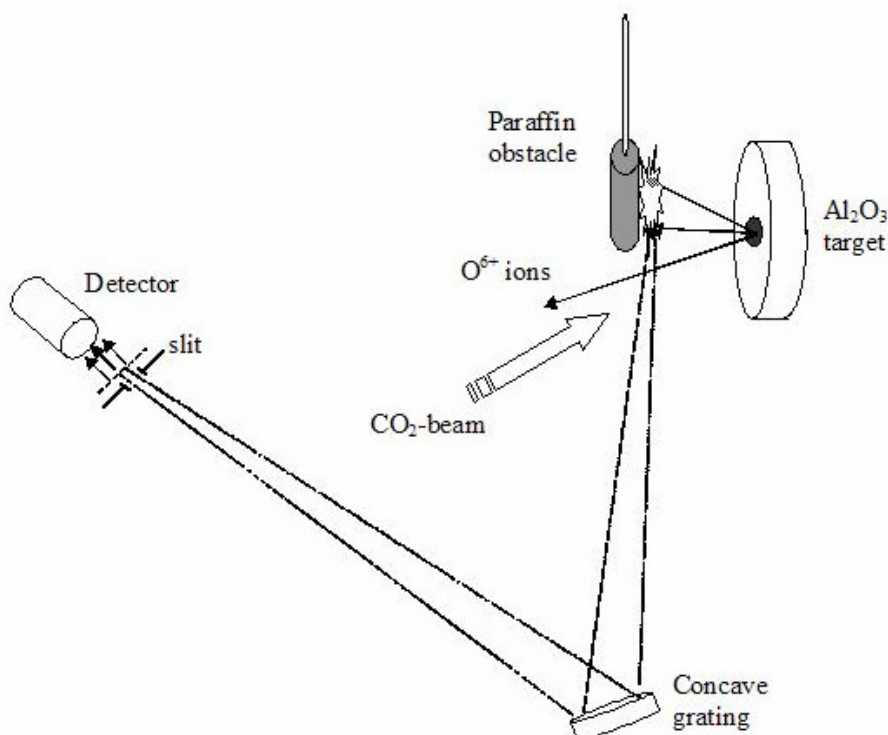


Figure 4.2 The scheme of experiment with oxygen plasma and paraffin obstacle to excite charge-transfer interaction.

The specifics of excitation of O^{5+} ions in the charge-transfer interaction $O^{6+} + H_2$ was studied in laser-produced plasmas expanded into uniform gas atmosphere by spectroscopic observation of main transitions of O^{5+} ions at specified conditions [Shaikhislamov I.F. 2001]. It was deduced that the luminosity of lines from the $n=4$ levels was induced solely by charge transfer, and, that their relative intensities show the sublevel distribution of charge transfer pumping. It should be mentioned that population of $4f$ sublevel is bound with the population of $3d$ sublevel by direct $4f-3d$ transition. Taking it into account, it was calculated that the charge transfer excitation

4. Status of experimental investigations on charge exchange

of O^{5+} ions in this reaction is distributed over sublevels for the distance 9 mm from the target in the following proportion: 4s – 11%, 4p – 28%, 4d – 36%, 4f – 25% as demonstrated in Fig. 4.4. There is also a tendency of populating the higher sublevels (4d, 4f) by moving closer to the targets, which makes better conditions for the 4f-3d lasing transition.

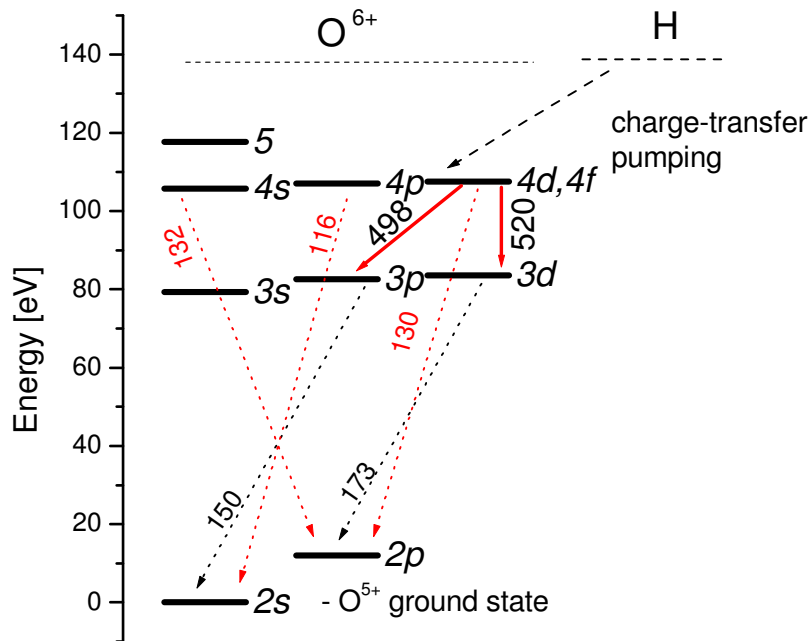


Figure 4.3 The simplified level diagram of O^{5+} ions (wavelengths are in Angstroms)

To realize proposed lasing experiment it is necessary to produce a sufficiently large amount of O^{6+} ions. They should be in the front of plasma so that other ionic components couldn't interfere with the interaction between O^{6+} ions and gas cloud. In the first preliminary experiment a flat Al_2O_3 target was irradiated by CO_2 -laser beam with total energy 100 J and 100 ns duration. A chosen focal spot with $d \approx 3$ mm corresponded to the intensity on the target surface ~ 10 GW/cm² which was estimated to be most suitable for the maximum output of O^{6+} ions. Plasma ion composition was determined by spectral measurements of visible lines of corresponding ions. For a good time resolution a photomultiplier with oscilloscope recording was placed at the exit plane of the spectrometer. The light was focused by an optical mirror and lens ($f=40$ cm), and the image of the entrance slit of the spectrometer in the interaction

4. Status of experimental investigations on charge exchange

region had a size of $0.1 \times 0.5 \text{ cm}^2$ and was aligned in parallel to the surface of plasma target and perpendicular to the axis of the gas target. The whole system from the mirror to the oscilloscope was calibrated for absolute measurements in the visible range. The measurements showed that the different ionic components were separated in space, and the O^{6+} ions are in the forefront of the plasma.

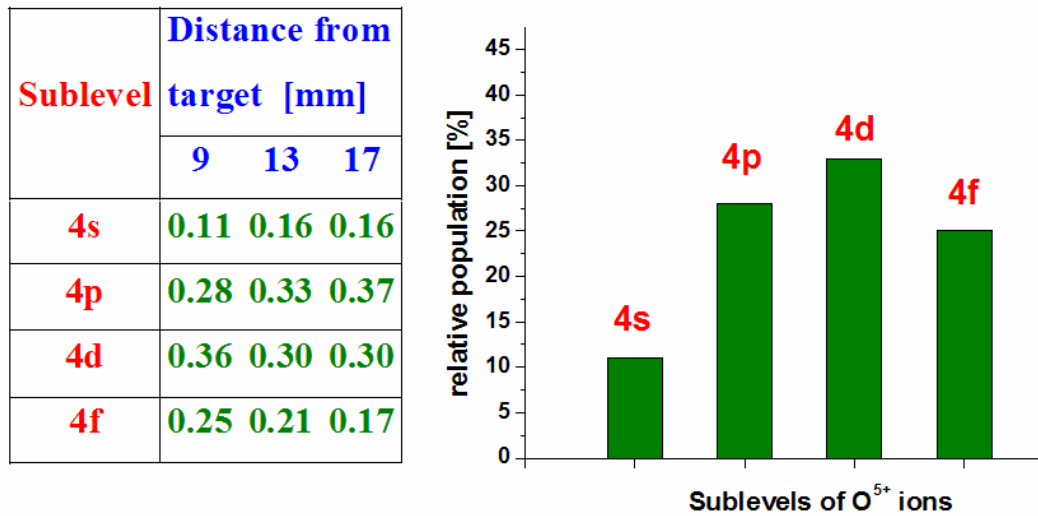


Figure 4.4 The relative population of sublevels ($n=4$) of O^{5+} ions pumped by charge transfer measured in experiments with laser plasmas expanding in background gas.

In fig. 4.5 time of flight diagrams deduced from measurements at various distances from the target are presented. The spectral measurements showed that generated plasma plume contained at its front a considerable fraction of O^{6+} ions with a total number of about 10^{16} cm^{-3} . The amount of ions with greater charge is very small due to the large ionization potential of helium-like O^{6+} ions, and one can see that the ions with smaller charges move slower and fly well behind of the O^{6+} ions.

4. Status of experimental investigations on charge exchange

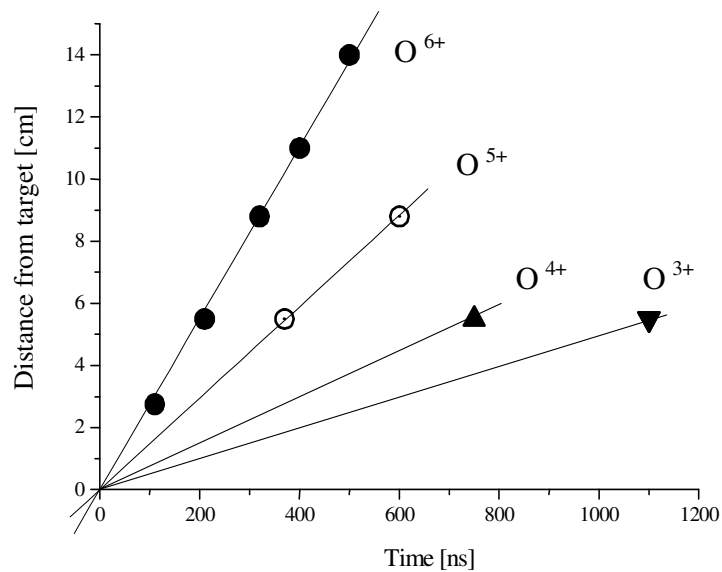


Figure 4.5 Time-of-flight diagrams of oxygen ions.

Having the desirable O^{6+} ions in the front of plasma, an obstacle made of paraffin in the form of a cylinder with $d=1$ cm was inserted on their way at the distance 3 cm from the plasma target in order to excite intensive and localized charge-transfer interaction. It was supposed that, being easily vaporized, paraffin emits neutral atoms due to the intense radiation coming from the plasma focus and due to the bombarding by fast ions.

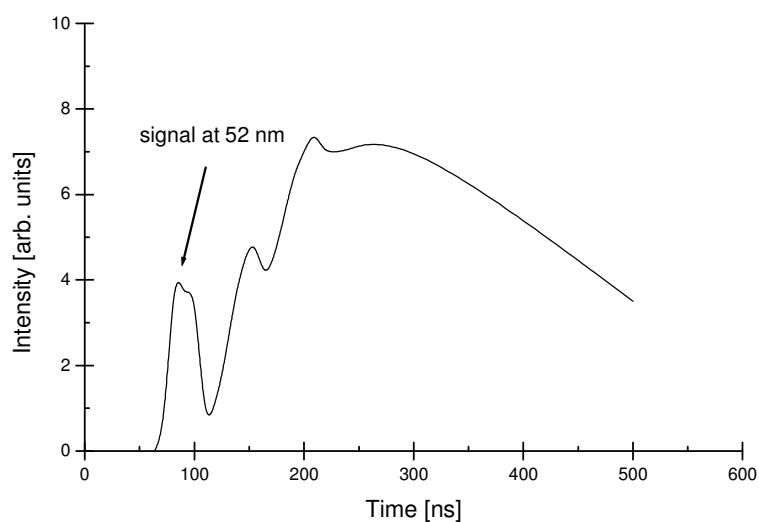


Figure 4.6 Luminosity of plasma at 52 nm. First narrow pick coincides with the time of flight of O^{6+} ions over paraffin target.

4. Status of experimental investigations on charge exchange

In the spectral range 50 ± 5 nm a specific signal against a background radiation was detected as shown in fig. 4.6. This signal was absent in the adjacent spectral ranges and when the obstacle was removed. By assumption that all O^{6+} ions are converted to excited O^{5+} ions and emit photons at 52 nm, the amplitude of the signal (pointed out by arrow) was consistent with the estimation that all O^{6+} shadowed by the obstacle undergo charge transfer reaction.

4.3 Conclusion

So far, the experimental attempts for creation of the lasers in the extreme ultraviolet spectral region with charge exchange excitation were able to demonstrate only the selective pumping of desired levels, and establish this pumping mechanism over recombination and other collisional interactions in plasmas. The pure charge exchange interaction was realized at the ion densities of the order of 10^{14} cm^{-3} [Dixon and Elton 1977], [Ponomarenko et. al. 1998], but at such low ion densities the charge transfer pumping rate is also very low, which made the approaches useless for the realization of XUV lasers. In experiments with hot and cold colliding plasmas [Ruhl et. al. 1997] the charge exchange interaction was realized at the densities of 10^{17} cm^{-3} , but due to a smoothed interaction region (Fig. 4.1b) and difficulties to control parameters of the interacting plasmas, no improvement has been reached in further experiments with colliding plasmas.

There is still no convincing results on the realization of pure charge exchange pumping at required densities of 10^{16} - 10^{17} cm^{-3} and appropriate geometries, and no gain with this type of pumping was demonstrated.

5. Novel experimental setup (charge-transfer reactions between fs-laser produced ions and neutrals from a gas jet)

Taking into account the difficulties with the realization of pure charge exchange interaction at desirable geometries and particle densities as outlined in the previous chapters and described in [Dixon and Elton 1977], [Ruhl F. et. al. 1997], [Ponomarenko et. al. 1998], one could think how the obstacles could be removed. According to an analytical model of charge-exchange interaction of dense interpenetrating flows developed in [Shaikhislamov I.F. 2000], for having an efficient charge-transfer pumping at relatively high densities of reagents, it is crucial to have a compact gas region as well as a well-localized plasma jet with sharp ion density gradient. At desired particle densities ($>10^{16} \text{ cm}^{-3}$), the characteristic length of charge exchange, which determines the interpenetration of ions into a gas medium, is less than 1 mm. Thus, effective pumping can only be realized on a spatial scale of the order of 1 mm or less, and the widths of the plasma and gas fronts should be correspondingly small.

Because of the difficulty to control the front of the ablation plasma, the only way to ensure the front sharpness is to use ultrashort laser pulses for the generation of the plasma and to realize a gas-plasma interaction as close to the plasma target as possible. The potential advantages of high contrast ultrashort laser pulses for charge-exchange pumping experiments are clear: (1) ionizing radiation from the focal spot is considerably less due to a higher electron density, (2) a low-density pre-plasma, that may prematurely effect the gas, is absent, and (3) the density gradient of the produced ion flow is sharper. From the other side, a pulsed gas jet can be applied to provide neutrals for the charge transfer interaction [Vorontsov et. al. 2003]. Compared to filling the vacuum chamber with background gas, this setup is much more suitable for XUV studies because it removes the problem of XUV-radiation absorption. Pulsed nozzles have the advantage of simple operation and variability of such important parameters as pressure, sort of gas and, especially, jet position and orientation relative to the target.

5.1 Experimental arrangement and diagnostics

This experimental scenario, consisting of a pulsed gas jet interacting with a plasma produced by ultrashort laser pulses, should allow to achieve a well-defined gas and plasma interaction zone and realize charge-exchange pumping near the target surface, where the ion density is large enough, which is important for XUV lasing experiments.

In Fig. 5.1, the basic experimental arrangement is shown. The plasma is produced by focusing of 250 fs Ti:sapphire laser pulses on a flat rotating target with a $f=250$ mm lens. The angle of incidence is normal to the target surface and the size of the focal spot is ~ 250 μm . Laser pulses with an energy of up to 70 mJ are used, corresponding to an intensity of 7×10^{14} W/cm^2 at the focal spot. XUV radiation of the produced plasma is analyzed by a single shot spectrometer (McPherson instrument 248/310G with a spectral resolution of 0.2 nm) equipped with a MCP-phosphor-CCD time-integrating detection unit. To obtain a spatial resolution in the direction normal to the target, a 200 μm slit is placed at a 2 cm distance from the focal spot (fig. 5.1). The entrance slit of the spectrometer was correspondingly aligned. In between, a further slit was introduced for protection of the instrument against plasma debris and gas particles and for better differential pumping.

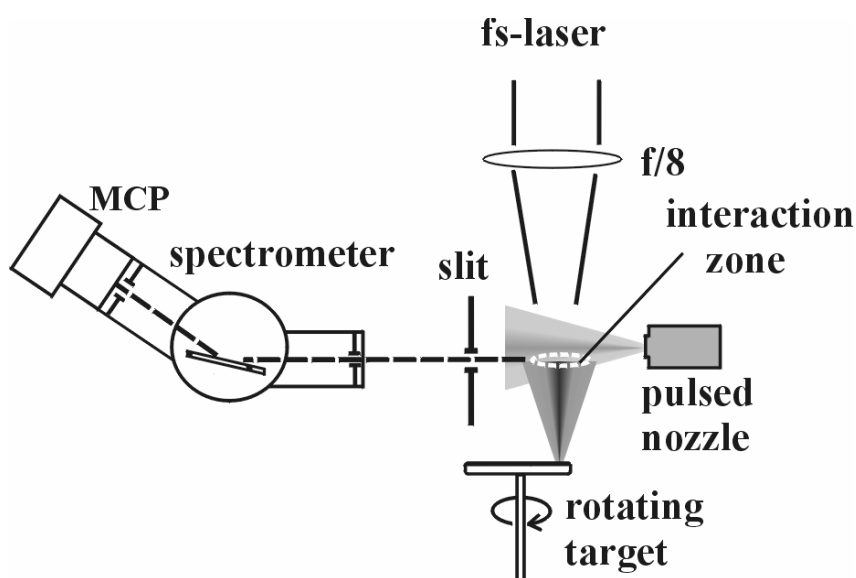


Figure 5.1 Experimental set-up.

The gas is injected into the vacuum chamber (evacuated to below 10^{-4} mbar) by a pulsed nozzle (General Valve Corporation) located close to the target surface near the focal spot. The pulsed nozzle has an opening time of about 1 ms and is operated at a backing pressures p of up to 3 bar. In most measurements the nozzle axis coincides with the optical axis defined by the slits. The position of the focal spot on the target surface relative to the nozzle opening (diameter 1 mm) can be easily varied by moving the target along its normal. The particle density n at the nozzle exit is determined from interferometric measurements and can be approximated by the following relationship

$$n (\text{cm}^{-3}) = 7 \times 10^{17} \times p (\text{bar}) \quad (5.1)$$

where p – is the backing pressure.

The gas-jet geometry was investigated by using laser pulses tightly focused into different regions of the gas jet and by observing the plasma emission. In these measurements a 90° spread of the gas-jet was established. Ti:sapphire laser and pulsed valve are operated at 10 Hz repetition rate. Single shot spectra are recorded in the spectral range of 10–50 nm. Since fluctuations from shot to shot of about 30% are observed, results presented below are averaged over ~100 shots.

In order to perform time resolved measurements to see the different nature of charge transfer pumping, a Jobin Yvon monochromator with fast MCP (micro-channel-plate) and oscilloscope instead of McPherson spectrometer was applied. In these measurements the time resolution was limited by both the oscilloscope and MCP and was about 1 ns, and the spatial resolution, which was determined by the same slit, shown in Fig. 5.1, was about 250 μm .

5.2 Ti:Sapphire laser system

Over the past decade, there has been rapid progress in the development of compact, very high power ultrafast optical lasers based on the technique of chirped-pulse amplification (CPA). Such short pulse high peak power lasers have led to reductions in the laser pump energy required for producing desirable high Z-ions for lasing experiments. In the CPA technique, a short seed pulse is first stretched in duration, then amplified, and finally recompressed to ideally its initial duration. The process allows us to obtain extremely high peak powers by the amplification of ultrashort pulses, while avoiding very high intensities in the amplification pulse that would damage the amplifiers. In this chapter, the femtosecond laser system used in our experiments will be briefly described. A general description of the CPA technique can be found elsewhere [Maine 1988], [Yamakawa et. al. 1994]. The detailed description of the Ti:Sapphire laser system applied in present experiments as well as the description all of the elements involved one can find in [Koch 2003].

5.2.1 Description of the system

The Ti:Sapphire laser system (Alpha 10/CS-3TW, Thales, France) used in our experiments can be characterized as a system operated at 10 Hz and delivering the pulses as short as 100 fs with fluent adjustment up to 3 ps and a maximum energy of 400 mJ. The diameter of the output radiation is 5 cm. The system is based on CPA mechanism that principle is illustrated in Fig. 5.2.

The short pulses from the MIRA 900- oscillator (Coherent) with the repetition rate of 76 MHz, energy of 10 nJ and pulse duration of 70 fs are initially chirped and stretched to 250 ps. At the same time the repetition rate of the laser pulses is reduced to 10 Hz with the help of a pulse-picker. The stretcher in its original design, consists of a pair of diffraction gratings in an antiparallel configuration. A laser pulse comprises many frequencies, according to its Fourier transform. By coming into a diffraction grating, the pulse spreads out in angle, each frequency component leaving at a slightly different dispersed angle. In travelling between two such gratings,

different frequencies take different paths, and the total distances of the different paths through this diffraction-grating system are not the same. Thus, at the output of the grating expander the frequency components arrive at staggered times, ordered by their frequencies. The result is a temporally stretched-out pulse of steadily rising frequency -- a positively chirped pulse. The chirped pulse amplification laser therefore dissects a laser according to its frequency components, and reorders it into a time-stretched lower-peak-intensity pulse of the same energy. These "long" pulses can then be amplified safely to high energy. There is one regenerative and two multi-pass amplifiers applied in our experiments. The amplifiers are optically pumped with a Q-switched frequency-doubled Nd:YAG lasers, as demonstrated in Fig. 5.3, where all parameters of the lasers are given as well. The radiation amplified with the use all of the three amplifiers is well in excess of 900 mJ with 790 nm central wavelength. Finally, the pulse is recompressed close to its original pulse width by a pair of identical parallel gratings that provide a negative group delay dispersion.

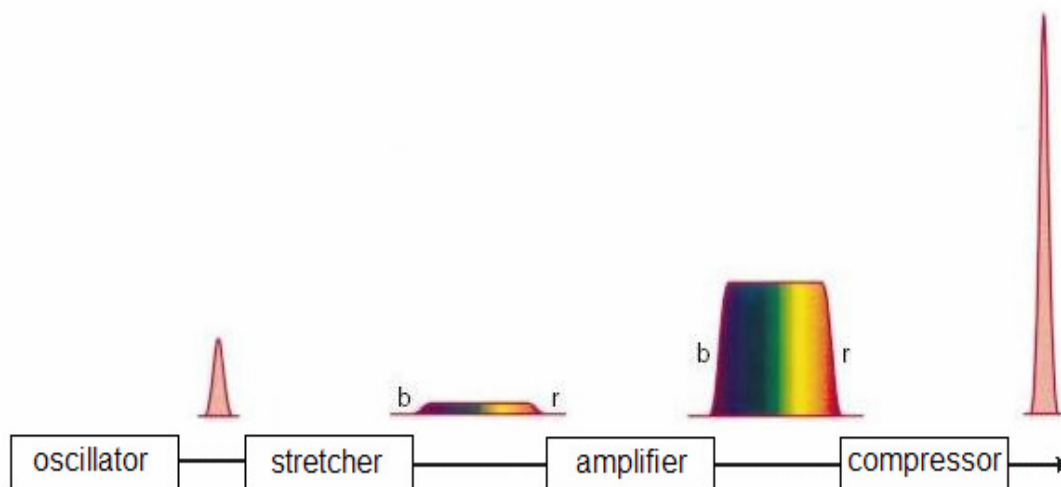


Figure 5.2 Diagram showing the principle of CPA. The oscillator output is stretched in the grating stretcher such that the red frequency components (r) travel ahead of the blue (b). The peak intensity is reduced in the process. The stretched pulse is then amplified in a regenerative and/or multipass amplifier before recompression in a grating-pair compressor.

Titan:Saphir-Hochleistungs-Lasersystem

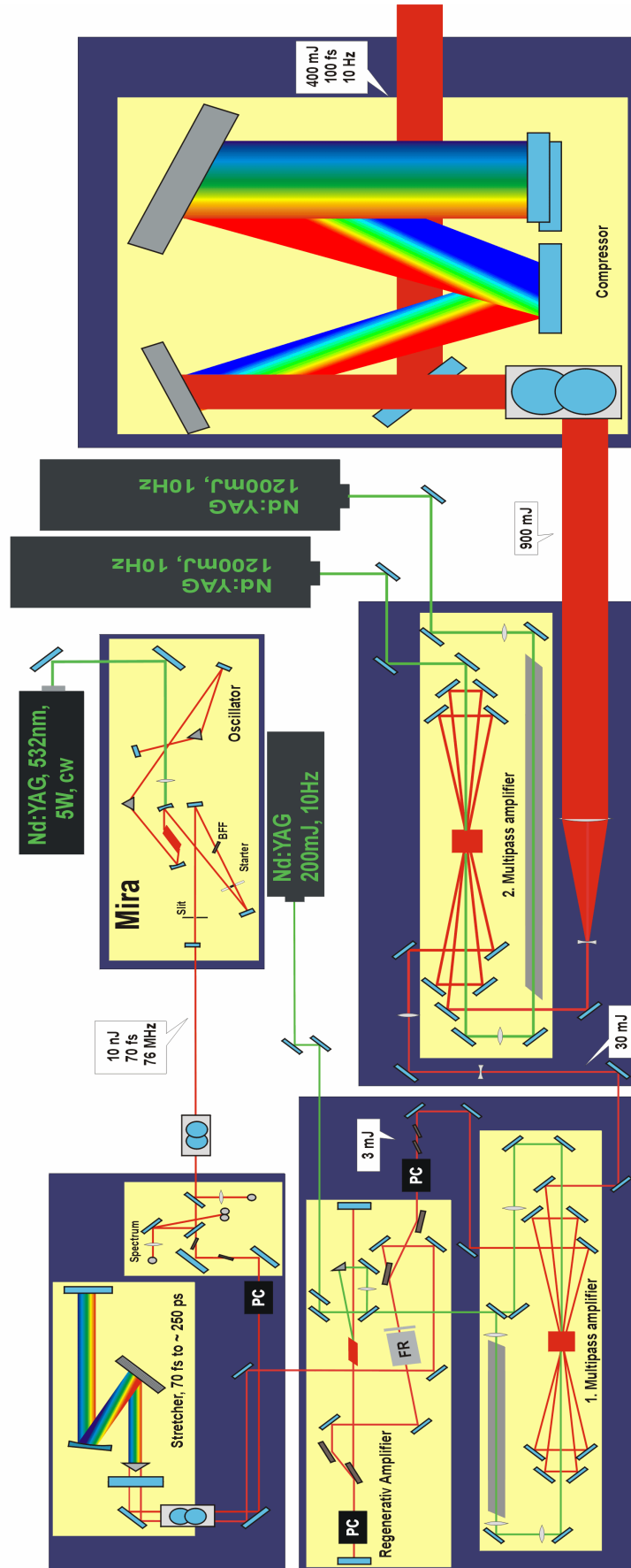


Figure 5.3 The scheme of the Ti:Sapphire laser system applied in the experiments.

5.2.2 Intensity in focus

For a Gaussian beam, the intensity is determined as

$$I = \rho c \quad (5.1)$$

where ρ - is the energy density given by

$$\rho = \frac{E}{(\pi/2)^{3/2} w^2 w_z} \exp\left[-\frac{2r^2}{w^2} - \frac{2(z-ct)^2}{w_z^2}\right] \quad (5.2)$$

E - is the total energy in the laser pulse, and w_z is the packet length:

$$w_z = \frac{c\tau}{\sqrt{2\ln 2}} \quad (5.3)$$

τ - is the total duration of laser pulse (Full Width at Half Maximum). In our case, for $\tau = 200$ fs, we have $w_z/c = 170$ fs, or $w_z = 51$ μm .

The transverse size of the beam during the propagation is described by

$$w = w_0 \left[1 + \frac{z^2}{z_R^2}\right]^{1/2} \quad \text{where } w_0 \text{ is the beam radius at } 1/e^2 \text{ in intensity} \quad (5.4)$$

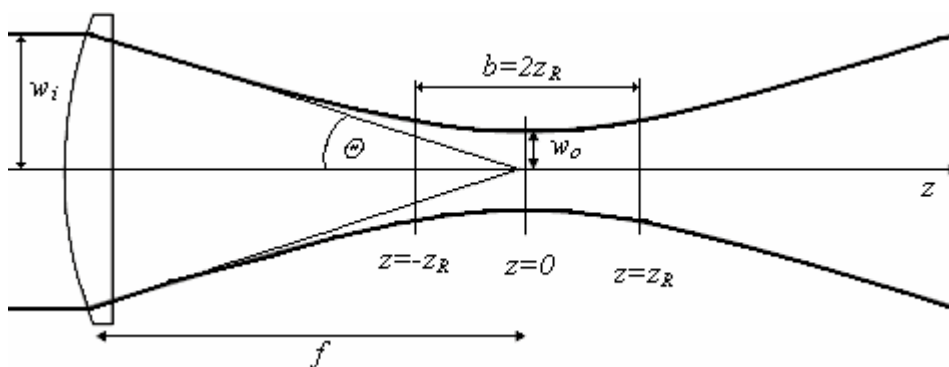


Figure 5.4 The designation of parameters by focusing a laser radiation with a lens.

By focussing the Gaussian beam, the waist in the focal plane w_0 is expressed as a function of waist of the incident beam w_i by

$$w_0 = M^2 \frac{\lambda f}{\pi w_i} \quad (5.5)$$

f is the focal length of the focussing optics, and M^2 characterizes the beam quality in comparison to an ideal Gaussian beam [Lawrence 1994]. For an ideal beam $M^2=1$.

At our experimental conditions, for the lens with $f=250$ cm, $\lambda=790$ nm, $w_i =2.5$ cm and $M^2=1$, the diffraction limited waist is $w_0= 25$ μ m.

The Rayleigh length is given by

$$z_R = \frac{\pi w_0^2}{\lambda M^2} = M^2 \frac{\lambda f^2}{\pi w_i^2} \quad (5.6)$$

and for the parameters above, the Rayleigh length is $z_R=2.37$ mm

On axis, the energy changes as $(1+z^2/z_R^2)^{-1}$. It is a Lorentz function with a half width at half maximum equal to z_R . For large z , the asymptotic behaviour $w \sim w_0 z/z_R$ allows to define the angular divergence $\delta = w/z \sim w_0/z_R$. The beam waist w_0 , and Rayleigh length z_R are both propotional to M^2 . Thus, the angular divergence does not depend on M^2 : only the beam properties in the vicinity of the focal plane are modified by the value of M^2 .

The maximum energy density is

$$\rho = \frac{E}{(\pi/2)^{3/2} w^2 w_z} \quad (5.7)$$

$$\text{or } \rho = \frac{4\sqrt{\ln 2} E}{\pi^{3/2} w_0^2 c \tau} \approx 0.598 \frac{E}{w_0^2 c \tau} \quad (5.8)$$

$$\text{The intensity is given by } I = \rho c \approx 0.598 \frac{E}{w_0^2 \tau} \quad (5.9)$$

With the typical parameters of our laser: $\tau \sim 200$ fs, energy of 200 mJ, $M^2=4$ and $w_0 \sim 100$ μ m, the typical intensity is $I \sim 6 \times 10^{15}$ W/cm².

In some cases, the different time duration laser pulses as well as different energies and focusing lenses were applied, the corresponding intensity is then given with the changed parameters.

6. Experimental results

In this chapter, the experimental results obtained with the novel set up suggested and in the previous chapter described are presented for a number of reactions. Firstly, detailed investigations on the reaction between laser produced C^{4+} ions and hydrogen gas jet were performed in order to optimize all of the parameters of the set up, since this reaction is well known as charge transfer reaction from the studies related to astrophysics [Dijkkamp et. al. 1985]. The novel set up was found to be capable to realize pure charge exchange interaction at densities of ions and neutrals in excess of 10^{16} cm^{-3} , which are necessary for lasing experiments. Detailed experimental studies of time behavior of the process provided additional information on the optimum conditions by comparison the results with the theoretical model described in chapter 3. This analysis proved also that charge exchange interaction at densities of ions undergoing the charge transfer reaction exceeding $2.8 \times 10^{16} \text{ cm}^{-3}$ was realized for the first time.

With this optimized set up, investigations for a number of promising reactions capable of creating a population inversion in the XUV spectral range have been done. Strong increase in intensities was observed for the $3d-2p$ ($\lambda=23.8 \text{ nm}$) and $2p3s-2p^2$ ($\lambda=37.4 \text{ nm}$) lines of O^{3+} and O^{2+} ions as a result of reactions $O^{4+} + H \rightarrow O^{3+} + H^+$ and $O^{3+} + H \rightarrow O^{2+} + H^+$ correspondingly. For the transition at 37.4 the gain was already achieved in an optically field ionization recombination scheme [Chichkov et. al. 1995]. Towards XUV gain experiments, the reaction $C^{6+} + H \rightarrow C^{5+} (n=3,4) + H^+$ was investigated, which is promising for lasing on the 4-2 and 3-2 transitions at 13.5 nm and 18.2 nm, the latter is well known from recombination pumped lasing experiments [Lee and Kim 2001].

6.1 Charge Exchange between C^{4+} ions and hydrogen as a model system.

The charge-exchange reaction $C^{4+} + H_2 \rightarrow H_2^+ + C^{3+}$ ($n=3$) is well-known as charge-transfer reaction from the studies related to astrophysics, and has been experimentally studied in detail in ion beam collision experiments [Dijkkamp et. al. 1985]. In this quasi-resonant reaction, which has a cross-section of $\sigma = 2.5 \times 10^{-15} \text{ cm}^2$, the quantum level $n=3$ is populated with a probability of over 90 %, followed by radiative transitions $3d-2p$ (38.4 nm), $3p-2s$ (31.2 nm), and $3s-2p$ (42 nm) as shown in the energy level diagram in Fig. 6.1. Note that for the ion velocities $>10^6 \text{ cm/s}$ this reaction goes with the energy defect of $\sim 10 \text{ eV}$. Instead of atomic hydrogen, molecular hydrogen is used here. With molecular Hydrogen the same quantum level is populated, with only a slightly different cross-section, and the main difference is in the relative population of the $3d, 3p, 3s$ sub-levels.

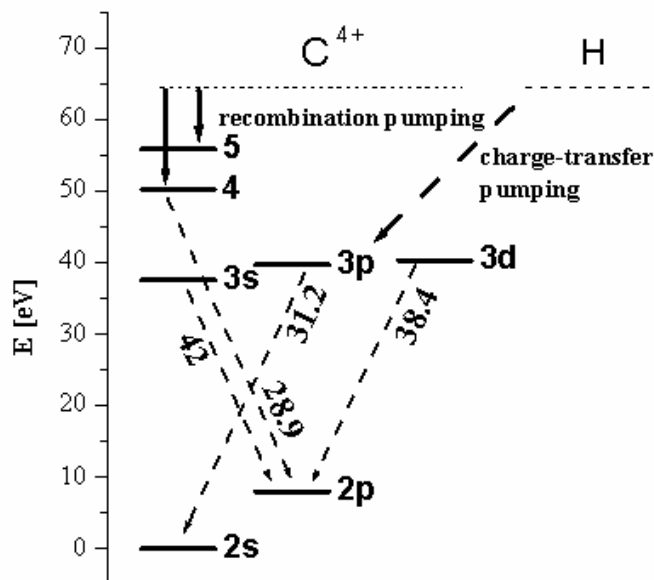


Figure 6.1 Simplified level diagram of C^{3+} ions with indication of charge-transfer pumping by collision of C^{4+} ions with atomic hydrogen (wavelengths are given in nm).

6.1.1 Observation of selective pumping of level $n=3$ of C^{3+} ions

To produce the necessary carbon ions for the above reaction, we applied short laser pulses with intensities of up to 10^{15} W/cm² in the focal spot at a pure Carbon target surface. At the target surface we can see lines from C^{5+} ions at 12.0, 13.5 and 18.2 nm, indicating that we partly produce fully ionized Carbon, but the strongest emissions results from C^{3+} and C^{4+} ions. Figure 6.2 depicts part of a spectrum recorded at the target surface, where all lines of interest of C^{4+} and C^{3+} ions are identified. Intensity is given in arbitrary units, that are the same for all other figures. When the plasma expands into the vacuum, the intensities of lines go down as the plasma density decreases. At a distance above 0.5 mm from the target, C^{4+} lines are practically absent, while C^{3+} and C^{2+} lines are observed up to distances of more than 4 mm. In Figure 6.3, a spectrum recorded at a distance of 1 mm is shown (dashed line), and one can see that C^{3+} lines are dominating. As described in chapter 3, the plasma parameters at this distance can roughly be estimated by an electron density $n_e \sim 10^{19}$ cm⁻³ and an electron temperature $T_e \sim 1.5$ eV . Thus, the main mechanism for the line emission from this plasma is three-body recombination.

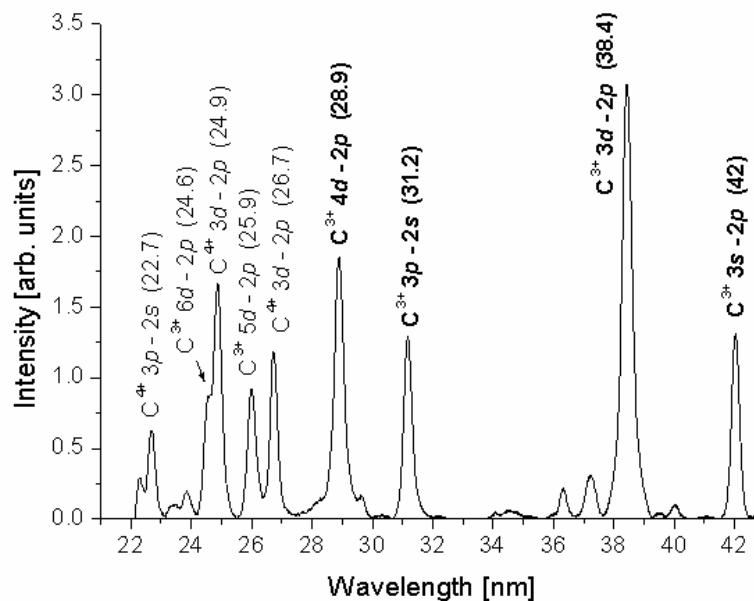


Figure 6.2 Typical carbon spectrum (part) recorded on target.

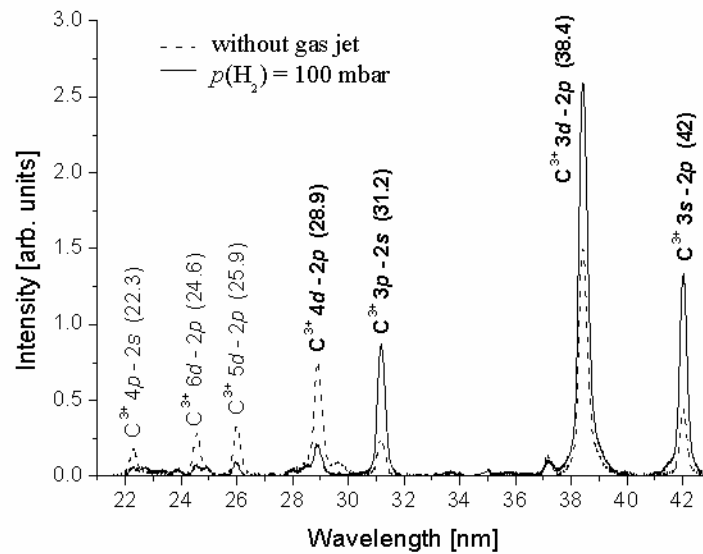


Figure 6.3 Example of carbon spectra recorded at 1 mm distance from the target surface. Dashed line: in vacuum, solid line: at 100 mbar H_2 backing pressure.

With the Hydrogen gas jet present, the signature of the spectra significantly changes (Fig. 6.3, solid line). C^{3+} lines from quantum level $n=3$ are strongly enhanced, while those from the quantum level $n=4$ and higher levels strongly decrease. This behavior is more or less pronounced for all relevant distances, gas jet pressures, and also for other interacting gases (see below) and is assumed to be an effect of the charge-exchange process, which preferentially populates the C^{3+} $n=3$ level. The strong effect on lines of C^{3+} ions allows simple optimization of various geometric and gas jet parameters. Best distances between the nozzle tip and laser focal spot are found to be in the range of 1-2 mm. For hydrogen, an optimum time delay between the valve opening and laser pulse is about 0.6 ms as shown in Fig. 6.4. Therefore, most of the results presented here were obtained with this optimal time delay. For heavier gases the optimum delay is larger (up to 1 ms). In the range of interest, the optimum delay is practically independent of the backing pressure. The sharp increase of the signal within a time interval of ~ 0.1 ms can be interpreted as the time required for the jet formation.

To verify the above assumption of charge-exchange population, the dependence of relevant line intensities on pressure, distance and sort of interacting gas has been investigated. When the plasma expands into vacuum, all C^{3+} lines

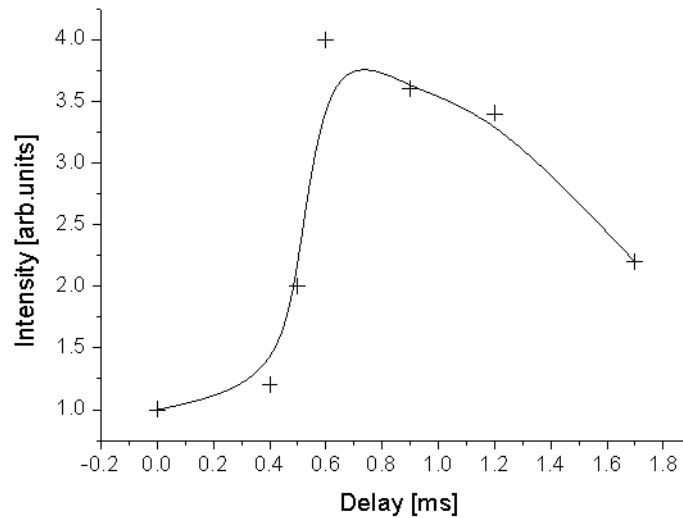


Figure 6.4 Dependence of line intensity ($3p - 2s$ line at 31.2 nm) on the delay between valve opening and laser pulse (the solid line just connects the measurement points).

show similar behavior, decreasing with the distance from the target as shown in the Fig. 6.5 for the $4d-2p$ and $3p-2s$ transitions. Only very close to the target (<0.2 mm) an initial rise, not resolved here, was observed.

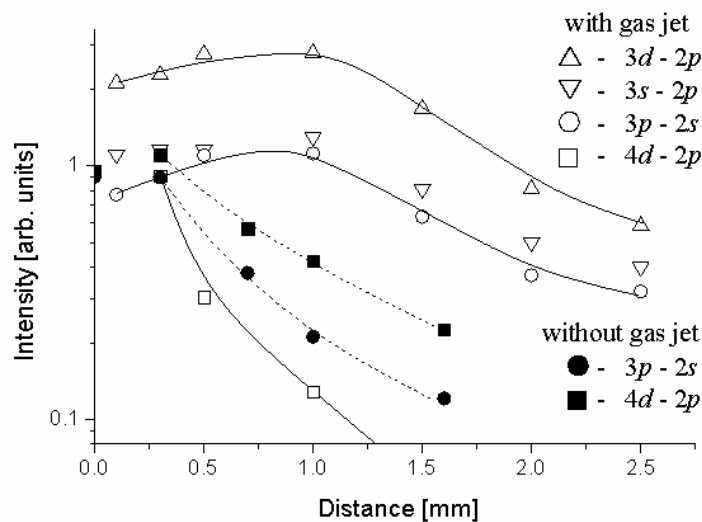


Figure 6.5 Intensity of C^{3+} lines versus distance from the target at a H_2 backing pressure of 100 mbar (solid lines) and for vacuum expansion (dashed lines). All lines just connect the measurement points.

With the gas jet present, the plasma conditions change as a result of charge-exchange and collisional interaction between ions, electrons and gas particles. The plasma density and temperature can rise if collisions between ions and neutrals are important, or the number of free electrons can increase and electron temperature decrease due to ionization of neutrals. Depending on the dominant effect, the line intensity may increase or decrease with respect to the vacuum case. As can be seen in Fig. 6.5, C^{3+} lines from the level $n=4$, which cannot be affected by charge-exchange, decrease even more faster when gas jet is present. The same is true for lines from higher levels as well. This can be attributed to a net heating of the plasma, as will be discussed below.

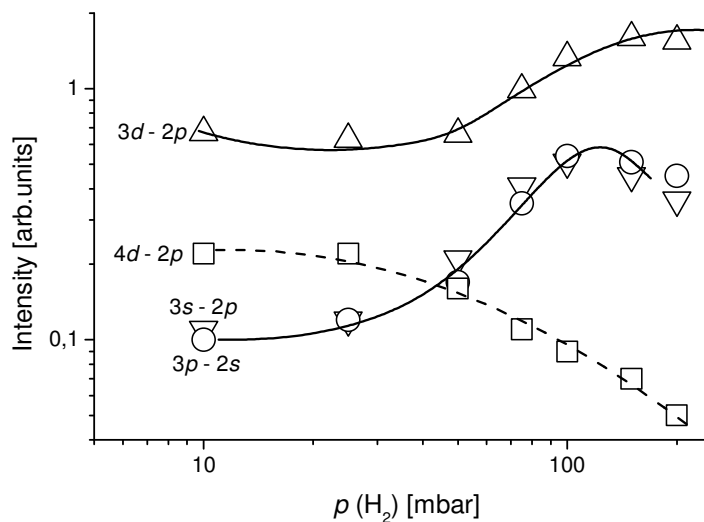


Figure 6.6 Intensity of C^{3+} lines versus backing pressure (H_2) at a distance of 1 mm from the target (the lines just connect the measurement points).

In contrast to this behavior, lines from the level $n=3$ clearly rise with distance until a maximum value, around 1 mm, is reached and then smoothly decrease. The effect of the gas jet compared to the vacuum case is strong even at smaller distances and can be explained only by charge-exchange pumping, since possible collisional de-excitation from level $n=4$ to $n=3$ cannot produce the same effect under the given plasma conditions.

Charge-exchange pumping, being proportional to the density of neutrals, can exceed recombination pumping only at sufficient gas pressures. This is shown in the Fig. 6.6. At low backing pressure even lines from level $n=3$ slightly decrease compared to the vacuum case, due to the plasma heating, but then the charge-exchange affected lines are increasing up to a maximum at about 100 mbar, while the lines from $n=4$ level continue decreasing. By applying of higher pressures the processes of collisional interaction and ionization of the gas jet particles are starting. In case of 150 mbar nitrogen gas jet, a transition to collisional interaction was clearly observed due to the appearance of ionized Nitrogen gas particles (the N^{2+} lines in Fig. 6.7), which are not there when the nitrogen gas jet at the lower backing pressure is applied. The same nature of ionization of gas particles was observed with other gases as well. It should be noted that at the optimum pressure of 100 mbar, the gas density in the interaction region of $\sim 7 \cdot 10^{16} \text{ cm}^{-3}$ is comparable to the estimated ion density $\sim 10^{17} \text{ cm}^{-3}$.

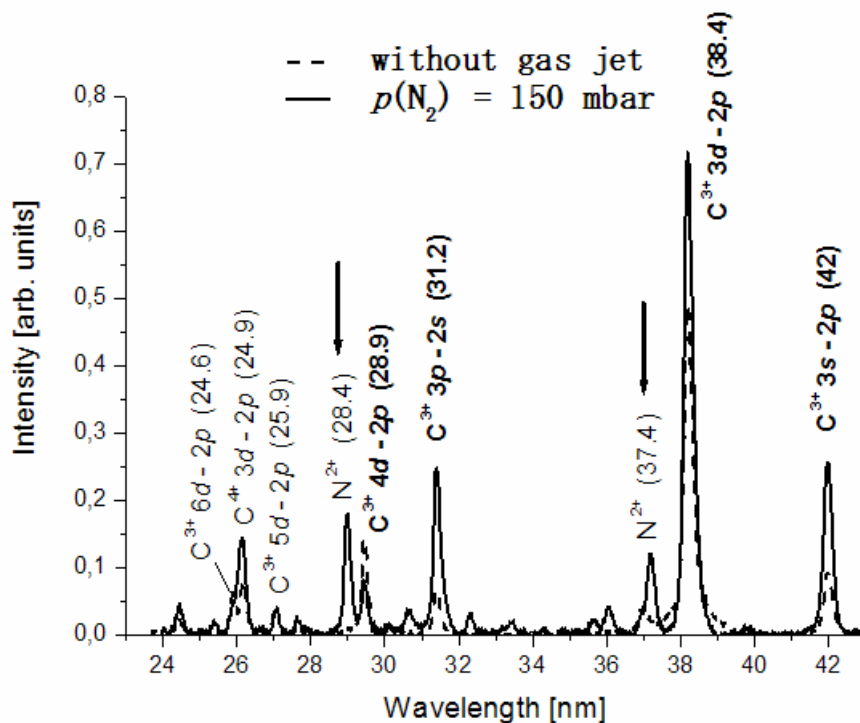


Figure 6.7 Carbon spectra recorded at a distance of 1 mm from the target. Dashed line: in vacuum, solid line: with a N_2 gas jet at 150 mbar backing pressure.

The different nature of excitation of the level $n=3$ is seen also in the time dependent behavior of the line intensity, which was investigated using a monochromator (Jobin Yvon) with fast MCP registration. In these measurements the time resolution was about 1 ns and the spatial resolution was around 500 μm . In Figure 6.8, time-of-flight luminosity of the $3p-2s$ line of C^{3+} ion is shown. Zero time corresponds to arrival of the fs-laser pulse. The signal rise time measured from 10 to 90 % of its maximum level is considerably shorter with the gas jet (~ 4.5 ns) than in vacuum (~ 7.5 ns). Opposite to this, the time behavior of the $4d-2p$ transition remains unchanged and the line intensity decreases in the presence of the gas jet (see for example Fig. 6.11).

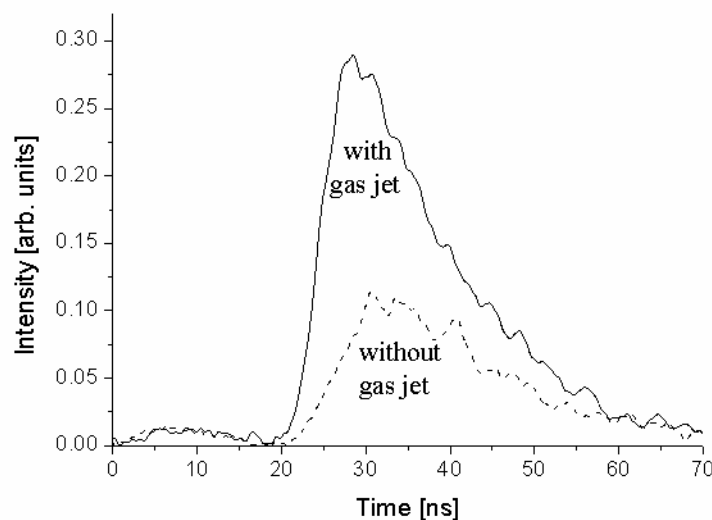


Figure 6.8 Time of flight luminosity of the C^{3+} $3p-2s$ line with gas jet (solid line; 100 mbar H_2 backing pressure) and in vacuum (dashed).

Charge-exchange pumping is a resonant process and consequently should depend on the ionization potential and atomic/molecular masses of the collision partners. Besides hydrogen, interactions with other gases such as N_2 , O_2 , Ar, and He was investigated. The obtained results are summarized in Fig. 6.9, where the maximum intensities of the charge-exchange $3p-2s$ and the recombination $4d-2p$ transitions are given for various gases at the same backing pressure of 50 mbar. At a pressure of 100 mbar (which is the optimum one for nearly all gases) the behavior for

the $3p-2s$ line is the same, while the intensity of the $4d-2p$ line is too small for a reliable measurement. Nitrogen and argon, having approximately the same ionization potentials as hydrogen, produce nearly the same effect on the $3p-2s$ transition, while the effect of helium with almost double ionization potential is very small and the signal is almost equal to that one in vacuum. It is known that for the C^{4+} ions the charge-transfer cross-section for the reaction with helium is much smaller than for hydrogen [Zwally and Koopman 1970], [Cederquist et. al. 1985]. For the $4d-2p$ line the influence of the different gases is just the opposite. All gases lead to an intensity decrease of this line with the strongest effect for the heavier gases.

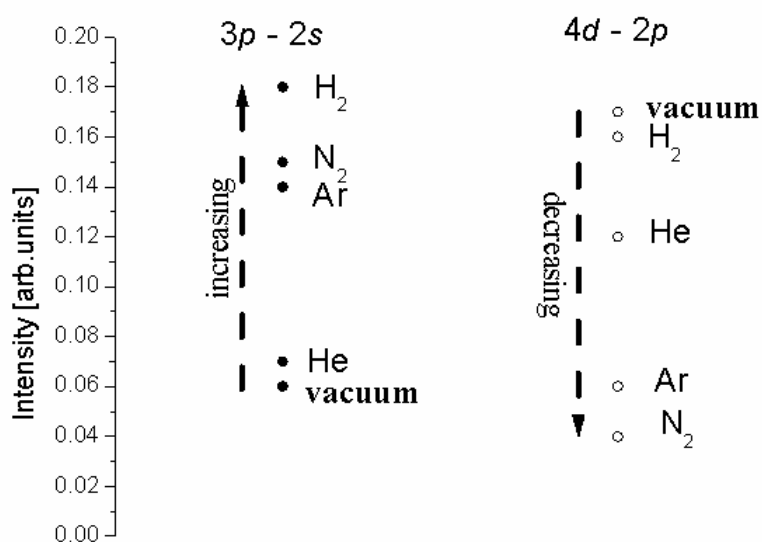


Figure 6.9 Maximum intensity of C^{3+} $3p-2s$ and $4d-2p$ lines at 1 mm distance from target for various gases, at backing pressures of 50 mbar, and for vacuum.

The observed behavior of lines originating from the level $n=3$ of C^{3+} ions is consistent with a charge-exchange population mechanism in every important aspect. Only these lines grow in the presence of the gas jet (Figs. 6.3, 6.7) and for a reagent not suitable for charge-exchange (helium) the effect is negligible (fig. 6.9). Another prominent feature is the opposite influences of the gas jet on transitions from high- n levels ($4d-2p$, $5d-2p$, $6d-2p$). In fact, an analogous behavior, but at much smaller gas

pressures and larger distances from the target, was described for the first time in [Orishich and Shaikhislamov 1992] for C^+ , C^{2+} and C^{3+} ions and later [Shaikhislamov 2003] for O^{5+} ions. In these experiments it was observed that the intensities of all lines initially decrease with the gas pressure. Only at sufficiently large pressures lines due to charge-exchange pumped transitions start to increase while others continue to decrease.

In the present experiments, a slight decrease in intensity at moderate pressures for lines originating from the level $n=3$ was also observed for H_2 (see Fig. 6.6) and more pronounced for a nitrogen gas jet. The reason for this behavior as proposed in [Shaikhislamov I.F. 2001] is that due to elastic collisions with gas the plasma becomes heated and recombination processes are slowed down. The heating of plasma and subsequent shock wave formation was observed in many other experiments with laser-produced plasmas and its effect on charge-transfer interaction was discussed in details in [Ponomarenko et. al. 1998]. This explains the decrease of intensity of highly lying transitions that are not affected by charge-exchange. Collisional heating of plasma interacting with gas is also consistent with the observation of a stronger reduction of $4d-2p$ recombination lines for heavier gases (Fig. 6.9).

6.1.2 Comparison of the results with different pulse duration lasers (10 ns, 0.1 ns, 200 fs)

As previously mentioned, it is expected that the charge exchange pumping will work better in case of a sharp plasma front interacting with the gas jet. That is why a short pulse laser was applied to produce the plasma. To check the role of the laser pulse duration, in addition to the 250 fs pulses also 100 ps pulses (realized by changing the pulse compression of the fs – laser system) and 10 ns pulses (from a Q-switch Nd:YAG laser system at 1060 nm) were applied for the generation of plasma jets. From the recorded spectra it follows that at equal laser energies the produced plasmas differ only by the presence or abundance of highly-charged C^{5+} , C^{6+} ions. For the 100 ps and 250 fs pulses the line intensities of C^{4+} ions are approximately 2 times larger than for ns-pulses, while the line intensities of C^{3+} ions are nearly the same.

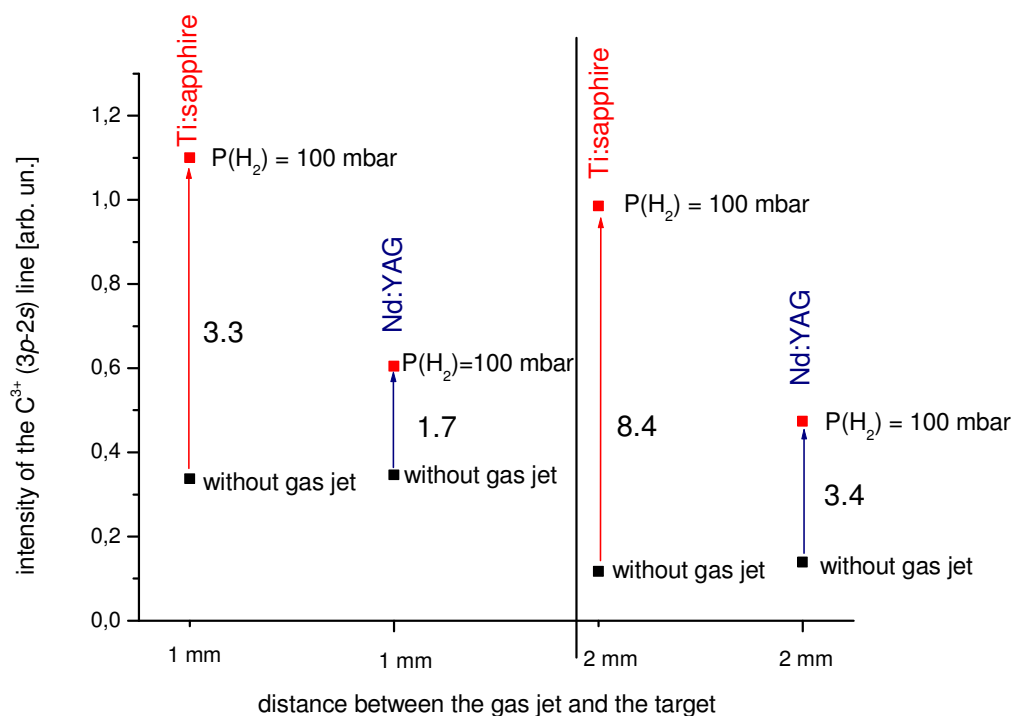


Figure 6.10 Comparison of charge transfer pumping of C^{3+} 3p-2s line at different distances from target with different pulse duration lasers (250 fs Ti:Sapphire laser, and 10 ns Nd:YAG) .

The influence of the gas jet on transitions of C^{3+} ions is qualitatively the same for all three pulses, an increase for lines from the quantum level $n=3$ and a decrease for lines from the level 4. However, quantitatively there is a clear tendency that for shorter pulses the charge-exchange effect is stronger. The gas jet induced increase of the $3p-2s$ line relative to the vacuum case was 1.5 times larger for 100 ps pulse and 2 times larger for 250 fs pulse compared to 10 ns pulse. The results of investigations with 250 fs Ti:Sapphire laser and 10 ns Nd:YAG lasers are summarized in Fig. 6.10. It is clearly seen that the effect for shorter pulses is better especially at larger distances from the target, where the difference is more pronounced. The observed small dependence of the time integrated line intensities on the laser pulse duration can be explained by long plasma expansion times which are responsible for the plasma front dispersion. Moreover, in the present experiments the exact pulse form and especially the contrast ratio of the ps- or fs- pulses, which is important for the initial plasma conditions, was not measured or controlled and therefore, a further improvement of the charge-exchange pumping with short pulses might be possible.

6.2 Theory versus experiment

In this chapter the experimental data and dependencies based on time resolved measurements are compared with the analytical model described in chapter 3.3. The experimental results were obtained with Jobyn Yvon monochromator as shown in Fig. 5.1, with space resolution of 250 μm , and time resolution of 1 ns. The analyses of these data allowed performing quantitative analysis of the results obtained by comparison with a kinetic model of charge exchange pumping. This provides additional information on the optimum conditions and proves that charge exchange interaction at densities of both reagents exceeding 10^{16} cm^{-3} was realized for the first time.

It has been shown in previous chapters, that by applying the Hydrogen gas jet all charge exchange influenced C^{3+} lines (from the $n=3$ level) are strongly enhanced in comparison to the case of expansion into vacuum and the lines which cannot be pumped by charge exchange (from the $n=4$ and higher) show even a decrease (Fig. 6.3). Such strong effect occurs at distances of 1-2 mm from target surface, hydrogen backing pressure of 100 mbar ($7 \times 10^{16} \text{ cm}^{-3}$), and at time delay between the valve opening and laser pulse of 600 ms.

Most informative data of the process are obtained from time resolved measurements. In Fig. 6.11, line intensities for two distances - close (0.5 mm) and far (1.5 mm) from the target surface are presented. The position of the gas nozzle relative to the line of sight of the monochromator was kept the same (Fig.5.1). These data demonstrate, that at relatively large distances between the target and the gas jet the lines from the level $n=3$ show an increase with respect to the vacuum case during the whole time when the plasma streams through the gas jet. At smaller distances, where the density of the plasma is comparable to or higher than the density of neutral particles, the lines show dramatic increase only at the plasma front. This increase of intensity at the plasma front exhibits a linear dependence with the gas jet pressure up to about 100 mbar (Fig. 6.12), exactly as expected for charge exchange pumping, since the rate of charge transfer pumping is proportional to the density of neutrals. At 100 mbar backing pressure the density of neutrals is getting comparable to the density of ions in the interaction region and, therefore, there should be no further increase in intensity of charge transfer pumped lines [Vorontsov et. al. 2004]. Near

the target the $4d-2p$ line doesn't show any change at all under the same conditions (Fig. 6.11), because it is not affected by the charge exchange.

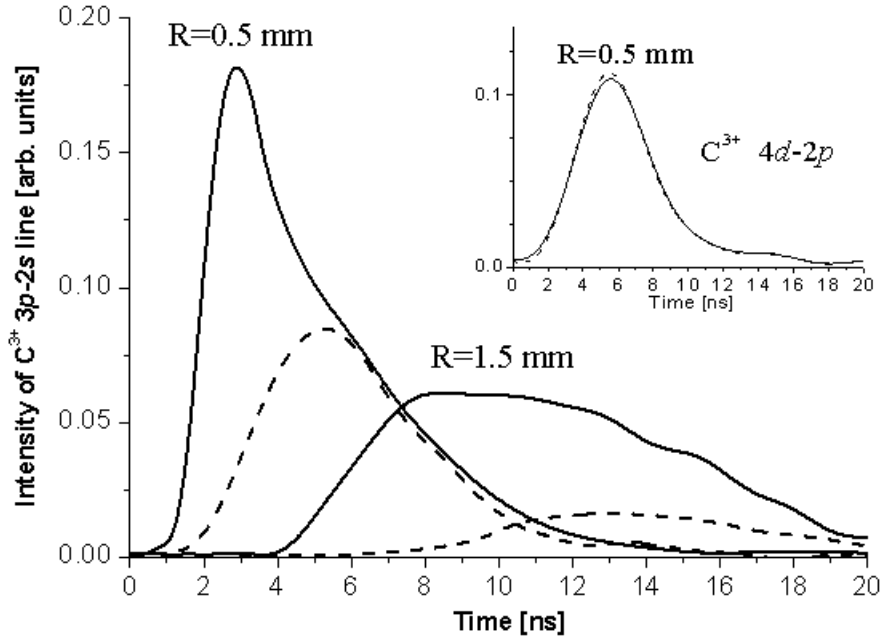


Figure 6.11 Time resolved intensity of C^{3+} 3p-2s line at two distances R from the target surface with gas jet (solid lines) and in vacuum (dashed lines). Insert: intensity of the $4d-2p$ line measured at $R=0.5$ mm distance with and without a Hydrogen gas jet.

In order to better understand the behavior of the lines, the experimental curve is analyzed with the existing model of charge exchange interaction. The pumping rate of charge exchange pumping J can be approximately expressed by the equation (see chapter 3)

$$J(R,t) = n_i^o(R,t) V_i n_a^o(R) \sigma_i k \quad \text{where} \quad k = \frac{e^{-N_i \sigma_i + N_a \sigma_i}}{[1 + e^{-N_i \sigma_i} (e^{N_a \sigma_i} - 1)]^2} \quad (6.1)$$

Here V_i is the ion velocity, n_i^o , n_a^o are the densities of species at a distance R and time t taken without interaction, σ_i is the charge exchange cross-section. The efficiency of interaction is described by a factor k , which depends on the integral densities N_a and N_i : where $N_a = \int^R n_a^o dR$ is the total number of neutrals along the path

from the target surface to the observation point R , and $N_i = \int n_i^o(R,t) V_i dt$ is the total number of ions passed through the unit square (located at the observation point) to the moment of observation t .

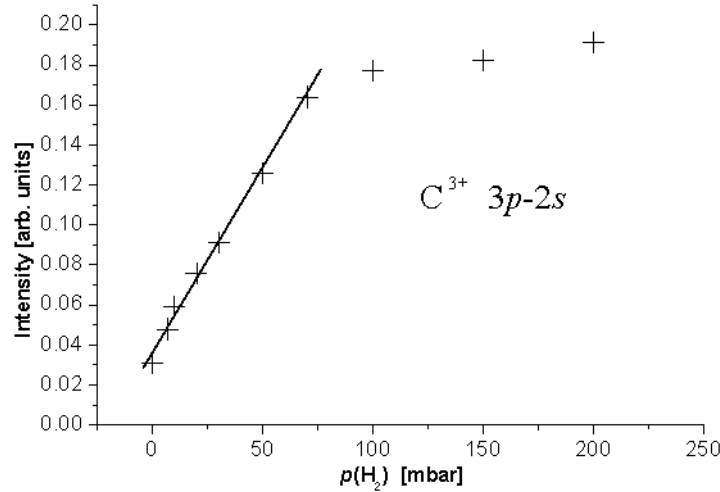


Figure 6.12 Maximum intensity of the $\text{C}^{3+} 3p-2s$ line versus the H_2 backing pressure at a distance of 0.5 mm from the target surface.

When the ion density is small and $N_i \ll 1/\sigma_i$ is fulfilled, the efficiency coefficient k_i is constant and can be approximated by $k \approx \exp(-N_a \sigma_i)$. In this case the line intensity, which is determined by the factor J , is proportional to the ion flux $n_i V_i$, see Eq. (6.1). In the opposite case of large ion density, it follows that $k \approx \exp(-N_i \sigma_i)$. Because N_i is the time integrated ion flux, the pumping rate exponentially decreases with time. In other terms, the pumping rate decreases because the number of neutral particles available for interaction decreases with time due to the charge exchange process. Thus, from Eq. (6.1) it follows that most effective interaction can be realized only if the number of neutrals and ions in front of the gas cloud and plasma flow, respectively, are approximately equal to each other, e.i. $N_i = N_a$. It is also desirable to keep this values not too large, $N_i, N_a \sim 1/\sigma_i$. Otherwise the length of charge exchange is too small and interaction takes place only in a thin layer. N_a can be calculated as $N_a = n_a \times L_a$, where L_a is the width of the jet boundary. For our experimental parameters, the estimation $N_a \sigma_i \sim 1$ is valid.

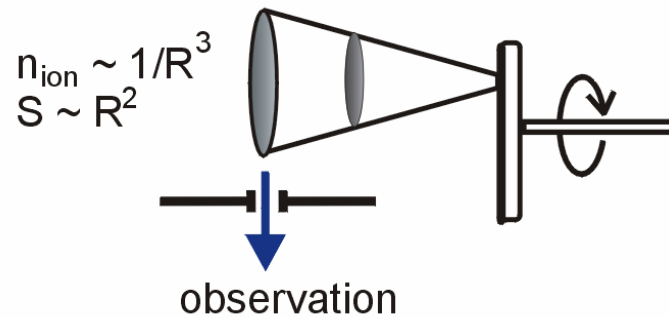


Figure 6.13 The simplified illustration of observation volume in the experiments.

At large distances R from the target, where N_{σ_i} is small, the line intensity J should be proportional to the ion flux $n_i V$. The measured line intensity J_m depends on the observation volume. Because the laser produced plasma expands in a cone with a cross section proportional to R^2 , and because the plasma density scales as $1/R^3$ (Fig. 6.13), the dependence of the line intensity on the distance from the target surface should be $J_m \sim 1/R$. And it is worth to show that the charge exchange influenced $3p-2s$ line has such a behavior (A mean square fit of the experimental data agrees very well with the $1/R$ scaling), while the behavior of the $4d-2p$ line is quite different as illustrated in Fig. 6.14.

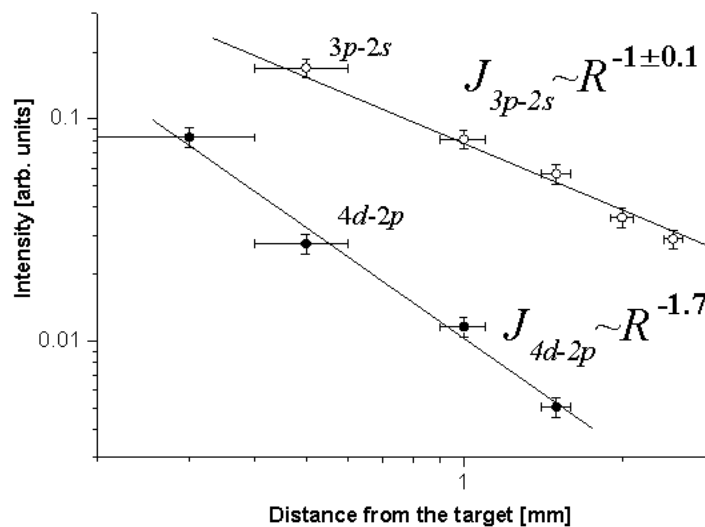


Figure 6.14 The dependencies of maximum line intensities on the distance from the target surface in the presence of the Hydrogen gas jet. Open circles - C^{3+} $3p-2s$ line; filled circles - C^{3+} $4d-2p$ line.

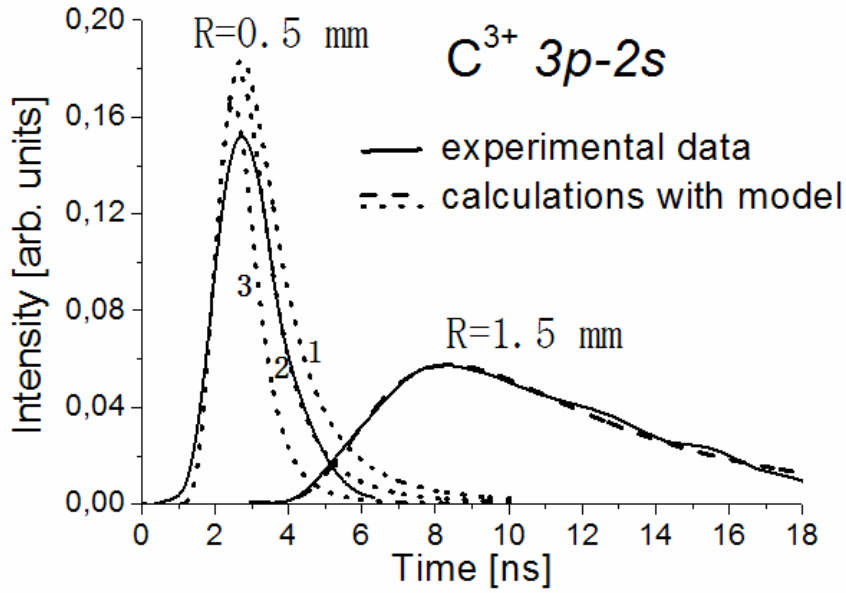


Figure 6.15 Solid curves: time dependent charge-transfer induced part of the $C^{3+} 3p-2s$ line at distances $R=1.5$ and 0.5 mm (calculated as difference between the solid and dashed curves shown in **Figure 6.9**).

Dashed curve: calculation results for a distance $R=1.5$ mm with the mean velocity $V_m = 1.27 \times 10^6$ cm/s obtained using Eqs. (1-2).

Dotted curves: calculation results for a distance $R=0.5$ mm with $V_m = 1.27 \times 10^6$ cm/s and three different values of a total number of ions N_{tot} : 1st: 3×10^{12} , 2^d: 4×10^{12} and 3^d: 6×10^{12} Sr⁻¹.

To calculate the time behavior of signals, a model of plasma expansion should be added to the solution of charge transfer equations. Plasma produced by a short laser pulse is described by a self-similar expansion of ions with Maxwell velocity distribution

$$n_i(R,t) = (4/\sqrt{\pi})N_{tot} \exp(-(R/V_m t)^2) / (V_m t)^3 \quad (6.2)$$

where N_{tot} is the total number of particles of interest (in our case C^{4+} ions) per unit solid angle, and V_m is their mean velocity. The velocity of each plasma element is given by $V=R/t$. The value of V_m can be found by fitting of the calculated curve to the experimental one. By the solid curves in Fig. 6.15, the difference between the line intensities measured with a gas jet and in vacuum are presented for two distances

$R=0.5$ and 1.5 mm (see Fig. 6.11). These curves represent the signals only due to charge exchange pumping. For the curve at $R=1.5$ mm, a best calculated fit is shown by the dashed line, which corresponds to $V_m = 1.27 \times 10^7$ cm/s and agrees very well with the experimental measurements, which can be derived from the Figure 6.11 as 1.3×10^7 cm/s. Because only relative line intensities were measured in these experiments, the value of N_{tot} cannot be derived from comparison with calculations as long as the ion density is small and the efficiency coefficient k is independent of it. However, near the target the behaviour of signals gets dependent on the total number of ions involved in the reaction. By dotted lines in Fig. 6.15, results of calculations are shown for the distance $R=0.5$ mm for three values of N_{tot} at the same mean velocity V_m found earlier. A best fit with $N_{tot}=4 \times 10^{12}$ Sr⁻¹ corresponds to an ion density of 2.8×10^{16} cm⁻³ at the signal maximum located at $t = 2.7$ ns, as follows from Eq. (6.2). This analysis not only confirms that highly selective charge exchange pumping has been realized at densities of both reagents exceeding 2.8×10^{16} cm⁻³, but also gives a possibility to see a time behavior of charge transfer influenced lines at different distances from the target.

As follows from this analysis, the time duration t_d of the charge exchange signal at a distance of 0.5 mm (half-width) corresponds to 2 ns (Fig. 6.15). It means, that the charge exchange interaction takes place on the spatial scale $S = V_m t_d$ which is about 200 μm . Even for the distance of 1.5 mm, where the interaction time is about 8 ns (Fig. 6.15), the interaction zone is less than 1 mm. Since the slit used in the experiment (Fig. 5.1) for providing the spatial resolution is 200 μm , the good scanning of the interaction region was possible.

These data prove our assumption, that the charge exchange is achieved on the spatial scale less than 1 mm, which is important as the characteristic length of charge exchange determines the interpenetration of ions into a gas, and according to theory [Shaikhislamov 2001] must be less than 1 mm to ensure the efficient charge exchange interaction at high densities.

6.3 Observation of charge transfer excitation in oxygen ions

Charge transfer processes due to collisions of ground state $O^{3+}(2s^22p)$ ions with atomic hydrogen were investigated using the quantum-mechanical molecular-orbital close-coupling (MOCC) method in [Wang et. al. 2003] for the energy range from 0.1 eV/a.m.u to 1 keV/a.m.u. It follows from their calculations that the capture of an electron to $O^{2+} 2p3s$ -state begins to dominate for the impact energies more than 20 eV/a.m.u., and the state cross section for the capture is as high as 10^{-15} cm^2 . The investigation of the capture of an electron into the $3s$ state is of interest since the lasing on the corresponding ground state transition $2p3s - 2p^2$ at $\lambda=37.4 \text{ nm}$ of O^{2+} ion was demonstrated with Optically Field Ionization recombination pumping mechanism [Chichkov et. al.1995]. The measurements of cross section for the O^{4+} and O^{3+} have been reported in [Grandall 1977]. Although the measurements were done for the higher impact energies, the clear tendency of coinciding results obtained in [Wang et. al. 2003] with the measurements in common impact range is observed. Based on this, one can expect that the cross section for the $O^{4+} + H \rightarrow O^{3+} (n=3) + H^+$ reaction can be as high as $3 \times 10^{-15} \text{ cm}^2$.

In the present experiments the interaction of O^{3+} and O^{4+} ions with hydrogen indicates strong charge exchange pumping of $O^{2+} (2p3s-2s^22p^2)$ and $O^{3+} (2s3d-2s^22p)$ lines at 37.4 and 23.8 nm.

6.3.1 Dramatic increase in intensities of O^{2+} and O^{3+} ions

Using the optimum experimental conditions found out in experiments with carbon targets, further experiments with the set up described in chapter 5 with Al_2O_3 targets were performed. In Fig. 6.16, two spectra are shown, recorded in vacuum (dashed line) and with a gas jet (H_2) at a backing pressure of 100 mbar (solid line) for a 1 mm distance from the target surface. The strongest effect shows the $3d-2p$ ($\lambda=23.8$ nm) line of O^{3+} ions with almost a factor of ten increase with respect to the vacuum level. Recall that for the level $n=3$ the higher value of cross-section as described above is supposed. The $2p3s - 2p^2$ ($\lambda=37.4$ nm) line to the ground state of O^{2+} ions, respectively shows very good increase in signal as well as the $2p3d - 2p^2$ line in O^{4+} ions, for which the cross section of is relative high as well [Grandall 1977].

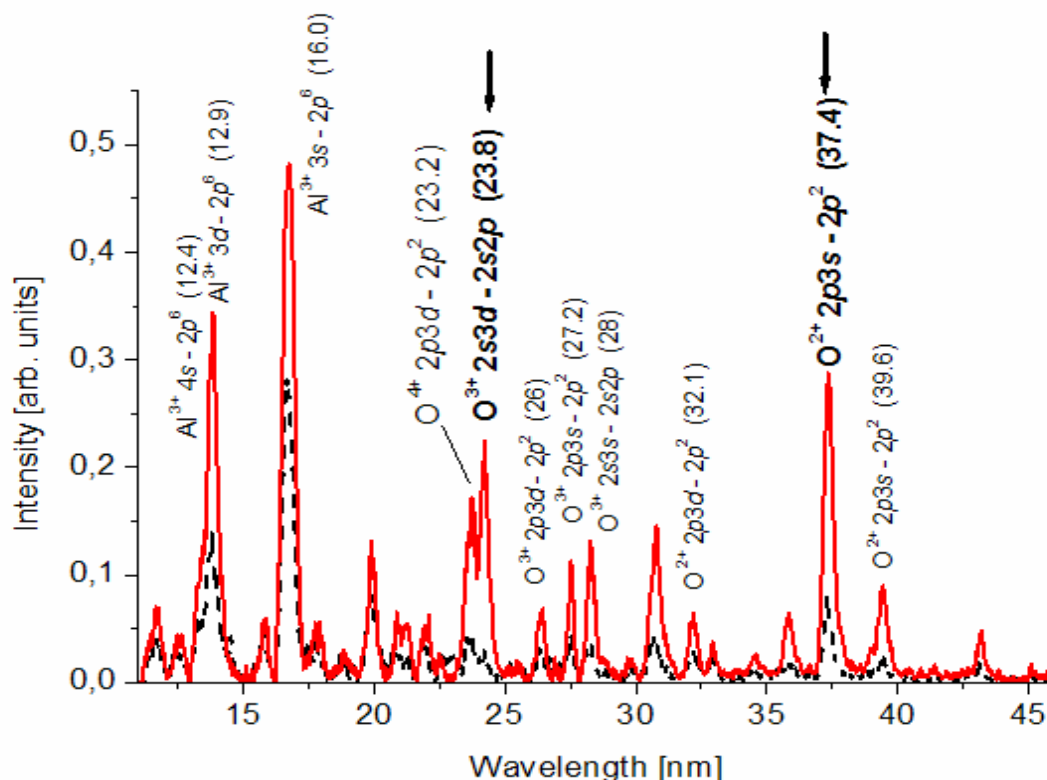


Figure 6.16 Oxygen spectrum recorded at a distance of 1 mm from the Al_2O_3 target at a gas jet backing pressure of 100 mbar (solid line) and in vacuum (dashed line).

We attribute this effect to the charge-transfer reaction, although the effects of collisional interaction begin to play a role, resulting in increasing intensities of other non-influenced charge exchange lines. At the backing pressure of 50 mbar only these two lines showed a good increase, while the others remained unchanged [Vorontsov et. al. 2004].

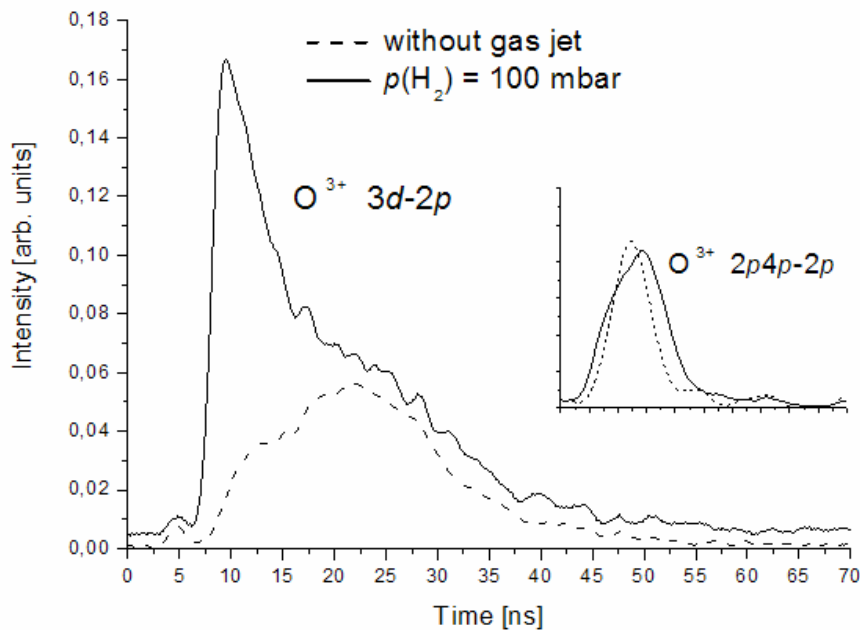


Figure 6.17 Time resolved intensities of the $3d-2p$ and $2p4p-2p$ lines of O^{3+} ions at a distance of 0.7 mm from the target with a gas jet backing pressure of 100 mbar (solid line) and in vacuum (dashed line).

The different nature of excitation of the level $n=3$ of the ions is seen also in the time dependent behavior of the line intensity, which was investigated using a monochromator (Jobin Yvon) with fast MCP registration. In these measurements the time resolution was about 1 ns and the spatial resolution was around 250 μm . In Fig. 6.17, time resolved intensity of the $3d-2p$ and $2p4p-2p$ transitions of O^{3+} ions at 23.8 nm and 17.1 nm correspondingly are shown. Zero time corresponds to arrival of fs-laser pulse. At distances smaller than 1 mm, when the plasma density is comparable or higher than the density of neutral particles, the $3d-2p$ line shows dramatic increase only at the plasma front, which is consistent with the results obtained for C^{3+} ions

analyzed with an analytical model, while the temporal behavior of the $2p4p$ - $2p$ line, which cannot be pumped due to the charge exchange, remains practically unchanged.

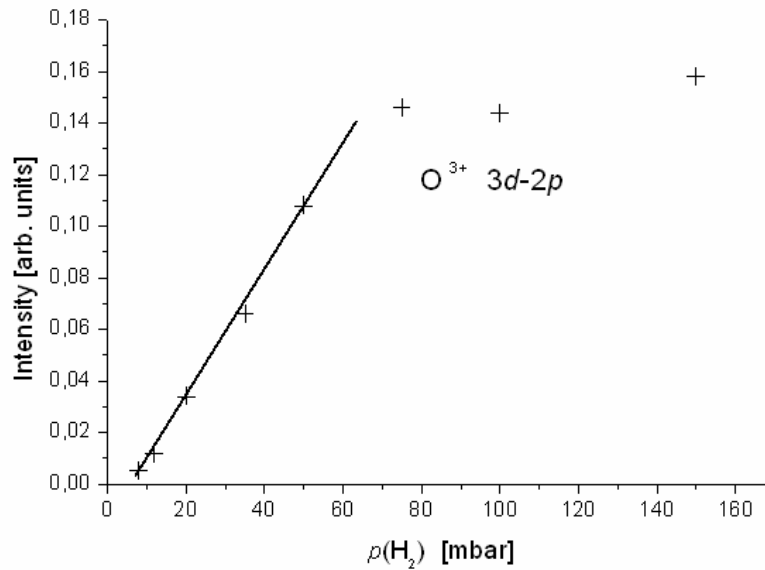


Figure 6.18 Maximum intensity of O^{3+} $3d-2p$ line versus backing pressure (H_2) at a distance of 0.7 mm from the target.

Charge-exchange pumping is proportional to the density of neutrals and therefore should have a linear dependence on the gas pressure. This corresponds to our experimental data shown in Fig. 6.18 for the $3d-2p$ line intensity at the plasma front. The line intensity exhibits a linear dependence with the gas jet pressure up to about 80 mbar, exactly as expected for the charge exchange mechanism, while at this backing pressure the density of neutrals is getting comparable to the ion density, and no more ions are present for further increase in intensity.

6.4 Investigations on possible lasing transition of C^{5+} ions at 18.2 nm

Another interesting XUV lasing candidate are C^{5+} ions on 3-2 transition at $\lambda=18.2$ nm, which can be pumped as a result of the reaction $C^{6+} + H \rightarrow C^{5+} (n=3,4) + H^+$. The lasing on this transition is related to the well known recombination laser [see for e.g. Lee and Kim 2001] and this mechanism is described in chapter 2. Attempts for creation of population inversion on this transition with charge exchange were done in experiments with hot and cold colliding plasmas [Ruhl et. al. 1997]. An increase in intensity of the C^{5+} ($3d-2p$) line at $\lambda=18.2$ nm was reported and explained as an effect of the reaction $C^{6+} + C^{2+} \rightarrow C^{5+} (n=3) + C^{3+}$. However, due to a smoothed interaction region and difficulties to control parameters of the interacted plasmas, no improvement has been reached in further experiments with colliding plasmas.

In this chapter new data obtained with the novel set up are presented to show that the pumping of the $n=3$ and $n=4$ levels of C^{5+} ions, resulted as charge exchange interaction between C^{6+} ions and hydrogen and helium gases, is realized at simple and desirable conditions with the novel experimental set up.

6.4.1 Selective pumping of $n=3,4$ levels with He and H_2 gases

The experiments were done on the same experimental scenario shown in Fig. 5.1. At the time of the experiments, we were limited in the energy of our Ti:Sapphire laser system. Therefore, for the production of bare Carbon ions from a solid carbon target, we have used the uncompressed pulses, which correspond to 100 ps, with the energy of 200 mJ. A corresponding intensity at the focal spot was 10^{13} W/cm².

In Fig. 6.19 examples of spectra recorded in vacuum and with a Hydrogen gas jet at a distance of 1.5 mm from the target surface are shown. One can see substantial intensity increase of the lines that should be pumped by the charge-transfer reaction, especially of the 4-2 line at $\lambda=13.5$ nm wavelength. On the other hand, the line from the higher level $n=5$ shows decrease, similar to the observations with C^{3+} ions discussed above.

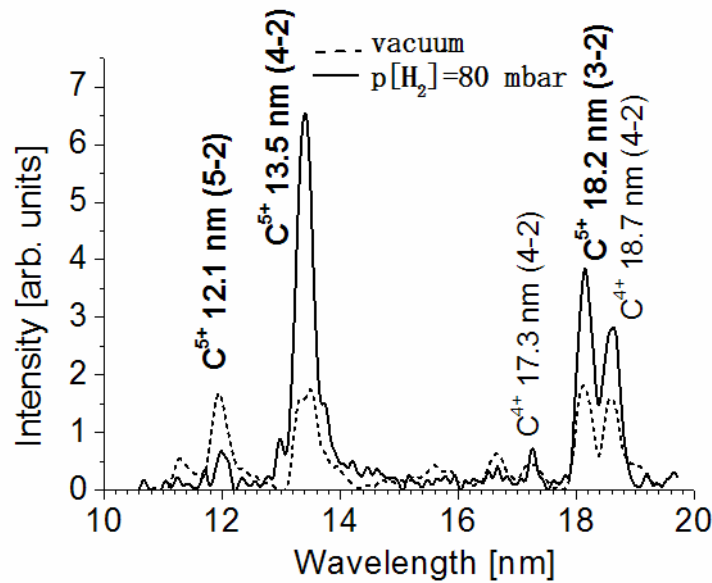


Figure 6.19 Carbon spectra recorded at a distance of 1.5 mm from the target. Dashed line: in vacuum, solid line: at 80 mbar H_2 backing pressure.

The time of flight measurements also show that there is a dramatic increase in the front of the signal for both lines with hydrogen gas jet (6.20, dashed lines) in comparison with the lines induced in vacuum.

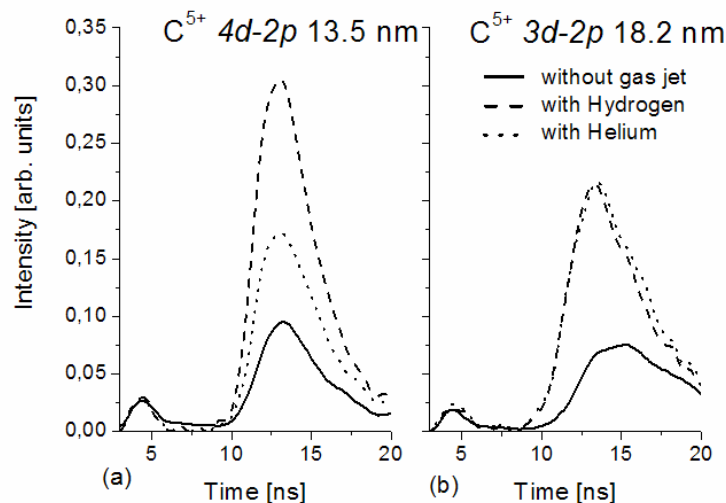


Figure 6.20 Time resolved measurements for C^{5+} $4d-2p$ (a) and $3d-2p$ (b) lines at a distance of 2.5 mm from the target: solid lines – expansion in vacuum, dashed lines – with hydrogen gas jet, dotted lines – with Helium gas jet.

Unlike the results of experiments with the plasma expanding into background gas [Dixon and Elton 1977], a clear dependence of measured line intensities on the sort of gas was observed. Charge-exchange, being a resonant process, depends mainly on the ionization potential of the collision partners. In case of C^{5+} ions, the level $n=4$ can better be pumped with hydrogen gas, but not with Helium which has higher ionization potential, and this is confirmed in our experiment (Fig. 6.20(a)), where the best increase is for the hydrogen gas jet. The level $n=3$, however, has the better decrement of energy with Helium gas, although the cross section is larger for the hydrogen gas, which explains the equal effect of these gases (Fig. 6.20(b)).

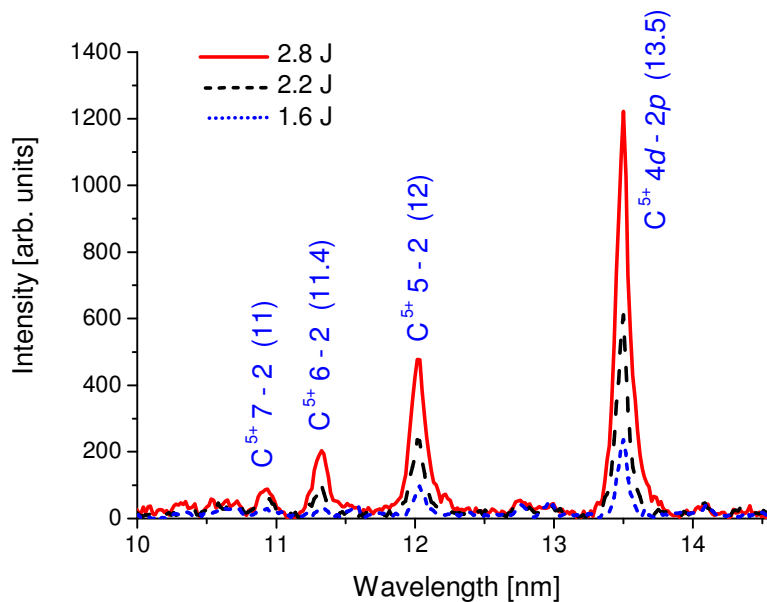


Figure 6.21 Carbon spectra for the different laser energies (recorded at Max Born institute with Nd: glass laser, 6 ps).

For the 18.2 nm line of the C^{5+} ion, a gain coefficient exceeding 10 cm^{-1} is expected for a length of medium of 1 cm with the densities of reagents of 10^{16} cm^{-3} as discussed in particular in chapter 3. In preliminary investigations towards XUV gain experiments, it has been found that about 2.5 J of energy in a ps-laser pulse is needed to produce sufficient amount of C^{6+} ions in a line focus of about 1 cm in length and 0.07 cm in width (Fig. 6.21). The latter experiment was conducted at the Max-Born Institute in Berlin, where a more powerful laser for this purpose is available, but unfortunately it was not possible to perform experiments with line focus and a corresponding gas jet.

6.5 Conclusion

Interaction of ions produced by short laser pulses with atoms from a pulsed gas jet has been studied by means of time and space resolved spectroscopy in the XUV range. The dependencies obtained on the gas pressure and gas sort are explained by direct and highly selective charge exchange pumping. Experimental results are in a good agreement with an analytical model and confirm that charge exchange pumping has been realized at densities of both reagents well in excess of 10^{16} cm^{-3} , which is at least one order of magnitude higher than in previous experiments (Chapter 4). At optimum conditions, a strong selective excitation of several potential lasing lines in the XUV range was observed in the presence of the gas jet. These observations provide new prospects for the realizations of XUV lasers with higher efficiency than in presently demonstrated schemes. For the 18.2 nm line of the C^{5+} ion, a gain coefficient exceeding 10 cm^{-1} is expected for a length of medium of 1 cm with the densities of reagents of 10^{16} cm^{-3} . In preliminary investigations towards XUV gain experiments, it has been found that about 2.5 J of energy in a ps-laser pulse is needed to produce a sufficient amount of C^{6+} ions in a line focus of about 1 cm in length and 0.07 cm in width.

7. Perspectives of charge exchange lasers

The results obtained in the previous chapter with the novel setup, consisting of a pulsed gas jet and a femtosecond laser produced plasma with focal spot ablation, demonstrated the selective charge transfer pumping for a number of reactions. However, for realizing of a charge transfer laser, the geometry of the experiment has to be slightly modified. Instead of the spot focus for laser ablation, the line focus has to be applied, and for an interaction of the whole elongated plasma column with neutrals, some kind of slit nozzle instead of the so far used cylindrical nozzle is needed. For this, ideal experimental geometries and possible ways for a realization will be introduced.

Advantages of new charge exchange schemes with potential lasing transitions in Na-like ions with an example for Chlorine and Calcium elements will be presented. These schemes promise even more efficient pumping as compared with the charge transfer excitation in Hydrogen like ions.

Another approach suggested is the idea of quasi-steady state charge transfer pumping, successfully realized with electron-collisional excitation. The idea is to pump by charge exchange both the upper and lower laser levels (or in ideal case, only the upper level). Then a population inversion is obtained if the lower state rapidly depopulates to the ground state. Some first experimental results on pumping in Ne-like Silicon ions will be presented.

In order to better evaluate parameters for charge transfer pumped lasers, it is suggested to construct a charge exchange laser operating in visible or ultraviolet spectral range in a normal operating laser regime with cavity. For this purpose the $3p-3s$ transition of O^{3+} at 307 nm is suggested and discussed.

7.1 Desirable geometry for lasing experiments – uniform plasma column interacting with a gas stream having a sharp boundary

As it was discussed in previous chapters, for any lasing experiments with charge exchange pumping there is a need to create an appropriate interaction zone of high Z-ions and neutrals (or low Z-ions). The interaction zone must be in a form of an elongated column, and the involved particles should have sharp and uniform density profiles along this zone.

Production of high Z-ions in line focus geometry

In most x-ray laser schemes, long narrow plasmas are produced by focusing the pump laser into a line via a cylindrical lens or with a spherical mirror. The line focus produced with a cylindrical lens provides normally a line of 100-200 μm in width, and has non-uniform intensity distribution along the line for a circular incident laser beam with Gaussian distribution. This is because the intensity at any point along the focused line is the integral of the laser intensity along a line normal to a focal line. This non-uniformity can be compensated either by shaping the aperture of the incoming beam into a rectangular form or by the use of deformable focusing optics.

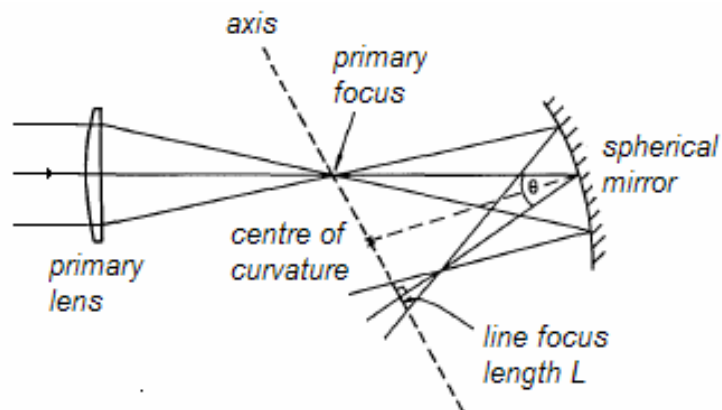


Figure 7.1 Schematic of a line focus design using a concave mirror.

An alternate method for focusing laser radiation into a line is with an off-axis concave mirror [Ross et. al. 1987]. In this case, a spherical mirror is added to the normal point-focus system (Fig. 7.1). Such a mirror is placed at the determined angle to the coming radiation that determines the length of focused line. At the fixed angle, the length of line can be varied by the limitation of the diameter of the incoming beam before it goes to the point-focus system.

Some new types of line focus geometries have been introduced to improve the uniformity along the line, that is, a cylindrical lens array in combination with a spherical lens [Wang et. al. 1992] or a segmented wedge array [Villeneuve et. al. 1991] with a cylindrical lens. Recently, a line focus system with a segmented prism array allowing to perform a uniform line focus for the length of 12 mm was developed in [Yamaguchi et. al. 1999].

Producing of gas streams with sharp boundary

There are two main types of gas nozzle constructions: sonic and supersonic. The first one is characterized by low Mach numbers ($M \approx 1$), has a parabolic gas density profile, and can be simply produced with a standard cylindrical nozzle [Li and Fedosejevs 1994]. The density profile from a sonic nozzle is only suitable for experimental needs at small distances from the nozzle, as in the far field it has a smeared density profile. The supersonic nozzle ($M > 1$) is capable for producing rectangular profiles, but requires low densities. Such nozzles have mostly conical geometries.

The conical nozzle with optimized length is easy to produce and provides a good density distribution. Such a nozzle was developed in [Semushin and Malka 2001] and is shown in Fig. 7.2, where all import parameters are designated. The optimal configurations were computed for different output jet diameters, and throat diameters. In Table 7.1 the optimal values of parameters presented in Fig. 7.2 are given with the resulting Mach numbers and mean exit densities at 0.5 mm. Smaller output diameters give lower Mach numbers and higher densities with smoother profiles. To produce steep profiles one needs to diminish the output density. The received profiles are nearly rectangular for a nozzle for critical and exit diameters given in the Table 7.1.

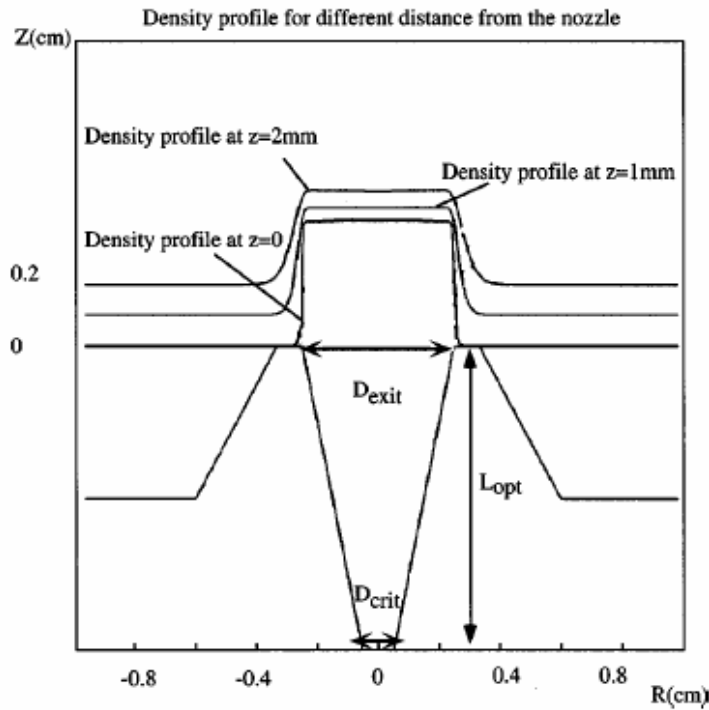


Figure 7.2 The conical nozzle construction. The optimal values of given parameters for providing a good density distribution are shown in the table 7.1.

Table 7.1 Optimized nozzles parameters D_{crit} , D_{exit} , and L_{opt} , which are defined in Fig. 7.2. M_{exit} - the Mach number and n_{exit} is the density at 0.5 mm from the nozzle.

| $D_{crit}(\text{mm})$ | $D_{exit}(\text{mm})$ | $l_{opt}(\text{mm})$ | M_{exit} | $n_{exit}(\text{cm}^{-3})$ |
|-----------------------|-----------------------|----------------------|------------|----------------------------|
| 1 | 2 | 6 | 3.5 | 18×10^{19} |
| 1 | 3 | 7 | 4.75 | 7.5×10^{19} |
| 1 | 5 | 10 | 7 | 2.7×10^{19} |
| 1 | 10 | 15 | 10 | 0.75×10^{19} |
| 0.5 | 1 | 4 | 3.3 | 16×10^{19} |
| 0.5 | 2 | 5 | 5.5 | 4.5×10^{19} |
| 0.5 | 3 | 5 | 6.2 | 2.1×10^{19} |
| 0.5 | 5 | 7 | 9.5 | 0.7×810^{19} |
| 0.5 | 10 | 15 | 14.5 | 0.2×10^{19} |

Such a conical nozzle, with critical D_{crit} and exit diameters D_{exit} of 0.5 mm and 2 mm, was tested in our experiments, and sharp boundary of gas jet region was observed by detecting the charge transfer signal scanned through the boundary region of gas jet. However, higher backing pressure was necessary due to large exit

diameter output. This caused too high pressure in the vacuum chamber and limited the further use of the nozzle.

For the planned lasing experiment it is important to produce a gas stream in a form of an elongated gas sheet with sharp boundary. The desirable parameters of such jet are: 10 mm in length and 1 mm in width. Unfortunately, there are no standard solutions, and in the simplest case, one could apply the standard cylindrical nozzle equipped with cylindrical tube flattened out at the end so that the exit slit was 10×0.5 mm. Such a construction was tested in our experiments and allowed us to create an appropriate gas stream with densities up to 10^{17} cm^{-3} .

Desirable geometry for lasing experiments

The ideal scenario for charge transfer pumping is depicted in Fig. 7.3. The required ions should be produced with the use of a femtosecond laser focused into a line as described above. The gas particles in a form of sheet with densities of 10^{17} cm^{-3} should be produced by a suitable nozzle design as well. The best distance in a line focus configuration is found to be 2 mm since the plasma expansion in such geometry is more directed and the density scales as $1/R^2$. The spontaneous emission then will be amplified along the elongated interaction zone and could be further amplified in a half-cavity configuration (by using one reflection from mirror).

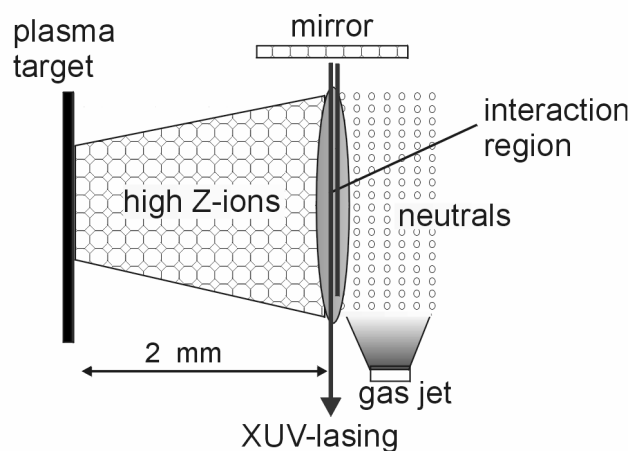


Figure 7.3 The ideal scenario for charge transfer laser: high Z-ions produced with fs-lasers in line focus geometry interacting with a gas jet having a sharp boundary.

7.2 Hydrogen like Beryllium as an ideal candidate for lasing

As it was shown in chapter 3, the charge transfer reaction is quasi-resonant, and it pumps better the levels of newly created $A^{(n-1)+}$ ions which have the energy E_u , corresponding to the energy of the upper laser level, determined by

$$E_{up} \approx E_{ion}(A^{(n-1)+}) - E_{ion}(B) - \Delta E \quad (7.1)$$

where $E_{ion}(A^{(n-1)+})$ is the ionization potential of $A^{(n-1)+}$ ions, $E_{ion}(B)$ is the ionization potential of the species (neutrals in our case) interacting with the ions, and $\Delta E \approx 10-20$ eV is the energy decrement discussed in chapter 3.

Of special interest is to pump selectively the level $n=3$ of hydrogen like ions with the subsequent lasing on 3-2 transition, which has been already demonstrated with recombination excitation mechanism for Carbon [Suckewer et.al. 1985] [Lee and Kim 2001] and Boron [Goltsov et. al. 1999] ions. The best appropriate gas reagent for an ion-neutral charge transfer reaction is found to be hydrogen, since it has usually the largest cross section compared with other gases.

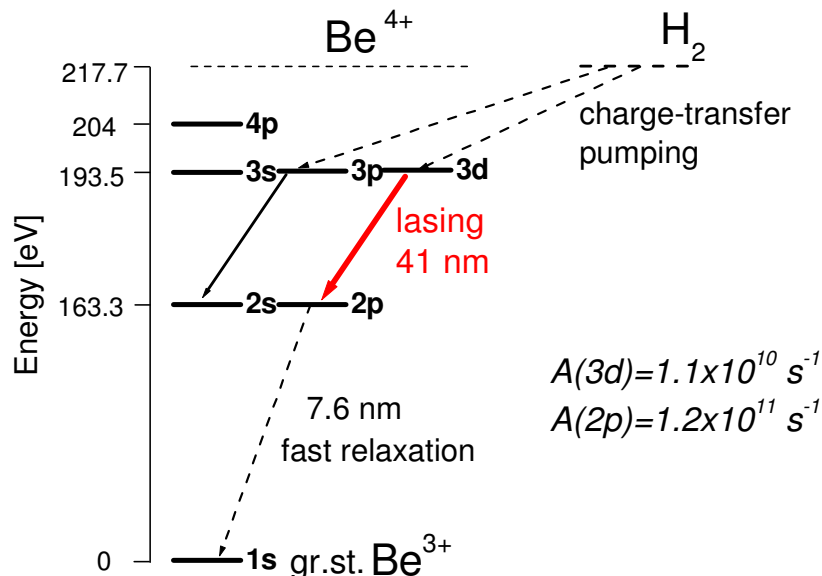
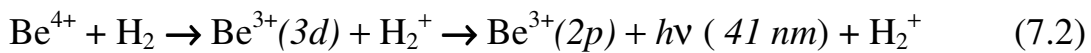


Figure 7.4 The simplified energy level diagram of Be^{3+} ions

According to these requirements, one can find that the ideal candidate for realization of lasing on 3-2 transition of Hydrogen like ions with charge transfer pumping is Beryllium. It has the optimum defect of energy $\Delta E \approx 11$ eV for the $n=3$ level by applying the hydrogen gas jet. The simplified scheme for relevant energy levels in Be^{3+} ions is shown in Fig. 7.4. Firstly, one needs to create the nuclear Beryllium ions and then make them interact with neutrals at relevant conditions for charge exchange pumping. At that time, according to equation (7.1), the level $n=3$ will be selectively pumped, and significant population can be build-up in the Be^{3+} 3d state. This process can be written as



The cross section of this reaction was calculated in [Harel et. al. 2001] and shown in Fig. 7.5, and it is as high as $2 \times 10^{-15} \text{ cm}^2$ for the laser produced Be^{4+} ions having velocities of about 0.15 a.u. ($3 \times 10^7 \text{ cm/sec}$).

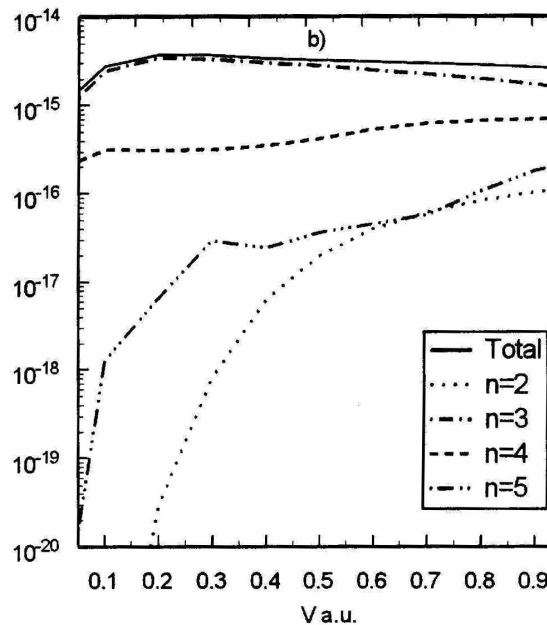


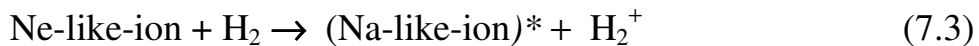
Figure 7.5 Total and n -partial cross sections as function of impact velocities for $\text{Be}^{4+} + \text{H}$ reaction calculated by [Harel et. al. 2001].

This analysis shows that Beryllium is an interesting candidate for lasing in Hydrogen like ions with charge transfer pumping. The lasing is possible on 3d-2p transition at 41 nm. Unfortunately, handling of Beryllium is difficult and Beryllium dust is very dangerous.

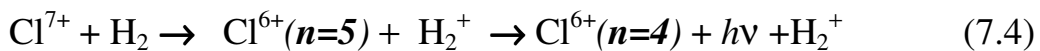
7.3 Extensions to non-Hydrogenic ions – lasing in Na-like ions with higher efficiency

A possible extension of the basic hydrogenic concept described above to plasmas that can be produced with greater efficiency is of interest. The best candidates are the ions with single outer electrons, as Li-like, Na-like, Cu-like ions, for corresponding lasing transitions between quantum numbers 4-3 (5-3), 5-4 (6,7,...-4), 6-5 (7,8,..-5) accordingly. This will open a great possibility to scale further to shorter wavelengths with the same required pumping power.

For charge exchange pumping experiments it is very important to have in the plasma only one desirable sort of ions, and the significant advantage for the above proposes is, that one can have only He-, Ne-, or Ni-like ions in the plasma, since these ions have a fully occupied outer shell and are hard to ionize. This results in a high relative abundance of the desirable ions over a wide range of plasma parameters. In the expanding plasma the ions with lower ionization stage are always behind these closed shell ions due to lower velocities. These abundant ions can further interact with neutral atoms with producing population inversion for Li-, Na-, Cu-like ions, as shown, for example, below for Na-like ions



A first suitable candidate for lasing in Na-like ions with charge exchange pumping is Chlorine. This process is described by the reaction



Since the lower laser level belongs to $n=4$, from which there is fast relaxation to a ground level, the first suitable for lasing situation takes place by capture of an electron into level $n=5$. The best decrement in energy of about 15 eV in this case is for the Cl^{6+} ions as depicted in Fig. 7.6, where the spontaneous rate coefficients are given for all transition of interest. It should be noted, that the lasing then is possible at a wavelength of 48.7 nm with the an energy required for producing of Cl^{7+} ions of 114

eV. It should be noted that the lasing in Na-like copper ions was already demonstrated with collisional recombination mechanism [Zhang et.al. 1996] on the $5g-4d$ transition at 11.1 nm. However, for this demonstration the authors needed to use a high power Nd:glass laser system delivering 20 J in 2 ps.

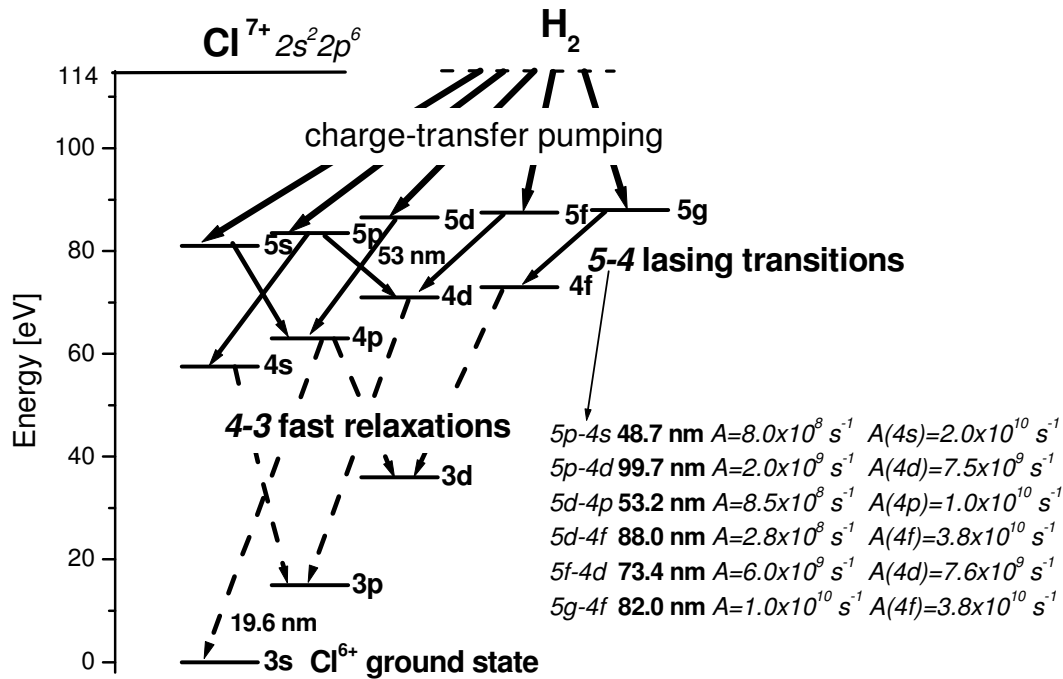
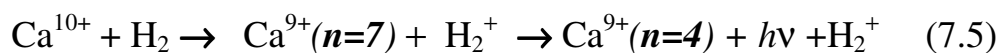


Figure 7.6 Simplified level diagram of Cl^{6+} ions with indication of charge-transfer pumped levels due collision of Cl^{7+} ions with hydrogen.

In order to go to shorter wavelengths, one has to realize appropriate conditions for the pumping of levels higher than $n=5$. One can find that, for example, for the interaction of Ne-like Calcium ions with Hydrogen gas jet described by the Eq. (7.5),



the appropriate levels of population belong in this case to the level $n=7$ as shown in Figure 7.7., with possible lasing on $7-4$ transitions at wavelength as short as 15.9 nm.

It should be noted, that as the charge exchange pumping takes place from the upper states (not by excitation from the ground state of a given ion to the upper laser level) a lasing might also be realized on the $7f-3d$ transition, since the state $3d$ is

placed relatively high from the ground 3s state, which corresponds to 51 eV and might be therefore unoccupied. This would allow the lasing at wavelength already at 9.4 nm.

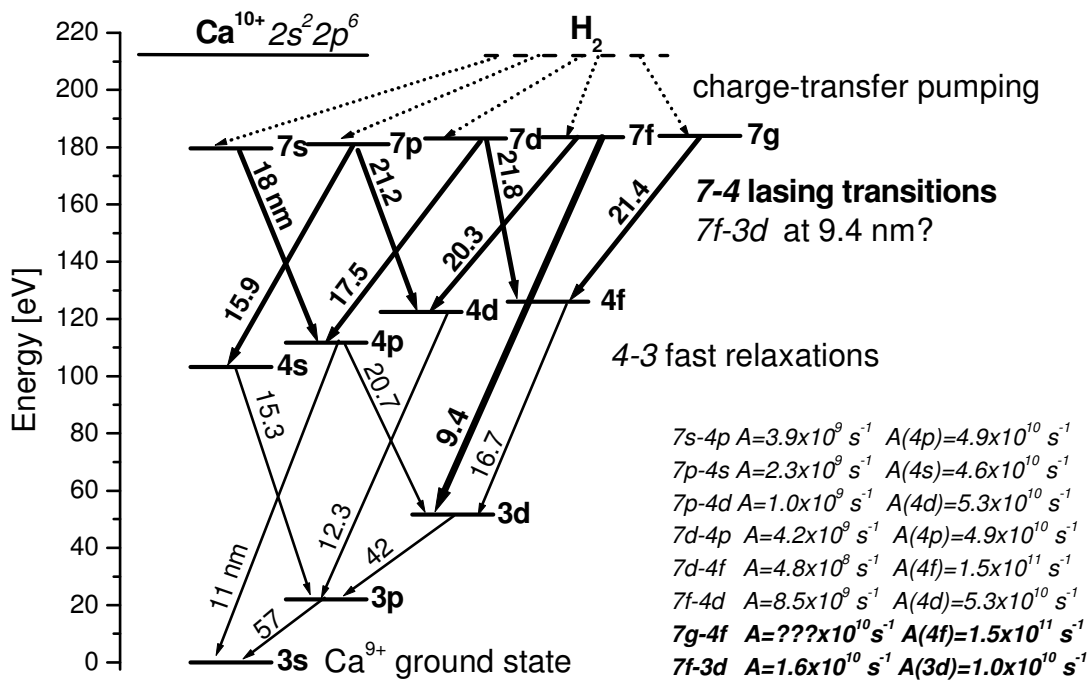


Figure 7.7 Simplified level diagram of Ca^{9+} ions with indication of charge-transfer pumped lines due to collision of Ca^{10+} ions with hydrogen.

The spontaneous emission rates for the lower laser levels ($n=4$), indicated in Figures 7.6 and 7.7, were calculated as a sum of probabilities for all possible decays from this level.

Finally, it should be concluded, that there are two main advantages by charge transfer pumping of Na-like ions:

- it requires the production of Ne-like ions, that allows to create a high abundance of such ions over a wide range of plasma parameters
- it opens a great possibility to scale to shorter wavelengths with the same required pumping power in comparison with hydrogen like ions.

This idea can be next extrapolated for the Cu-like ions with further improvement in efficiency.

7.4 The idea of quasi-steady state charge transfer pumping

The lasing in quasi-continuous regime was successfully realized with electron collisional excitation and in particular was described in chapter 2.3.1. And, therefore, it is of great interest to check whether it is possible to apply charge exchange pumping in quasi-steady state operation. The idea is to pump by charge exchange both the upper and lower laser levels (or in ideal case, only the upper level). Then a population inversion is obtained if the lower state depopulates rapidly to the ground state.

7.4.1 Results on pumping of Ne-like Silicon ions

The first attempts in the direction of quasi-continuous pumping by charge exchange were done with Ne-like Silicon. A simplified energy level diagram is shown in Fig. 7.8. For the $3p$ - $3s$ transition of Ne-like silicon the gain was already demonstrated in [Li et. al. 1997] with electron collisionally excitation.

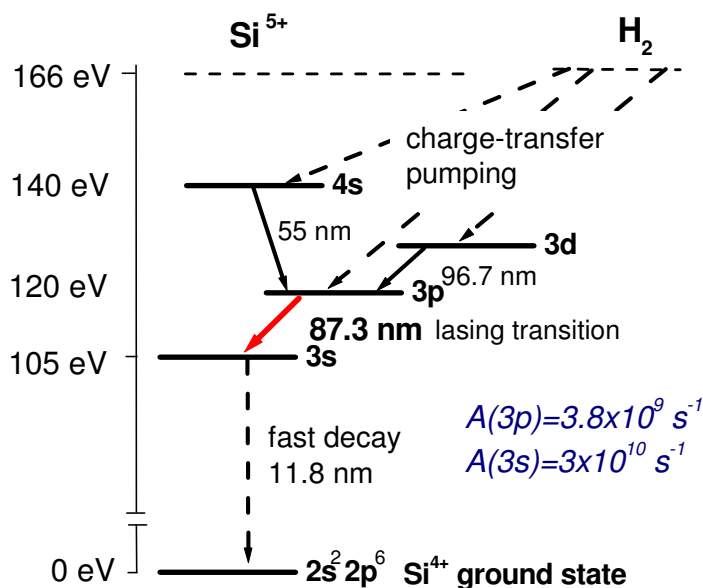


Fig. 7.8 Simplified level diagram of Si^{4+} ions with indication of charge-transfer pumped lines due to collision of Si^{5+} ions with hydrogen

This scheme is not ideally suited for direct pumping the $3p$ level by charge exchange, since the level $4s$ has more suitable decrement in energy to be pumped firstly. However, the level $3p$ can be populated due to three distinct processes: - direct charge exchange pumping, - population due to $4s-3p$ transition, and, lastly, - due to $3d-3p$ transition as depicted in fig. 7.8. On the other hand, the level $3s$ can be populated only due to charge transfer excitation but already at a slower rate, and moreover it depopulates rapidly to the ground state. Since the level $3p$ is metastable, the condition for lasing on the $3p-3s$ transition is fulfilled.

The experimental arrangement was similar to that described in chapter 5, but with two differences. Instead of Jobin Yvon the “Minuteman 302VM” monochromator was applied in order to record the spectra in range from 500 nm to 150 nm, where all lines of interest of Silicon ions are presented, and secondly, the radiation of Ti:sapphire laser was focused into a line (not a spot-focus). The laser radiation was focused via two cylindrical lenses ($f_1=240$ mm, $f_2=160$ mm) into a line of 2 mm in length and about 200 μm in width, the lenses were placed perpendicular to each other and the distance between them was about 3-5 cm (for different lengths of line focus). The spectroscopic resolution of the “Minuteman 302VM” monochromator was about 3 nm, and, therefore, the lines recorded are broad, but still good identified.

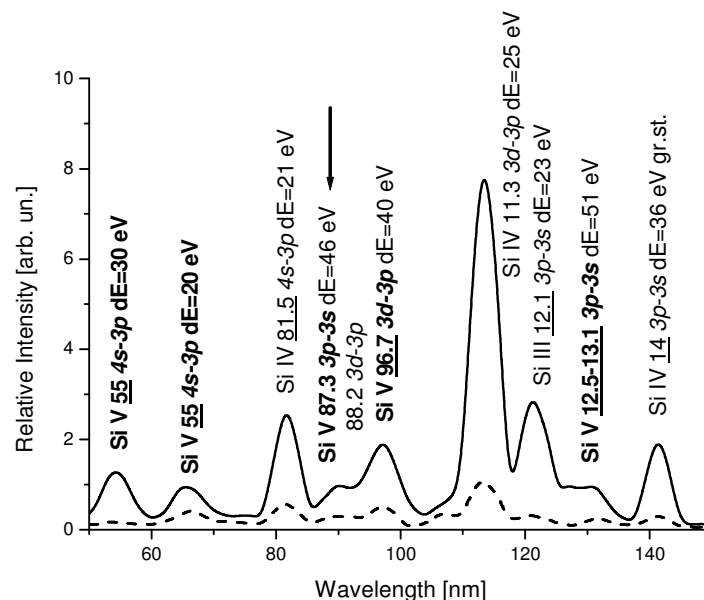


Figure 7.9 Example of Silicon spectra recorded at 2.5 mm distance from the target surface with 2 mm line focus ablation. Dashed line: in vacuum, solid line: at 100 mbar H_2 backing pressure.

Part of a recorded spectrum is shown in Fig 7.9. The spectrum was obtained with a laser energy of 200 mJ, and pulse duration of 100 fs, which was the maximum energy available at that time. An increase in the transition of interest at 87.3 nm and another $3p$ - $3s$ transition at 12.5 nm was observed, although the best increase was observed for the transitions from high lying levels $4s$ and $3p$ which have more suitable energy decrement ΔE as can be seen from Fig. 7.8 for the reaction below



The increase in intensities of different lines, shown in Fig. 7.9, as a function of the energy decrement ΔE is shown in Fig. 7.10 for Si^{4+} and in Fig. 7.11 for Si^{3+} . One can see that for charge transfer reaction between Si^{5+} and H_2 as well for similar reaction between Si^{4+} and H_2 , there is a clear maximum for an energy decrement of 10-20 eV. This proves experimentally, that the charge transfer reaction has a quasi-resonant character and is most probable for $\Delta E \approx 10$ -20 eV.

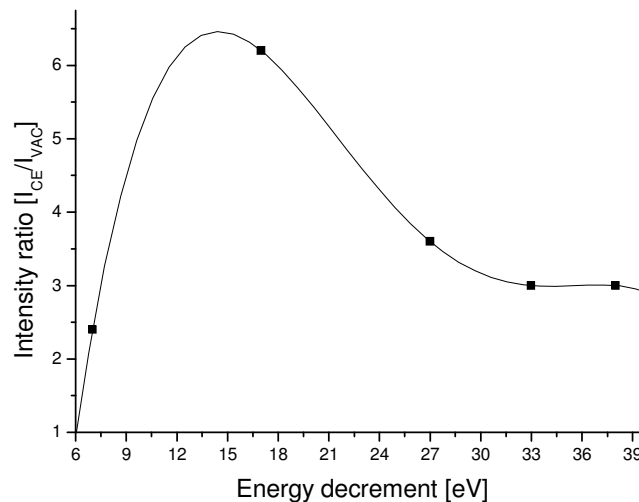


Figure 7.10 The increase in intensities of different lines of Si^{4+} ions (shown in Fig. 7.9) as a function of energy decrement ΔE (solid line just connects the measurement points)

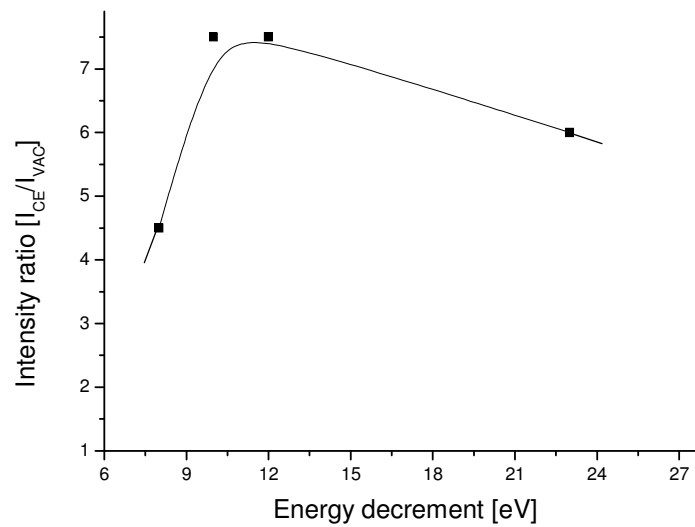


Figure 7.11 The increase in intensities of different lines of Si^{3+} ions (shown in Fig. 7.9) as a function of energy decrement ΔE (solid line just connects the measurement points)

Although the good increase in intensity of $3p$ - $3s$ lines was observed, for lasing experiments a line focus of more than 10 mm in length [Li et. al. 1997] is necessary. The further scaling with the Ne-like sequence to shorter wavelengths with charge transfer pumping is difficult while the energy defect of is too high, and therefore the higher levels ($n=5,6,..$) will be pumped firstly and the population inversion between $3p$ and $3s$ states can be achieved only due to cascade transitions from the higher levels, which makes the scheme more complicated and implies additional losses. As an alternative way, one can try to find appropriate interacting components for lasing in Ni- or Pd-like ions.

7.4.2 $3p$ - $3s$ transition of O^{3+} at 307 nm as an ideal tool to check lasing by charge transfer in a normal operating laser mode with cavity

In order to better understand the relevant conditions for the operation of charge exchange lasers in XUV range, it would be of great interest to construct first such a laser in the visible or ultraviolet spectral region, where one could use mirrors and operate a laser in a normal mode with cavity.

One of the possible candidates could be Boron-like Oxygen. The simplified energy levels of O^{3+} ions are depicted in Fig. 7.12.

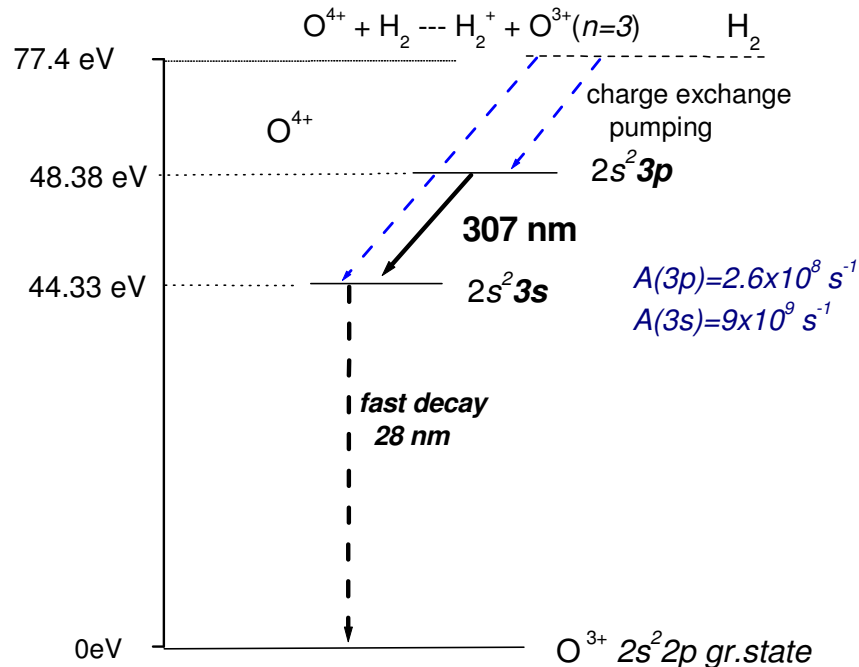


Fig. 7.12 Simplified level diagram of O^{3+} ions with indication of charge transfer pumped levels due to collision of O^{4+} ions with hydrogen.

Here, both the $3p$ and $3s$ states will be populated by charge exchange with rapid depopulation of the $3s$ state. Since the spontaneous rate of the $3s$ state is almost 2 orders of magnitude higher than that of the $3p$ state, the condition for quasi-steady state operation is fulfilled for the $3p$ - $3s$ transition at 307 nm. And for this wavelength one can simply apply mirrors to construct a resonator in a way similar as depicted in Fig. 7.3. The ions can be produced by laser ablation of oxygen containing solid targets (for example Al_2O_3 , SiO_2 or other) in a line focus configuration as described above. A big increase in line intensities for transitions to the ground state from the lower laser $3s$ state at 28 nm was already observed (Fig. 6.16).

It can be estimated that production of O^{4+} will not require very powerful pump lasers, and a potential gain and lasing at the 307 nm transition is more easily detectable as compared to the XUV range.

8. Summary

In this dissertation a novel experimental scheme for studying charge exchange interactions between ions and neutrals is introduced and investigated as a potential tool for the pumping of the lasers in the extreme ultraviolet (XUV) spectral range. The basic idea behind the new setup is the use of a femtosecond laser for the plasma production by ablation of solid targets and a gas jet for the supply of the neutrals. By this, steep density gradients of the emerging plasma front and of the gas jet can be achieved, those are necessary for an effective charge transfer interaction at high densities of ions and neutrals in the interaction zone. To achieve sufficient gain for lasing at XUV transitions, the densities of ions and neutrals in the interaction region should be more than 10^{16} cm^{-3} . At these densities the interpenetration length will be well below 1 mm, which means that the transversal dimension of the inverted volume will only be at the order of several hundreds of micrometers. That is why steep density gradients are essential.

For optimization of the new setup and principal investigations on parameter dependencies, the charge transfer reaction $\text{C}^{4+} + \text{H}_2 \rightarrow \text{C}^{3+} (n=3) + \text{H}_2^+$, well known from studies related to astrophysics, was explored. For this, the short pulse pump laser radiation is focused to a spot of about 200 μm at the surface of a solid Carbon target. Plasma is produced at intensities of about 10^{15} W/cm^2 . The gas jet is located at distances of 1 mm from the target surface. Spectral intensities of plasma lines are used as indicators for the pump processes. Clear selective pumping of levels $n=3$ of C^{3+} ions up to a few mm distance from the solid target was observed at densities of the gas jet around $7 \times 10^{16} \text{ cm}^{-3}$, while the population of other levels with $n \geq 4$, which could not be pumped with charge transfer mechanism, remained unchanged or even slightly decreased. By the use of laser pulses with different pulse durations it was also demonstrated, that in fact the short pulses are more favorable for the production of the plasma, leading to a steeper density gradient of the plasma front. The selectivity of the charge transfer pumping was further tested by using a Helium gas jet instead of the hydrogen, and this resulted in an equal effect for all lines as predicted, since Helium is non-resonant to all lines due to higher ionization potential.

For the first time, time resolved measurements of the charge exchange process have been performed. This allowed to specify the time behaviour of the interaction and to perform a quantitative comparison with a developed analytical model. From this analysis it can be seen that strong charge exchange pumping occurs predominantly at the plasma front, and it can be deduced, that in fact charge exchange pumping at densities of both reagents exceeding $2 \times 10^{16} \text{ cm}^{-3}$ was achieved, which should be sufficient for XUV lasers.

With the optimized setup, investigations on a number of promising reactions capable of creating a population inversion in the XUV spectral range been performed. A strong increase in line intensities was observed for the $3d-2p$ ($\lambda=23.8 \text{ nm}$) and the $2p3s-2p^2$ ($\lambda=37.4 \text{ nm}$) lines of O^{3+} and O^{2+} ions as a result of the reactions $\text{O}^{4+} + \text{H} \rightarrow \text{O}^{3+} + \text{H}^+$ and $\text{O}^{3+} + \text{H} \rightarrow \text{O}^{2+} + \text{H}^+$, correspondingly. Interestingly, for the 37.4 nm line gain was recently demonstrated in an optically field ionization recombination scheme [Chichkov et. al. 1995]. As this is a ground state transition, it is, however, doubtful at present to forecast whether a population inversion by charge exchange alone will be sufficient for producing gain.

To explore a transition where gain and lasing in the XUV is well known, the reaction $\text{C}^{6+} + \text{H} \rightarrow \text{C}^{5+} (n=3,4) + \text{H}^+$ was investigated. The $3-2$ transition in C^{5+} is operated since long time as a recombination laser transition [Suckewer et. al. 1985], implying that already in a pure C^{6+} plasma expanding into vacuum an inversion may be generated. Again, a clear increase of line intensities originating from the levels $n=4$ and 3 of the C^{5+} ions was obtained with the hydrogen jet present as compared to the vacuum case, where the levels are pumped by recombination. To generate the C^{6+} plasma with a spot focus ablation, an energy of about 200 mJ was necessary. To explore the possibility for producing gain (lasing), instead of a point focus a line focus at the target has to be used to generate an elongated plasma column. Extrapolating from the point focus intensity, this would require a short pulse pump laser energy of about 3 J for a line focus of about 1 cm length. As such a laser energy can not be delivered from the here used laser system, some first test experiments have been performed at the Max Born institute in Berlin, where a more powerful laser exists. It was revealed, that with 2.5 J of a 6 ps laser pulse, a sufficient amount of C^{6+} ions can be generated for a line focus of about 1 cm in length and 0.07 cm in width. To perform charge exchange lasing experiments with such a line focus plasma, in addition a specific nozzle, such as a slit nozzle, for producing an elongated gas jet

area has to be used. A corresponding experimental scheme with suitable optics for an optimal line focus and an improved nozzle design is briefly outlined.

Since lasing in hydrogen like ions with charge transfer excitation requires the production of bare ions such as, for example, C^{6+} ions for the $C^{6+} + H_2$ reaction, the high energies are necessary. Therefore, some novel schemes are described those might overcome the problem of high energy requirements. Instead of lasing on transitions in Hydrogen-like ions, corresponding transitions in Na-like ions such as Chlorine or Calcium are considered, starting with producing Ne-like ions. For example, in case of the reaction $Ca^{10+} + H_2 \rightarrow Ca^{9+}(n=7) + H_2$, lasing is possible at a wavelength as short as $\lambda=15.9$ nm which is even shorter than in case of lasing in C^{5+} ions with $\lambda=18.2$ nm, but requires much less pump energy due to smaller ionization potential of needed Ca^{10+} ions (211 eV) in comparison with C^{6+} ions (490 eV). In case of the reaction $Cl^{7+} + H_2 \rightarrow Cl^{6+}(n=5) + H_2$ with possible lasing at 48.7 nm, the needed pump energy is even smaller, as ionization potential of Cl^{7+} is only 114 eV. For lasing in Na-like ions, it is necessary to produce the Ne-like ions, which have the closed shell and hard to be ionized further. This is a big advantage, since one can create a high abundance of such ions over a wide range of plasma parameters.

In so far considered schemes, inversion will only be generated in a short time interval. It might also be interesting to explore quasi steady state charge exchange pumping, in a similar way as this is known from electron collisional excitation laser schemes. The idea consists in pumping by charge exchange both the upper and lower laser levels. If the upper level is pumped at a slightly higher rate (having the larger cross section) and the lower level is rapidly depopulated by radiative decay, steady state inversion is possible. A potential scheme with Si^{5+} ions for this purpose is suggested and first results are presented.

As XUV lasers are difficult to realize, it might be of interest to first demonstrate a charge exchange pumped laser with the new scenario at a laser transition in the visible or near UV spectral range, where the stimulated emission cross section is larger and where the possibility exists to use a cavity for a further reduction of the inversion density and necessary pump power. Such a transition might be the $3p-3s$ transition at 307 nm in O^{3+} ions.

In conclusion, considerable progress on charge exchange pumping for XUV lasers has been achieved in this work with a new developed experimental scheme. For the first time charge exchange pumping at densities necessary for gain has been

demonstrated, and a variety of new schemes have been proposed. This gives big hopes that with further possible improvements of the experimental setup and with more powerful pump lasers, charge exchange pumped lasers at XUV transitions will be realized in the future.

REFERENCES

Afanasiev Yu. A. and Shlyaptsev V. N. "Formation of a Population Inversion of transitions in Ne-like ions in steady state and transient plasmas" 1989 *Sov. J. Quantum Electron.* **19** 1606

Barany A., Danared H., Cederquist H., Hvelplund H., Knudsen H., Pedersen J.O.K., Cock C.L., Tunnel L.N., Wagonner W., and Gisce G.P. "Stueckelberg angular scattering oscillations in two-electron capture by C^{4+} from He at low energies" 1985 *J.Phys. B.* **19** L427

Beijers J. P. M., Hoekstra R., Schlatmann A. R., Morgenstern R. and F.J. de Heer "State-selective electron capture in slow collisions of C^{6+} and O^{6+} with He" 1992 *J. Phys. B* **25** 463

Boehly T., Russotto M., Craxton R. S., Epstein R., Yaakobi B. Da Silva L. B., Nilsen J., Chandler E. A., Fields D. J., MacGowan B. J., Matthews D. L., Scofield J. H., and Shimkaveg G. "Demonstration of a narrow-divergence x-ray laser in neonlike titanium" 1990 *Phys. Rev. A* **42** 6962

Brabec T. and Krausz F. "Intense few-cycle laser fields: Frontiers of nonlinear optics" 2000 *Phys. Rev. Mod.* **72** 545

Bransden B.H. and McDowell M.R. "Charge exchange and the theory of ion-atom collisions" *Clarendon Press, Oxford* 1992

Bohr N. and Lindhardt J. K. 1954 *Dan.Vid.Sel.Mat.Phys.Medd.*, **28** No7

Cederquist H., Andersen L. H., Barany A., Hvelplund P., Knudsen H., Nielsen E. H., Pedersen J. O. K. and Sorensen J. "State-selective single- and double-electron capture processes in slow $C^{4+} + He, Ne, Ar$ and Xe collisions" 1985 *J. Phys. B* **18** 3951

Chichkov B. N., Egbert A., Mayer S., Wellegehausen B., Aschke L., Kunze H.J., and Kato Y. "Soft-X-Ray Lasers with Charge Transfer Pumping in a Mixture of Clusters and Atomic Gases" 1999 *Jpn. J. Applied Phys.* **38** 1975

Chichkov B. N., Egbert A., Eichmann H, Momma C, Nolte S and Wellegehausen B., "Soft-x-ray lasing to the ground states in low-charged oxygen ions" 1995 *Phys. Rev. A* **52** 1629

Daidoo H. "Review of soft x-ray laser researches and developments" *Rep. Prog. Phys.* 2002 **65**1513

Dijkkamp D., Ciric D., De Heer F. J., and Vlieg E. " (n,l) -Subshell electron capture cross sections in collisions of C^{4+} , N^{5+} and O^{6+} with atomic hydrogen" 1985 *Nucl. Instr. Meth. Phys. Res. B* **9** 403

Dixon R.H. and Elton R.C. "Resonance Charge Transfer and Population Inversion Following C^{5+} and C^{6+} Interactions with Carbon Atoms in a Laser-Generated plasma" 1977 *Phys. Rev. Letters* **38** 1072

Dixon R.H., Seely J.F., and Elton R.C. "Intensity Inversion in the Balmer spectrum of C^{5+} " 1978 *Phys. Rev. Letters* **40** 122

Duguay M. A. and Rentzepis P. M. "Some approaches to vacuum and X-ray lasers" 1967 *Appl. Phys. Lett.* **10** 350

Elton R. C. "X-Ray Lasers" *Academic Press, London* 1990

Emma P., Bane K., Cornacchia M., Huang Z., Schlarb H., Stupakov G., and Walz D. "Femtosecond and Subfemtosecond X-Ray Pulses from a Self-Amplified Spontaneous-Emission-Based Free-Electron Laser" 2004 *Phys. Rev. Lett.* **92** 074801

Errea L. F., Gorfinkiel J. D., Harel C., Jouin H., Macías A., Méndez L., Pons B. and Riera A. "Model potential treatment of $C^{4+} + H_2$ collisions at low impact energies" 2000 *J. Phys. B* **33** 3107

Errea L. F., Harel C., Illescas C., Jouin H., Méndez L., Pons B. and Riera A. "Convergent molecular close-coupling calculations for ion-atom collisions from low to intermediate energies" 1998 *J. Phys. B.* **31** 3199

Goldstein W.H., Zigler A., Burkhalter P.G., Nagel D.J., Bar-Shalom A., Oreg J., Luk T.S., McPherson A., and Rhodes C.K. „X-ray emission from a 650-fs laser produced barium plasma“ 1993 *Phys. Rev. E* **47** 4349

Goltsov A, Korobkin D, Morozov A and Suckewer S "Very compact soft x-ray lasers and their potential applications" 1999 *Plasma Phys. Control. Fusion* **41** A595

Grandall D.H., Mallory M.L., and Kocher D.C. "Charge exchange between multicharged ions of C, N, and O and molecular hydrogen" 1977 *Phys. Rev. A* **15** 61

Griem H. "Plasma Spectroscopy" McGraw-Hill, New York, 1964

Grozdanov T.P. 1980 "Classical model for electron capture in collisions of highly charged, fully stripped ions with hydrogen atoms" *J. Phys. B.* **13** 3835

Gudzenko L. I. and Shelepin L. A. 1965 *Sov. Phys. Doki.* **10** 147 *Dokl. Acad. Nauk SSSR* **160** 1296

Hagelstein P. L., *Proc. OSA Meeting on Short Wavelength Coherent Radiation: Generation and Applications*, edited by R. W. Falcone and J. Korz, 1988 p. 28

Harel C., Jouin H., Pons B., Errea L.F., Gorfinkiel J.D., Illescas C., Macias A., Méndez L., and Riera A. "Calculations of Charge Transfer and Ionization Cross Sections in Collisions between Multicharged ions A^{q+} ($1 \leq q \leq 8$) and atomic Hydrogen" 2001 *APID* **9**

Ilcisin K. J., Aumayr F., Schwob J. L., and Suckewer S. „Demonstration of resonant fluorescence in Mo VII induced by Mo XII for possible lasing near 600 Å“ 1994 *J. Opt. Soc. Am. B* **11** 1436

Irons F.E. and Peacock N.J. “A spectroscopic study of the recombination of C⁶⁺ to C⁵⁺ in an expanding laser-produced plasma” 1974 *J. Phys. B* **7** 2084

Keane C. J., Ceglio N. M., MacGowan B. J., Matthews D. L., Nilson D. G., Trebes J. E. and Whelan D. A. “Soft x-ray laser source development and applications experiments at Lawrence Livermore National Laboratory” 1989 *J. Phys. B* **22** 3343

Key M.H., Barbee J.R., DaSilva L. B., Glendinning S. G., Kalantar D. H., Rose S. J., Weber S. V. „New plasma diagnostic possibilities from radiography with x.u.v. lasers“ 1995 *J. Quant. Spectrosc. Radiat. Transfer* **54** 221

Koch L. “Untersuchungen an einem Hochleistungs-Titan-Saphir-Lasersystem - Experimenten an laserinduzierten Lithiumplasmen” *Institut für Quantenoptik der Universität Hannover*, Diplomarbeit, Februar 2003

Lawrence G.N. “Proposed international standards for laser beam quality falls short” *Laser Focus World*, July 1994, 109

Lee K. and Kim D. “Another regime of operation for a 18.2 nm recombination laser using a capillary-discharged carbon plasma” 2001 *Appl. Phys. Lett.* **79** 1968

Li Y.M. and Fedosejevs R. “Density measurements of a high-density pulsed gas jet for laser-plasma interaction studies” 1994 *Meas. Sci. Technol.* **5** 1197

Li Y., Lu P., Pretzler G., Fill E. E. “Lasing in neonlike sulphur and silicon” *Opt. Commun.* 1997 **133** 196

MacGowan B. J., Da Silva L. B., Fields D. J., Keane C. J., Maxon S., Osterheld A. L., Scofield J. H., and Shimkaveg G. „Observation of $3d^8 4d-3d^8 4p$ soft-x-ray laser emission in high-Z ions isoelectronic to Co I” 1990 *Phys. Rev. Lett.* **65** 2374

MacGowan B. J., Maxon S., Hagelstein P. L., Keane C. J., London R. A., Matthews D. L., Rosen M. D., Scofield J. H., and Whelan D. A. „Demonstration of soft x-ray amplification in nickel-like ions“ 1987 *Phys. Rev. Lett.* **59** 2157

Maiman T.H. “Stimulated Optical radiation in ruby” 1960 *Nature* 187 493

Maine P., Strickland D., Bado P., Pessot M., and Mourou G. “ Generation of Ultrahigh Peak Power Pulses by Chirped Pulse Amplification” 1988 *IEEE J. Quant. Electron.* **24** 398

Mapleton R.A. “Theory of Charge Echange” *Wiley, New York* 1972

Matthews D.L., Hagelstein P.L., Rosen M.D., Eckart M.J., Ceglio N.M., Hazi A.U., Medeck H., MacGowan B.J., Trebes J.E., Whitten B.L., Campbell E.M., Hatcher C.W., Hawryluk A.M., Kauffman R.L., Pleasance L.D., Rambach G., Scofield J.H., Stone G. and Weave T. A., “Demonstration of a Soft X-ray Amplifier” 1985 *Phys. Rev. Lett.* **54** 110

Neil G. R. and Merminga L. “Technical approaches for high-average-power free-electron lasers” 2002 *Rev. Mod. Phys.* **74** 685

Nickles P. V., Shlyaptsev V. N., Kalachnikov M. P., Schnürer M., Will I. and Sandner W. “Short Pulse X-ray Laser at 32.6 nm based on Transient Gain in Ne-like Titanium” 1997 *Phys. Rev. Lett.* **78** 2748

Orishich A.M. and Shaikhislamov I.F. 1992 *Russian J. of Applied Mech. and Tech. Phys.* **3** 13

Ozaki T., Ganeev R. A., Ishizawa A., Kanai T. and Kuroda H. “Highly Directive 18.9 nm Nickel-like Molybdenum X-Ray Laser Operating at 150 mJ Pump Energy” 2002 *Phys. Rev. Lett.* **89** 253902-1

Ponomarenko A.G., Shaikhislamov I.F., Zakharov Yu.P., Antonov V.M., Posukh V.G., Melekhov A.V. „Charge Exchange Pumping of Laser Produced Plasma colliding with vapor Cloud for lasing in XUV“ 1998 *J. Phys. D* **31** 2117

Porter J. L., Spielman R. B., Matzen M. K., McGuire E. J., Ruggles L. E., Vargas M. F., Apruzese J. P., Clark R. W., and Davis J. „Demonstration of population inversion by resonant photopumping in a neon gas cell irradiated by a sodium Z pinch“ 1992 *Phys. Rev. Lett.* **68** 796

Proceedings of 8-th Conf. on X-ray Lasers 2002 Aspen, Colorado.

Qi N., Hammer D. A., Kalantar D. H., and Mittal K. C., “Fluorescence in Mg IX emission at 48.340 Å from Mg pinch plasmas photopumped by Al XI line radiation at 48.338 Å” 1993 *Phys. Rev. A* **47** 2253

Rigazio M., Kharchenko V. and Dalgarno A. “X-ray emission spectra induced by hydrogenic ions in charge transfer collisions” 2002 *Phys. Rev. A* **66** 064701

Rocca J.J. “Table-top soft x-ray lasers” 1999 *Rev. Sci. Instr.* **70** 3799

Ross I. N., Boon J., Corbett R., Damerell A., Gottfeldt P., Hooker C., Key M. H., Kiehn G., Lewis C. and Willi O. „Design and performance of a new line focus geometry for x-ray laser experiments“ 1987 *Appl. Opt.* **26** 1584

Ruhl F., Aschke L., Kunze H.-J. „Selective Population of the n=3 level of hydrogen-like Carbon in Two Colliding Laser-produced Plasmas“ 1997 *Physics Letters A* **225** 107

Ryufuku H., Sasaki K. and Watanabe T. “Oscillatory behavior of charge transfer cross sections as a function of the charge of projectiles in low-energy collisions” 1980 *Phys. Rev. A* **21** 745.

Seely J.F. and McKnight "Soft x-ray laser pumped by charge exchange between C VII and Ar III in expanding laser-produced plasma" 1977 *Appl. Phys. B* **48** 3691

Semushin S. and Malkaa V. "High density gas jet nozzle design for laser target production" 2001 *Rev. Sci. Instrum.* **72** 2961

Shaikhislamov I.F. "Kinetika processa peresaryadnogo vsaimodeistviya plotnyx potokov" 2000 *Russian J. of Applied Mech. And Tech. Phys.* **41** 212

Shaikhislamov I.F. "Spectroscopic investigation of charge-transfer pumping of lithium-like O^{5+} ion" 2001 *J. Phys. D* **34** 1646

Shaikhislamov I.F., Zakharov Yu.P., Ponomarenko A.G., Posukh V.G., Melekhov A.V., Antonov V.M. and Vorontsov V.A. "Charge-transfer scheme of EUV laser" 2001 *Laser Physics* **11** 1069

Silfvast W.T., Macklin J.J. and Wood I.I.O.R. "High-gain inner-shell photoionization laser in Cd vapor pumped by soft-x-ray radiation from a laser-produced plasma source" 1983 *Opt. Lett.* **8** 551

Smirnov B.M. "Atomnye stolknoveniya i elementarnye processy v plasme" *Atomisdat, Moscow* 1968

Smith R. F., Dunn J., Nilsen J., Shlyaptsev V. N., Moon S., Filevich J., Rocca J. J., Marconi M. C., Hunter J. R., and Barbee T. W. "Picosecond X-Ray Laser Interferometry of Dense Plasmas" 2002 *Phys. Rev. Lett.* **89** 065004-1

Suckewer S., Skinner C.H., Milchberg H., Keane C. and Voorhees D. "Amplification of Stimulated Soft X-ray Emission in a confined plasma column" 1985 *Phys. Rev. Lett.* **55** 1753

Svelto O. "Principles of Lasers" *Plenum Press, New York* 1998

Theobald W., Haßner R., Kingham R., Sauerbrey R., Fehr R., Gericke D. O., Schlanges M., Kraeft W.-D. and Ishikawa K. "Electron densities, temperatures, and the dielectric function of femtosecond-laser-produced plasmas" 1999 *Phys. Rev. E* **59** 3544

Villeneuve D. M., Enright G. D., Baldis H. A., and Kieffer J. C. "Novel laser line focus geometry applied to X-ray lasers" 1991 *Opt. Commun.* **81**, 54

Vinogradov A.V. and Sobel'man I.I. "K probleme lasernyx istochnikov islucheniya v dalekoi ultravioletovoi i rengenovskoi oblasti spectra" 1973 *Sov. Phys. JETP* **63** 2113

Vorontsov V.A., Born M., Shaikhislamov I.F., Chichkov B.N., and Wellegehausen B. "Charge-transfer pumping for XUV lasers" 2003 *J. Phys. B* **36** 3865

Vorontsov V.A., Born M., Shaikhislamov I.F., Chichkov B.N., and Wellegehausen B. "Investigations on novel XUV-laser schemes" 2004 *Appl. Phys. B* **78** 979

Vorontsov V.A., Shaikhislamov I.F., Born M., Chichkov B.N., and Wellegehausen B. "Charge Transfer as Alternative Pumping Scheme for XUV Lasers" *Proceedings of IX Intern. Conf. on X-ray Lasers* Beijing, China, May 24-29, 2004

Wagner T., Eberl E., Frank K., Hartmann W., Hoffmann D. H. H., and Tkotz R. "XUV Amplification in a Recombining z-Pinch Plasma" 1994 *Phys. Rev. Lett.* **76** 3124

Wang J. G., Stancil P. C., Turner A. R., and D. L. Cooper "Charge transfer of O^{3+} ions with atomic hydrogen" 2003 *Phys. Rev. A* **67** 012710

Wang S. *et al.*, *X-Ray Lasers 1992*, edited by E. E. Fill IOP, Bristol, 1992

Xu Z.Z. Fan P.Z., Lin L.H., Li Y.L., Wang X.F., Li R.X., Lu P.X., Han S.S., Sun L., Qian A.D., Zhang Z.Q., and Zhou J.Z. "Short-wavelength Soft X-ray Amplification in a Lithiumlike Calcium Plasma" 1994 *Phys. Rev. A* **49** 485

Yamaguchi M., Ohchi T., Fujikawa C., Ogata A., Hisada Y. , Kazunobu Okasaka, Hara T., Tsunashima T., Yutaka Iizuka Y. “Line focus system with a segmented prism array for compact x-ray laser experiments” 1999 *Rev. Sci. Instrum.* **70** 1285

Yamakawa K., Chiu P.H., Magana A., and Kmetec J.D. “ Generation of high peak power femtosecond pulses at 10 Hz repetition rate in a titanium-doped sapphire laser” 1994 *IEEE J. Quant. Electron.* **30** 2698

Zhang J., Fill E.F., Li Y., Schlögl D., Steingruber J., Holden M., Tallents G. J., Demir A., Zeitoun P., Danson C., Norreys P. A., and Walsh F., Key M.H., Lewis C. L. S., McPhee A.G. “High-gain x-ray lasing at 11.1 nm in sodiumlike copper driven by a 20-J, 2-ps Nd:glass laser” 1996 *Optics Letters* **14** 10351

Zhang J., Key M.H., Norreys P.A., Tallents G.J., Behjat A., Danson C., Demir A., Dwivedi L., Holden M., Holden P.B., Lewis C.L.S., McPhee A.G., Neely D., Pert G.J., Ramsden S.A., Rose S.J., Shao Y.F., Thomas O., Walsh F. and You Y.L. “Demonstration of a High Gain in Recombination XUV Laser at 18.2 nm driven by a 20 J, 2 ps Glass Laser” 1995 *Phys. Rev Lett.* **74** 1335

Zherikhin A.N., Koshelev K.N. and Letokhov V.S. 1976 “On amplification in the far VUV region in multiply-charged ion transitions” *Sov. J. Quantum Electron.* **6** 82

Zwally H.J. and Koopman D.W. “Single electron capture by C^{4+} in Helium, Neon and Argon below 40 keV” 1970 *Phys. Rev. A.* **2** 1851

Acknowledgements

This thesis is the result of the coherent team-work of many people and was done during my PhD-study in the European Graduate College “Interference and Quantum Applications” at the Institut für Quantenoptik, supervised by Prof. Dr. Bernd Wellegehausen. And it is my pleasure to thank all who made this thesis possible.

First of all I would like to thank Prof. Dr. Bernd Wellegehausen for his excellent supervision and advice over the course of this PhD. I am very grateful to him for his extensive attention he paid to the work presented in the thesis, including many discussions, supporting this work with ideas and criticism, and much-needed proof reading. His continual support and encouragement gave me a big help and kept going over these years.

I would particularly like to thank Prof. Dr. Eberhard Tiemann for giving me the opportunity to study in the College and providing me with very valuable input not only in science, but also with organization skills. He was able to combine a relaxed atmosphere in our college with a great dedication to doing high quality research.

My special thank I would like to address to my supervisor Dr. Ildar Shaikhlislamov, who guided my scientific life in Novosibirsk and kept doing this in Hannover. I am very thankful for his help, guidance, and friendly and successful team-work everywhere.

It is my pleasure to thank Prof. Dr. Boris Chichkov for the fruitful discussions, great ideas and comments for evaluating this thesis. His suggestions and guidance were always much appreciated.

For their assistance, advices and support during the whole period of this work I would like to say a big 'thank-you' to all my colleges and in particularly M. Born, L. Koch, C. Reinhardt, S. Passinger and M. Klug.

I acknowledge all members of the European Graduate College. It is very nice to have someone on the same path that you can talk to and share knowledge on research and daily life with.

Acknowledgements

I would like to thank all staff of 'Institut für Quantenoptik' and especially 'Werkstatt' for their all time helpfulness, and 'Sekretariat' for the fruitful and warm working environment.

I would also like to say 'thank-you' to Dr. S. Sebban and Dr. T. Mocek for their support and enthusiastic and efficient team-work during my stay at Laboratoire d'Optique Appliquée in France.

My first steps into the world of scientific research I took at the Institute of Laser Physics in Novosibirsk, and I gratefully acknowledge all staff of our 'Department of Laser Plasma' and among them Vitaliy Posukh, Dr. Yuriy Zakharov and Prof. Dr. Arnold Ponomarenko.

Finally, I have to say 'thank-you' to all my friends and family, particularly my Mum and Dad, who always believed in me.

Lebenslauf

Persönliche Daten

Valeriy Vorontsov
geboren am 08.11.1975 in Omsk, Rußland
Eltern: Aleksei Vorontsov
Natalia Vorontsova, geb. Ivonina

Schulbildung

1982 – 1992 Oberschule N12 in Novoaltaisk, Rußland

Hochschulausbildung und wissenschaftliche Arbeit

1992 – 1996 Studium der Physik an der Technischen Universität in
Novosibirsk, Rußland

06/1996 Abschluß des Studiums als Bakkalaureus der Physik

1996 – 1998 Studium der Physik an der Technischen Universität in
Novosibirsk, Rußland

06/1998 Abschluß des Studiums als Magister der Physik

1998 – 2001 Wissenschaftlicher Mitarbeiter im Institute of Laser Physics
SB RAS, Novosibirsk, Rußland

2002 – 2004 Stipendiat im Graduiertenkolleg „Interference and Quantum
Applications“ im Institut für Quantenoptik der Universität
Hannover

List of publications

T. Mocek, C. M. McKenna, B. Cros, S. Sebban, D. J. Spence, G. Maynard, I. Bettaibi, V. Vorontsov, A. J. Gonsavles, and S. M. Hooker “ *Dramatic enhancement of xuv laser output using a multi-mode, gas-filled capillary waveguide*” Phys.Rev. A **71** 013804 2005

V.A. Vorontsov, M. Born, I.F. Shaikhislamov, B.N. Chichkov and B. Wellegehausen “*Investigations on novel XUV-laser schemes*” Appl. Phys. B **78** 979 2004

V.A. Vorontsov, I.F. Shaikhislamov, M. Born, B.N. Chichkov and B. Wellegehausen “*Charge Transfer as Alternative Pumping Scheme for XUV Lasers*” Proceedings of IX Intern. Conf. on “X-ray Lasers” Beijing, China, May 24-29, 2004

M. Born, S. Passinger, V.A. Vorontsov, I.F. Shaikhislamov, B.N. Chichkov and B. Wellegehausen “*Investigations on short-pulse laser pumped XUV laser schemes*” Proceedings of IX Intern. Conf. on “X-ray Lasers” Beijing, China, May 24-29, 2004

V.A. Vorontsov, M. Born, I.F. Shaikhislamov, B.N. Chichkov and B. Wellegehausen “*Charge-transfer pumping for XUV lasers*” J. Phys. B **36** 3865 2003

I.F. Shaikhislamov, Yu.P. Zakharov, A.G. Ponomarenko, V.G. Posukh, A.V. Melekhov, V.M. Antonov and V.A. Vorontsov “Charge-transfer pumping of OVII ions with emission at 51.2nm”. J. Phys. France **11** Pr2-267 2001

I.F. Shaikhislamov, Yu.P. Zakharov, A.G. Ponomarenko, V.G. Posukh, A.V. Melekhov, V.M. Antonov and V.A. Vorontsov “Charge-transfer scheme of EUV laser” Laser Physics **11** 1069 2001

I.F. Shaikhislamov, Yu.P. Zakharov and V.A. Vorontsov “Charge-transfer in diagnostics of Laser-produced ions” Proc. of XXIV Intern. Conf. “Phenomena in Ionized Gases” Warsaw, Poland, July 11-16, v.III, p.79-80 1999